NTNU
Norwegian University of
Science and Technology

Analysis and Design of Mooring and Turret Systems for Ship-shaped Floating Production Systems (FPSOs)

Øystein Ølund Bertelsen

Marine Technology
Submission date: June 2018
Supervisor: Kjell Larsen, IMT

Norwegian University of Science and Technology
Department of Marine Technology

MASTER THESIS SPRING 2018

for

Stud. tech. Øystein Ølund Bertelsen

Analysis and Design of Mooring and Turret Systems for Ship-shaped Floating Production Systems (FPSOs)

Analyse og design av forankrings- og turretsystemer for flytende produksjonsskip (FPSO)

Background

Floating production concepts for oil and gas are often designed as turret moored ships; Floating Production, Storage and Offloading units (FPSOs). The purpose of the turret mooring system is to keep the vessel safely at a required position due to the integrity of the production risers. It normally consists of 12-20 mooring lines of heavy chain, steel wire ropes and/or synthetic polyester ropes connected to a seabed anchor.

During the past years, the requirements to the mooring and station keeping systems of mobile and permanent units have become more complex;
- The industry is moving into new frontiers (ultra-deep water down to 3000m depth and into arctic areas).
- There are more operations adjacent to other installations (floatel operations and tender support vessel operations).
- The new mobile units are becoming larger and many units are at the end of their lifetime.
- There are too many anchor line failures.
- The design lifetime of the units must in many cases be extended due to increased oil recovery.

The overall objective of this thesis is to assess different design concepts and design methods for mooring systems for a turret moored ship and to study the resultant load effects in the turret structure. A typical FPSO unit designed for Norwegian Continental Shelf shall be studied. The assessments shall be limited to ULS and ALS design.

A large part of the work is related to establish numerical analysis models and to perform numerical analysis using the numerical tools SIMO/RIFLEX/SIMA. Numerical simulations in the time domain shall be the basic method.

.

Scope of Work

1) Review relevant literature and describe possible mooring and station keeping systems for mobile and permanent units. Focus on station keeping principles and main hardware components. Describe the main differences between a system in deep water and a system to be operated in shallow water.

2) Review relevant literature for time domain simulation of mooring systems and describe the theory related to coupled and un-coupled analysis methodology. Describe the relevant simulation tools available in SIMO/RIFLEX/SIMA and how SIMA can effectively be utilized and how extreme vessel motions and line tension can be estimated for a turret moored FPSO. In particular, a description of a model for sway/yaw stability of a turret moored ship shall be included.

3) Describe the design limit states for mooring systems with corresponding acceptance criteria outlined in rules and regulations (use ISO 19901-7 and DNVGL-OS-E301). Focus on ULS and ALS limit state, but fatigue limit state (FLS) shall also be described.

4) Continue to develop a model of a turret moored FPSO in the SIMA software package. Based on a proposed mooring configuration, compliance with the requirements for ULS and ALS design shall be documented. The candidate shall document the differences between a fully coupled analysis using SIMO/RIFLEX and the simple quasi-static approach using SIMO only.

5) Establish a simple model for estimating the support forces of the turret structure. Characteristics of the turret is to be agreed with the supervisor. Establish ULS design loads of the turret and discuss the risk of turret uplift in extreme sea states.

6) Conclusions and recommendations for further work.

General information

All necessary input data for the simulation case is assumed to be provided by Statoil.

The work scope may prove to be larger than initially anticipated. Subject to approval from the supervisor, topics may be reduced in extent.

In the thesis the candidate shall present his personal contribution to the resolution of problems within the scope of work.

Theories and conclusions should be based on mathematical derivations and/or logic reasoning identifying the various steps in the deduction.

The candidate should utilise the existing possibilities for obtaining relevant literature.

Report/Delivery
The thesis report shall be organised in a rational manner to give a clear exposition of results, assessments, and conclusions. The text should be brief and to the point, with a clear language. Telegraphic language should be avoided.

The report shall be written in English and edited as a research report including literature survey, description of relevant mathematical models together with numerical simulation results, discussion, conclusions and proposal for further work. List of symbols and acronyms, references and (optional) appendices shall also be included. All figures, tables and equations shall be numerated.

The original contribution of the candidate and material taken from other sources shall be clearly defined. Work from other sources shall be properly referenced using an acknowledged referencing system.

The report shall be submitted in two copies:
- Signed by the candidate
- The text defining the scope included
- In bound volume(s)
- An electronic copy to be sent to the supervisor

Ownership
NTNU has according to the present rules the ownership of the project results. Any use of the project results has to be approved by NTNU (or external partner when this applies). The department has the right to use the results as if the work was carried out by a NTNU employee, if nothing else has been agreed in advance.

Thesis supervisor**:**
Prof. II Kjell Larsen, NTNU/Statoil

Deadline: June 11, 2018

Trondheim, January 18th, 2018

Kjell Larsen (date and signature):
Kjell Larsen, 6/6-2018
Øystein Ølund Bertelsen (date and signature):
Øystein Ø. Bertelsen 06.06.18 Trondheim

Preface

This thesis represents the end of my two year Master's and Science Program in Marine Technology with specialization in marine hydrodynamics at the Norwegian University of Science and Technology (NTNU). The thesis has been performed with Professor II. Kjell Larsen as my supervisor.

Thank you Kjell Larsen for your guidance and support along the way. Our talks have inspired and motivated me to give my best. This last year, specializing in one subject, have been very challenging but also interesting and fun. Thank you for breaking heavy hydrodynamics expressions and phenomenons down to a level I can understand.

I want to thank Equinor for providing the FPSO model, and all additional data that was necessary for my thesis.

I want to thank Yuna Zhao for your great help in the process of performing analyses within Sima. Thank you for always keeping your door open.

I want to give a thanks to the guys in my cubicle for all the good and frustrated hours we have spent together in the office. I also want to thank the class of 18 for two great years together here at MTS.

Finally I want to thank my family and my dear Helena for their support and encouragement through this past year, and I want to give a special thanks to my brothers, Eivinn and Torleif, for sharing their words and knowledge with me in the last couple of days.

Abstract

From 2010-2014 there have been in total 18 mooring line failures in the Norwegian Continental Shelf, thus line failures are still an existing problem of moored floating structures. The motivation in this thesis is thus to study the line tensions and top end motions of floating structures in extreme weather conditions.

A literature study of the different permanent and mobile keeping systems, and their hardware components is conducted in order to build a fundamental knowledge about mooring. When designing permanent station keeping systems the ultimate, accidental and fatigue design limit state requirements must be satisfied. Ultimate and accidental limit state analyzes are conducted in this thesis.

Time domain simulations of a turret moored FPSO are performed in this thesis, and a literature study of the time domain analysis methods is conducted. The software Sima is used to perform the time domain analyzes, however there are two features within Sima that performs the analyzes: Simo and Riflex. A literature review of these programs and their simplifications are conducted.

The FPSO's RAOs show that the most critical response is in roll with a maximum response of 9.9 deg/m. It is thus very important that the vessel is able to weathervane up against the weather such that roll motions is prevented. Sway-yaw stability calculations are performed for different distances between the center of gravity and the turret to investigate the weathervaning ability of the vessel.

In this master's thesis, quasi-static and dynamic simulations of a turret moored FPSO are performed in the software Sima in ULS and ALS during co-linear and spread environments. Before performing the ULS and ALS simulations, a surge decay test is conducted to investigate if the surge natural period is the same between the system in Simo and Simo-Riflex. Also a system characteristic test is conducted to investigate if there exist any stiffness differences between Simo and Simo-Riflex. A convergence test of the line tension's standard deviation is conducted to investigate how many simulations are necessary before the standard deviation becomes stable. The number of simulations performed in the ULS and ALS analyzes are based on the convergence test.

The system responses studied in this thesis are the vessel's six degree of freedom motions, mooring line tension responses and the turret loads. These responses have been studied in 100 year wave and wind period, and a 10 year current period. The

characteristic most probable maximum line tensions are found through the Gumbel extreme distribution, and is compared with the line breaking strength according to the requirements for permanent mooring units on the Norwegian Continental Shelf. The turret design loads are calculated, and turret uplift is investigated in ULS and ALS during co-linear and spread environmental conditions. The motion and line tension response is compared between system in Simo and in Simo-Riflex to study the difference between them.

The results show that Simo does not capture the WF forces caused by the dynamic behaviour of the mooring lines, and thus the surge and sway LF motions are not dampened by the mooring lines. In Riflex, the leeward line Longest 4 and windward line Long 4 achieves the largest most probable maximum line tension in ULS spread and co-linear weather respectively. The minimum 90% fractile design load in one boogie is negative, thus the turret uplift requirement is not satisfied in ULS and ALS during both weather conditions.

Sammendrag

Fra 2014 til 2018 har det oppstått 18 linebrudd på Norsk sokkel, og linebrudd er dermed fortsatt et eksisterende problem. Motivasjonen i denne oppgaven er derfor å studere linestrekkene og toppbevegelsene av flytende konstruksjoner under ekstreme værforhold.

En litteraturstudie av de forskjellige permanente og mobile forankringssystemer, og deres forankringskomponenter er gjennomført for å bygge et kunnskapsgrunnlag om forankring. Ved design av permanente forankringssystemer så må systemet tilfredsstille kravene til brudd-, ulykkes- og utmattingsgrensetilstand. Analyser i brudd- og ulykkesgrensetilstand er utført i denne oppgaven.

I denne masteroppgaven utføres simuleringer i tidsdomenet av en turret forankret FPSO, og ulike analysemetoder i tidsdomenet er studert. En analyse i tidsdomenet simulerer naturkreftene og beskriver oppførselen til fartøyet, fortøyningssystemet og eventuelle risere. Hvor godt oppførselen blir beskrevet er avhengig av analysemetoden, og det er to metoder: separat og koblet analyse.

Analyser i tidsdomenet kan utføres i programvaren Sima, og det finnes to delprogrammer som utfører analysene: Simo og Riflex. Et litteraturstudie av programmene og deres forenklinger og bereningsmetoder er gjennomført.

FPSO'ens RAOer viser at den mest kritiske responsen er i rull med en maksimalrespons på 9,9 grader / m. Det er derfor meget viktig at fartøyet er i stand til å rette seg opp mot været slik at store rullebevegelser forhindres. Enkle svai-gir stabilitetsberegninger er utført for ulike avstander mellom fartøyets tyngdepunkt og turret, for å undersøke fartøyets evne til å rette seg opp mot været.

I denne mastergradsoppgaven utføres det kvasi-statiske og dynamiske simuleringer av en turret forankret FPSO, i programvaren Sima i brudd- og ulykkesgrensetilstand under rett og spredt værretning. For å undersøke om systemets egenperiode i jag er den samme i Simo og Simo-Riflex, så er det blitt utført en jag demping test. Også en systemkarakteristikk er funnet med hensikt i å undersøke om det finnes noen stivhetsforskjeller mellom forankringsmodellen i Simo og Simo-Riflex. En konvergensprøve av standard avviket til linestrekket i en line utføres for å undersøke hvor mange simuleringer det tar før standardavviket blir stabilt, og antall simuleringer utført i brudd- og ulykkes-analysene er basert på konvergensprøven.

I denne oppgaven studeres følgende responser: fartøyets bevegelsesrespons i seks frihetsgrader, linestrekkresponser og turretbelastninger. De maksimale linestrekkene er Gumbel fordelt, og de karakteristiske mest sannsynlige maksimale linestrekkene er funnet gjennom denne fordelingen og er sammenlignet med linens bruddstyrke, i henhold til kravene til permanente enheter på norsk sokkel. Turretens designbelastning er funnet fra Gumbel's fordeling, og turretoppløfting undersøkes i brudd- og ulykkesgrensetilstand under rett og spredt vær. Bevegelses- og linestrekkresponsen blir sammenlignet mellom forankringssystemet i Simo og Simo-Riflex for å studere forskjellen mellom dem.

Resultatene viser at Simo ikke simulerer de bølgefrekvente kreftene som kommer av den dynamiske oppførselen til forankringslinene, og dermed blir ikke fartøyets lavfrekvente jag- og svai bevegelser dempet av linene. I Riflex oppnår le line Longest 4 og lo line Long 4 de største og mest sannsynlige linestrekkene i henholdsvis ULS spredt og rett vær. 90% fractile design lasten i en boogie er negativ, og dermed er kravet til turret oppløft ikke tilfredsstilg i ULS og ALS under begge værtilstander.

Nomenclature

The nomenclature describes several symbols that will be later used within the Master's thesis.

$\bar{F}_{wf}$ Mean wave drift force

$\bar{U}$ Mean wind velocity

$\bar{U}_{cu} = V_{cu}$ Current velocity

β Is related to the standard deviation in the Gumbel probability distribution

$\ddot{\theta}$ Turret's COG angular acceleration

$\dot{x}$ Low frequent vessel velocity

$\eta_1, \eta_2, \eta_3, \eta_4, \eta_5, \eta_6$ Surge, sway, heave, roll, pitch and yaw motion

$\frac{dF_{sway}}{d\psi}$ Change in sway force with respect to change in weather heading

$\frac{dM_z}{d\psi}$ Change in yaw moment with respect to change in weather heading

γ_F Safety factor in fatigue design limit state

Λ Damping ratio

μ The mean value

ω_d Damped natural frequency

ϕ Line angle with respect to x-axis

ρ_{air} Air density

ρ_w Water density

$\sum F_x$ The sum of the forces in x-direction

$\sum F_y$ The sum of the forces in y-direction

$\sum M_{COG}$ The sum of the moments about the center of gravity

θ Standard Deviation

ξ Damping ratio

$_I$ Initial coordinate system

$_L$	Local coordinate system
$_R$	Body-related coordinate system
$_{GL}$	Global coordinate system
a	Catenary: weight moment arm, Taut: horizontal distance from vessel to anchor
$A(\omega)$	Frequency dependent added mass
A_{cu}	Projected current area
A_{wi}	Projected wind area
$B^L_{Q,cu}$	Linear current damping
$B^L_{Q,wi}$	Linear wind damping
B_L	Linear surge damping
B_{LF}	LF damping
$C(\omega)$	Frequency dependent damping
$C^{cu}_{sway,\psi}$	Sway current coefficient
$C^{cu}_{yaw,\psi}$	Yaw current coefficient
$C^{wi}_{sway,\psi}$	Sway wind coefficient
$C^{wi}_{yaw,\psi}$	Yaw wind coefficient
C_c	Critical damping
$C_{D,cu}$	Current drag coefficient
$C_{D,wi}$	Wind drag coefficient
C_{LF}	LF stiffness
C_{wd}	Wave drift force coefficient
$D = y$	Water depth
D	Normal external current force
d_c	Accumulated fatigue damage in a mooring line
d_i	Fatigue damage in loading sequence i

D_l Linear damping

D_q Quadratic damping

EA Axial stiffness

F Tangential external current force

$F(x)$ Gumbel cumulative density function

$f(x)$ Gumbel probability density function

F_1^M Mooring system's total surge force

F_2^M Mooring system's total sway force

F_6^M Mooring system's total yaw moment

F_h Restoring force

F_v Vertical force

F_x^{CT} Shear Mooring force

F_x^{RAD} Radial wheel force

F_Y Sway force

F_z^{BOG} Vertical boogie force

F_z^{CT} Axial mooring force

F_z^{FK} Dynamic wave pressure

H_S Significant wave height

I_θ Moment of intertia from turret and added mass

$K(r)$ Non-linear stiffness

k_E Elastic system stiffness

k_G Geometric system stiffness

k_T Total system stiffness

l Line length

M Body mass

M^{BOG} Boogie moment

M^{CT} Mooring moment at the top end

M_T Total turret moment

$M_z = M_{yaw}$ Yaw moment

M_{sway} Sway moment

Mg Turret gravitation force

n Number of amplitudes between the chosen amplitude peaks

$Q(t, r, \dot{r})$ Total environmental loads

q_{cu} Current loads

q_{th} Thruster loads

q_{wa} Wave loads

q_{wi} Wind loads

s Total motion of a random point on a floating structure

S_η Wave spectrum

$S_{F,LF}(\omega, LF)$ LF spectral density

sf^{DLS} Design limit state safety factor

T Line tension force

T_d Damped natural period

T_n Natural period

T_P Wave peak period

$T_x = T_H$ Horizontal top tension

T_{BS} Line breaking strength

T_{Ch}^{DLS} Characteristic design limit state line tension

$u(t)$ Dynamic wind gust

u_{dyn} Dynamic response

u_{st} Static response

w Line unit weight in water

W_w	Line weight in water
x, y, z	Cartesian coordinates
X_l	Horizontal distance from the vessel to the anchor
x_{GT}	Distance between the COG and turret
u	The value where the Gumbel probability density function reaches its peak

Contents

List of Figures

List of Tables

Chapter 1

Introduction

1.1 Background

During the past years, the requirement for mooring and station keeping systems of mobile and permanent units have become more complex. The oil and gas industry is continuously searching for new fields, and is moving into deeper and colder frontiers. Mooring systems are often necessary to maintain a stable positioning of an operating Floating, Production, Storage and Offloading (FPSO) vessel in an oil field. This is mainly because the vessel's motions often shall be restrained during a marine operation. The vessel has risers connected to it where petroleum liquids are flowing from the seabed and on board the vessel. These risers have a maximum allowed breaking load, and in order to prevent the risers from breaking, the vessel motions must be restrained.

It is of special interest to study the motions of a turret moored FPSO in extreme offshore environment. The environmental loads in extreme weather conditions have a large impact on the mooring lines. From 2010-2014 there have been in total 18 mooring line failures on the Norwegian Continental Shelf. These line breaks have occured due to fatigue, overload, mechanical damage and production defects. 7 of the mooring line failures in this period are due to overloads, according to Vegard Aksnes (2016), thus it is interesting to investigate the line tensions in extreme weather conditions.

Turret uplift is a phenomenon that can occur under extreme weather conditions. This may damage components in the turret which are important to the oil and gas flow transportation and then production must shut down. Turret uplift must therefore be prevented and thus it is interesting to study the turret loads during extreme weather conditions.

1.2 Scope of Work

This Master's thesis is a continuation of the Project Thesis Øystein Ølund Bertelsen (2017), and the main objective of the Master's thesis is to acquire knowledge about design of station keeping systems, and be able to model and perform numerical simulations of a turret moored FPSO in a given oilfield using the Simulation Workbench for Marine Applications (SIMA) software.

The thesis is divided into five parts:

1) Review literature about station keeping systems for mobile and permanent units in shallow and deep waters, and a description of the main hardware components in a mooring system.

2) Review literature for time domain simulation of mooring systems and describe the theory related to coupled and un-coupled analysis methodology. Describe SIMA/SIMO/RIFLEX and how extreme vessel motions and line tension can be estimated for a turret moored FPSO. A description of a model for sway/yaw stability of a turret moored ship shall be included.

3) Describe the design limit states for mooring systems with corresponding acceptance criteria outlined in rules and regulations. Focus on Ultimate Limit State (ULS) and Accidental Limit State (ALS) limit state, but Fatigue Limit State (FLS) shall also be described.

4) Continue to develop a model of a turret moored FPSO in the SIMA software package. Based on a proposed mooring configuration, compliance with the requirements for ULS and ALS design shall be documented. The candidate shall document the differences between a fully coupled analysis using SIMO/RIFLEX and the simple quasi-static approach using SIMO only.

5) Establish a simple model for estimating the support forces of the turret structure. Characteristics of the turret is to be agreed with the supervisor. Establish ULS design loads of the turret and discuss the risk of turret uplift in extreme sea states.

Chapter 2

Station Keeping Systems, Hardware and Design Requirements

This chapter includes a description of different station-keeping systems, the main hardware components in a mooring system and a description of the design limit states.

2.1 Mooring Hardware

This section is based on the references Larsen (2017) and ISO (2013).

The mooring system may consist of several different components depending on which type of mooring system that is used. An illustration of the main hardware components of a mooring system is showed in Figure 2.1.

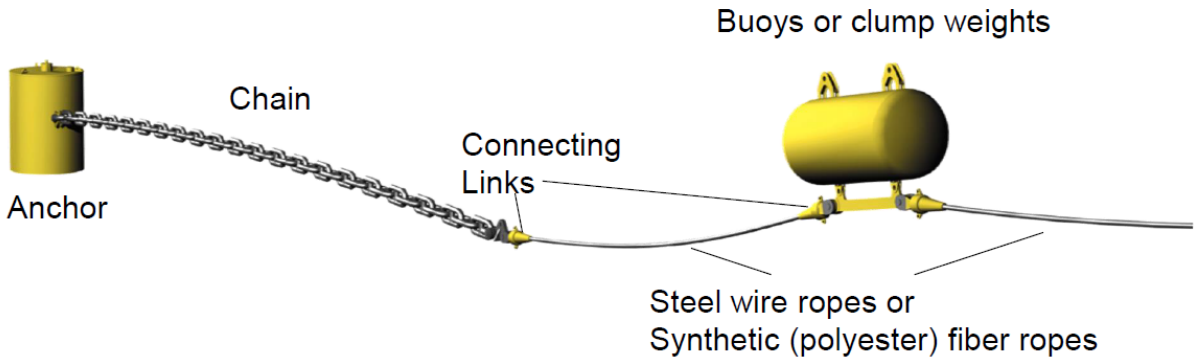

Figure 2.1: Main mooring line components, Larsen (2017).

Chain

Chain mooring lines are commonly used in designing of a catenary mooring system, and are either studded or studless. It has a large weight which provides stiffness to the system, and it has good abrasion characteristics. However, an all chain configuration

in deep water is very heavy, thus the payload capacity of the floating vessel will be reduced with a mooring configuration of just chain.

Steel Wire

There are several different steel wire configurations, and some examples are the plastic sheathed spiral strand and the unsheathed six-strand configuration. Steel wire provides large stiffness to the system, and are much lighter than chain which as mentioned becomes important in deep water. However, an all wire configuration are not used for permanent mooring due to abrasion at the sea floor.

Synthetic Fibre

Synthetic fibre lines provides stiffness due to its elastic elongation properties. The lines are very light compared to chain and steel lines and are usually made out of polyester. Due to its low weight and high stiffness properties, synthetic fibre lines are usually used in deep water mooring configurations. Also, the fatigue life of synthetic fibre lines are longer compared with steel wire lines.

Anchor

Several anchors have been developed for station keeping systems, and some of them are drag anchors, anchor piles, suction anchors, gravity anchors, plate anchors etc. The anchor decision making is based on parameters like the soil configuration, water depth, holding capacity etc.

Buoyancy Elements and Clump Weights

Buoyancy elements are connected to the mooring lines with the intention of reducing the line weight, effects of line dynamics and the vessel's offset. However, the unfavorable effects are installation complexity and dynamic response of the buoys in bad weather, which may increase the tension in the mooring lines. Clump weights however, is added to the mooring lines with the intention of increasing the weight, thus increasing the stiffness of the mooring system.

Connection Links

Mooring lines often consists of a combination between chain, steel wire and fibre lines, and connection links are used to connect these components.

2.2 Station Keeping Systems

This section is based on the references Larsen (2017), ISO (2013), DNV (2013) and Faltinsen (1990).

Several station-keeping systems have been developed over the years and is used to maintain the positioning and motion control of marine offshore vessels. These are divided into permanent and mobile station keeping systems. Permanent station keeping systems are designed to incorporate a long service life. Mooring systems are used in permanent systems and according to section 5.1 in the Offshore Standards, fatigue analysis of the mooring lines shall be performed. For mobile station keeping systems, for example drilling rigs, the station keeping system may consist of mooring lines or dynamic positioning (DP) system. The permanent and mobile station keeping systems will be described in subsection 2.2.1 and 2.2.2 respectively.

2.2.1 Permanent Station Keeping Systems

This subsection is based on the references ISO (2013) and Larsen (2017).

Permanent station keeping systems are used in offshore operations where a vessel shall be operating at least 5 years at the same location, Larsen (2017). The common solution for these "permanent" operations is to use mooring systems, thus mooring lines controls the positioning of the vessel. The main task of the mooring system is to restrain the vessel motions from exceeding the acceptable limit of horizontal offset.

The mooring lines consists of either steel chain, steel wire, synthetic fibre or a combination of these. These lines can be attached to the vessel in different configurations like mooring winches or turrets, and are fastened to the seabed by anchors. The lines create an important restoring stiffness to the system, which is provided by elastic and geometric properties which will be described later in the thesis. There are several different mooring systems, and in this section certain mooring systems will be presented.

Spread Mooring

The spread mooring system fixes the orientation of the floating structure, and is commonly used for semi-submersibles which are insensitive to the weather direction. However this mooring system can also be applied for ship shaped vessels when

the prevailing weather in the field only comes from one direction. The ship is then moored with the bow towards this direction.

The spread mooring system can be of catenary, taut or semi-taut configuration. This means that the spread mooring can have lines consisting of chain, steel wire, polyester and a combination of these.

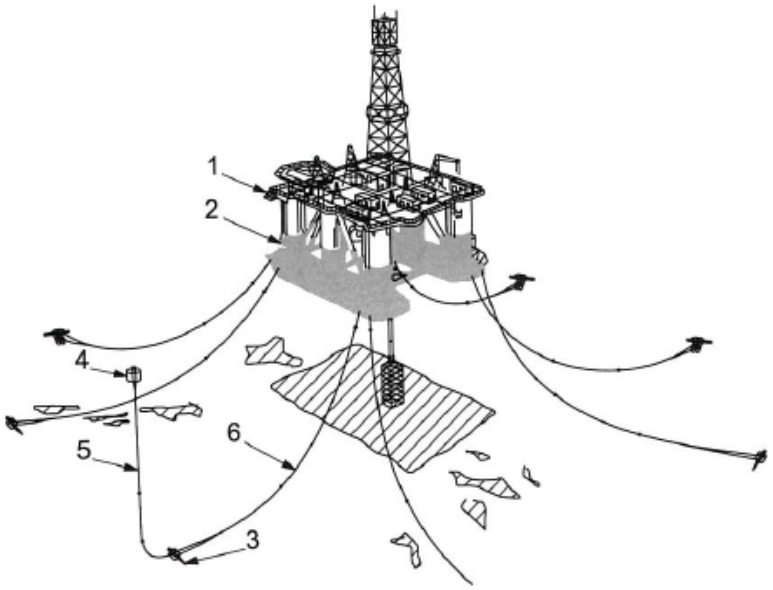

Figure 2.2: Spread mooring system, ISO (2013).

Single Point Mooring

The single point mooring setup is typically the case for streamlined ship shaped floating vessels, like for example an FPSO or an Floating Storage and Offloading (FSO) vessel. The weather direction is very critical with respect to an FPSO, and the single point mooring makes it possible for the ship to weathervane. Weathervane means to head the vessel's bow against the weather. There exist different single mooring systems, but they essentially have the same function. Single anchor leg mooring (SALM), catenary anchor leg mooring (CALM) and turret mooring are examples of typically used single point mooring systems. The latter which is the mooring system that is to be further investigated will be more closely described in the next page..

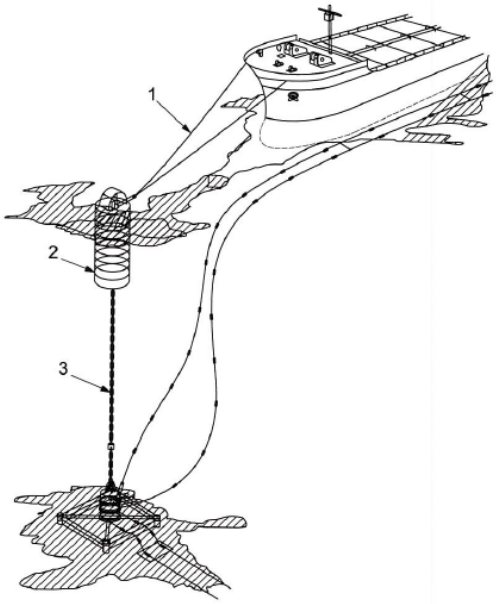

Figure 2.3: Catenary anchor leg mooring, ISO (2013).

Turret Mooring

It is called turret mooring because the catenary mooring lines and risers are all connected to a turret. Two important properties of a turret moored FPSO is (as mentioned earlier) that it can weathervane by rotating about the turret, and that it rotates independently of the mooring and riser system. The latter means that the mooring lines and risers are not affected by the yaw motion.

There exist three designs of a turret mooring: internal turret, outer turret and turret with a disconnection ability. The inner turret is practical since it usually has a shorter transportation distance of oil and gas to the tanks. The outer turret is (among other things) commonly used to maintain the sway-yaw stability by increasing the distance between the turret and the centre of gravity (COG) of the ship. The sway-yaw stability will be discussed more closely later in the report. The disconnection design is used when the vessel is exposed to storms larger than what the vessel is designed for in general and during production. When it disconnects, the mooring lines are self-floating a distance under the sea surface due to connected buoyancy elements.

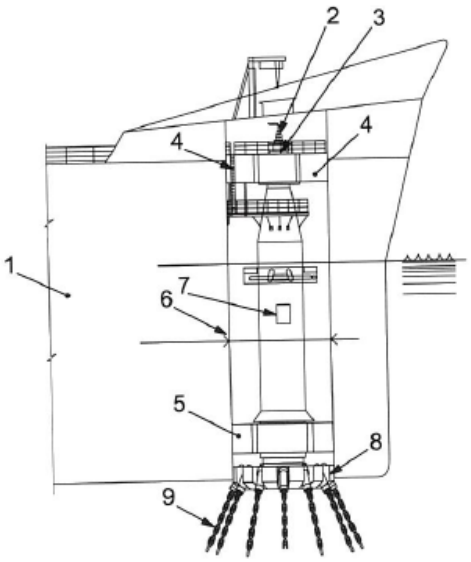

Figure 2.4: Turret mooring, ISO (2013)

Thruster-Assisted Mooring Systems

A mooring system might not be sufficient for maintaining heading direction or positioning in general. Thrusters are often installed in addition to the mooring system to maintain stable positioning, and this is called a thruster-assisted mooring system.

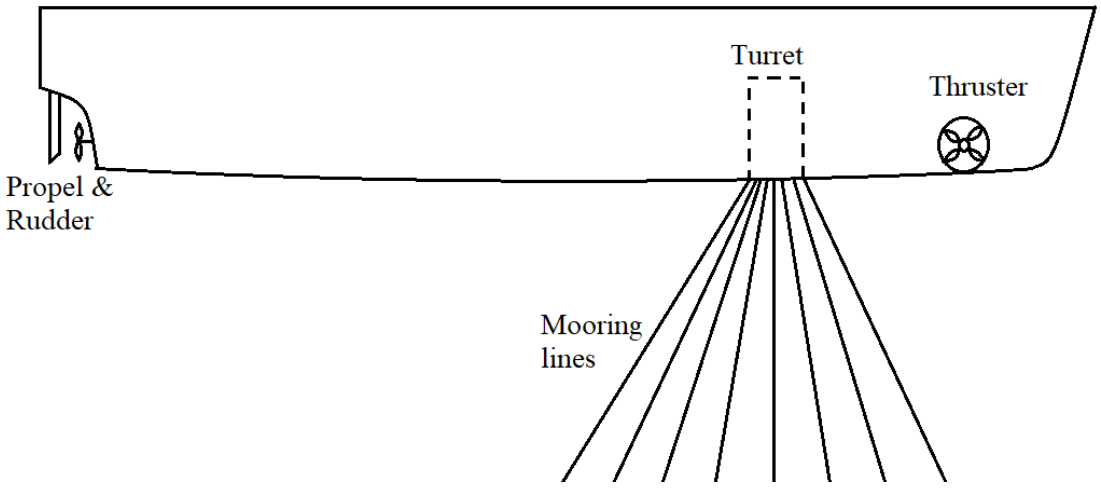

Figure 2.5: Thruster assisted mooring.

2.2.2 Mobile Station Keeping Systems

This subsection is based on the references Larsen (2017) and ISO (2013).

Mobile station keeping systems are used for operations with a short duration of time. Two types of mobile station keeping systems will be presented in this section: DP-systems and mobile mooring systems.

Dynamic Positioning Systems

Some marine operations lasts for a short duration of time, and it is very costly to set up a mooring system. Instead dynamic thruster systems are commonly used for maintaining stable positioning in short-period operations. The DP-system is common for drilling and maintenance vessels.

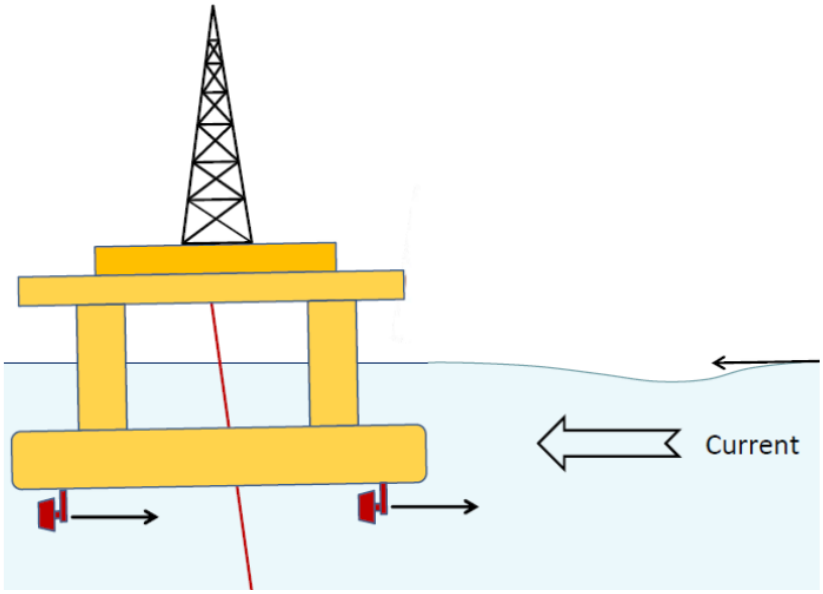

Figure 2.6: Dynamic positioning system ,Larsen (2017)

Mobile Mooring Systems

Mooring systems are usually applied for long-term or permanent operation vessels were the consequence for failure is high, as showed in Figure 2.7. However mooring systems are also used for weather restricted operations in shorter operation periods, for example drilling operations. These mobile mooring systems are designed for operations period less than 5 years. The decision of either using a mooring system or a

dynamic positioning system is illustrated in Figure 2.7.

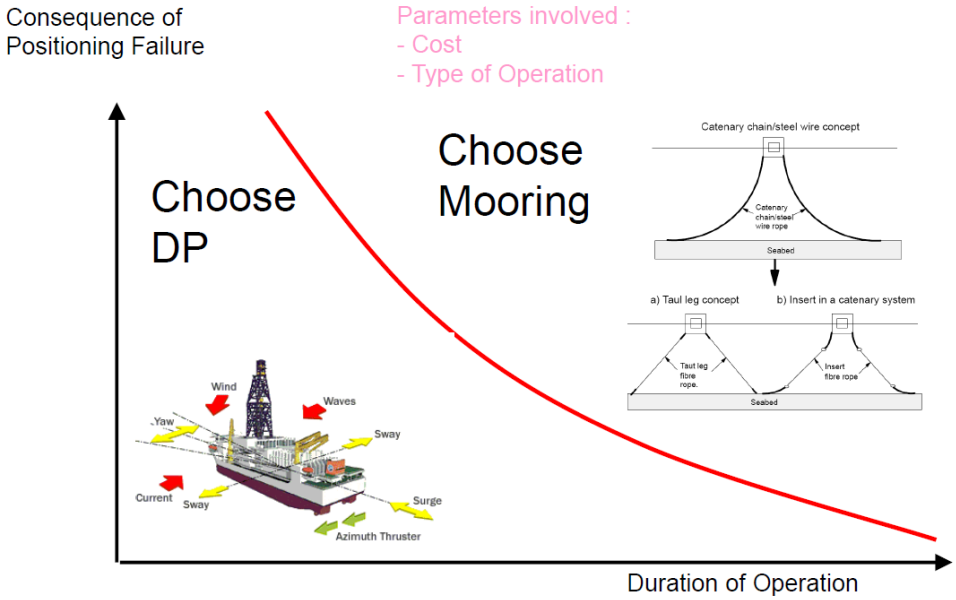

Figure 2.7: Choosing a DP- or a moored system with respect to the consequence of positioning failure as a function of the operation duration, Larsen (2017).

2.2.3 Station Keeping Systems in Deep and Shallow Water

This subsection is based on the references Larsen (2017) and ISO (2013).

As mentioned in the background of this project thesis, the oil and gas production is moving into colder and deeper sea areas. Mooring systems are commonly used for shallow water operations, but also for deep water operations. However the choice of line material is of significant matter. A catenary system with pure chain mooring lines can ,as mentioned earlier, be used in shallow water but not deep water due to its too heavy weight. A catenary system with a chain and steel wire line configuration however can be used in medium deep water, because of the lighter weight of the steel wire. Taut systems of polyester fibre lines are used in deep water moorings and is a much lighter and cheaper alternative. A combination between a catenary and taut system is called a semi-taut mooring system. The semi-taut lines can consists of a combination between chain, steel wire and polyester fibre, and can be used in shallow- and deep water fields. Figure 2.8 shows the mooring configurations of a catenary, taut and semi-taut system.
A maintenance vessel with a DP-system can operate in both shallow- and deep water,

however these vessels are restrained from performing long-term operations due to a large risk of positioning failure.

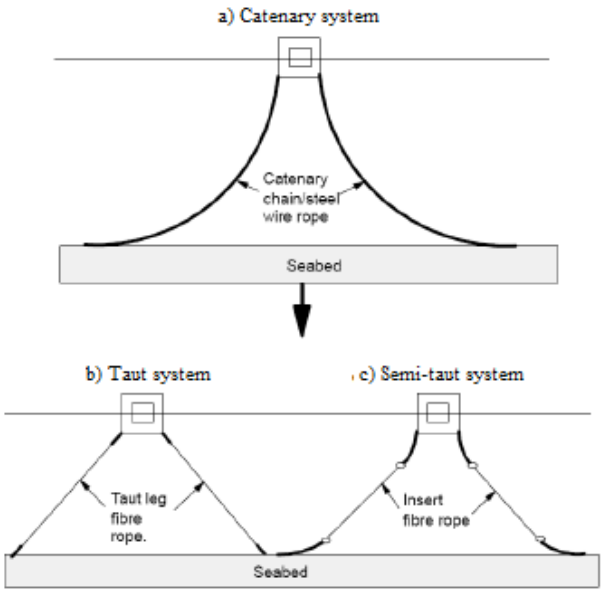

Figure 2.8: The different mooring system configurations: a) Catenary system, b) Taut system and c) Semi-taut system, Larsen (2017).

2.3 Design Limit States of Station Keeping Systems

This section is based on the references DNV (2013) and Larsen (2017).

When designing station keeping systems there are three important design limit states that must be designed for:

- Ultimate Limit State (ULS) - this design ensures that the mooring lines remain intact in a storm with a 100 year return period.
- Accidental Limit State (ALS) - the system is designed to remain stable after one or two line failures in a storm with 100 year return period.
- Fatigue Limit State (FLS) - the system is designed to ensure that each mooring line withstands cyclic loading.

These will be more closely discussed in the following subsections.

2.3.1 Ultimate- and Accidental Limit State

This section is based on the references DNV (2013) and Larsen (2017).

Mooring systems for vessels operating at the norwegian continental shelf shall be designed according to DNV Offshore Standard, DNV (2013). According to DNV Offshore Standard the design requirements for ULS and ALS are 100 year return period waves and wind, and 10 year return period for current.

When the vessels is exposed to these environmental loads, the breaking strength of the mooring line shall be larger than the characteristic maximum tension multiplied by a safety factor. This is expressed in the equation below:

$$T_{Ch}^{DLS} * sf^{DLS} < T_{BS} \tag{2.1}$$

Where T_{Ch}^{DLS}, sf^{DLS} and T_{BS} are the characteristic design limit state tension, the corresponding safety factor and the mooring line breaking strength, respectively. There is a large difference with respect to the design safety factor between Norwegian and International standards. This is shown in Table 2.1 for permanent oil storage and production units.

Table 2.1: The Norwegian and International safety factors of permanent oil storage or production units for ULS condition and ALS 1 and 2 line breaks, Larsen (2017).

	Norwegian safety factors		
Weather condition	ULS	ALS: 1 line break	ALS: 2 line break
10 year storm	N/A	N/A	1.5
100 year storm	2.2	1.5	N/A
	International safety factors		
Weather condition	ULS	ALS: 1 line break	ALS: 2 line break
10 year storm	N/A	N/A	N/A
100 year storm	1.67	1.25	N/A

2.3.2 Fatigue Limit State

This section is based on the reference DNV (2013).

The mooring lines must be designed to withstand fatigue fracture due to cyclic loading during the design life, and satisfying the FLS requirement ensures that. The accu-

mulated fatigue damage in a mooring line component due to cyclic loading during the design life (d_c) is given as:

$$d_c = \sum_{i=1}^{i=n} d_i \tag{2.2}$$

Where d_i is the fatigue damage to the component in state i. Any component in an individual mooring line must be able to resist fatigue fracture, and the design equation for FLS is given in chapter 6.1 in the DNV Offshore Standards and states the following:

$$1 - d_c * \gamma_F >= 0 \tag{2.3}$$

Where γ_F is the safety factor for the fatigue limit state. The fatigue safety factor for polyester ropes and mooring lines which are not regularly inspected, are given in the following table:

	When $d_F <= 0.8$	When $d_F > 0.8$
γ_F	5	5+3$((d_F - 0.8)/0.2)$

Table 2.2: The fatigue safety factor for tension fatigue according to the DNV Offshore Standards

Where d_F is the ratio between the fatigue damage d_c in two adjacent lines, and it cannot be larger than one. The fatigue safety factor for polyester ropes shall cover the uncertainties in a fatigue analysis, and is given as γ_F = 60. The fatigue limit state will not be studied further in this thesis.

2.3.3 Analysis and Weather Direction Recommendations

This section is based on the reference DNV (2013).

According to section 2.5.2 in the DNV Offshore Standards, all vessels should be analyzed with in-line and in-between environmental directions. Section 2.5.5 in the DNV Offshore Standards states that if the site specific data is not available, the vessels should be analyzed with a co-linear and non-co-linear environment:

- Co-linear environment analysis - is when the wind, waves and current is acting in the same direction, and the initial weather direction should be 15^o relative to the bow of the vessel.

- Non-co-linear (spread) environment analysis - is when the waves are propagating towards the bow of the vessel, and direction of the wind and current is 30^o and 45^o relative to the wave direction.

Similar weather analysis will be performed in SIMA in both ULS and ALS weather conditions, and these are more closely described in chapter 5.

Chapter 3

Theoretical Background

The governing excitation for extreme line tension of a floating vessel, is the top end motion which is excited by the environmental loads. This chapter will describe the top end motions, equation of motion and the time domain analysis for mooring systems. It will also include a short introduction to SIMA, the coordinate systems within this software, sway-yaw stability and decay calculations.

3.1 Top End Motions

This section is based on the reference Faltinsen (1990).

The motions of a moored floating vessel are excited by environmental forces, and can be categorized into four different motions:

1) Mean drift motion

2) High frequency (HF) motion

3) Wave frequency (WF) motion

4) Low frequency (LF) motion

The total motion of any point on a floating vessel can be expressed as:

$$s = \eta_1 i + \eta_2 j + \eta_3 k + \omega \times r \tag{3.1}$$

, where r and ω are respectively the position and rotation vector, given as r=xi+yj+zk and ω=$\eta_4 i$+$\eta_5 j$+$\eta_6 k$. $\eta_4 i$, $\eta_5 j$ and $\eta_6 k$ are the identified as the roll, pitch and yaw motion. The complete equation of the total motion then becomes:

$$s = (\eta_1 + z\eta_5 - y\eta_6)\, i + (\eta_2 - z\eta_4 + x\eta_6)\, j + (\eta_3 + y\eta_4 - x\eta_5)\, k \tag{3.2}$$

, where i, j and k are unit vectors along the x-, y- and z axis, respectively. $\eta_1 i$, $\eta_2 j$ and

$\eta_3 k$ are the surge, sway and heave motion, and all rigid body motions can be seen in Figure 3.1. The motion of any point on the vessel can be estimated by this equation when the motion response in every degree of freedom are known.

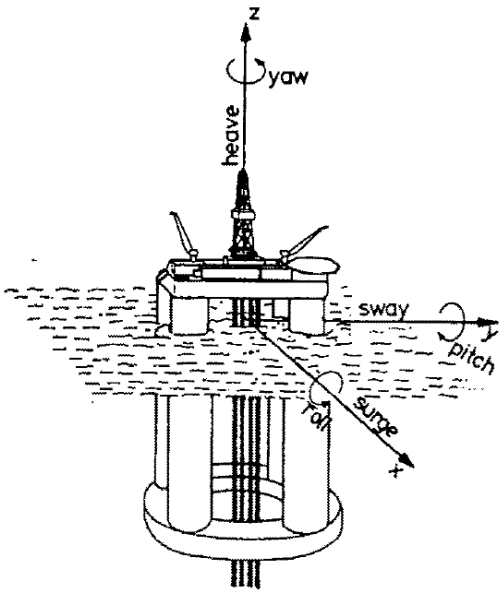

Figure 3.1: Rigid-body motion modes, Faltinsen (1990).

3.1.1 First order wave motions of a moored vessel

This section is based on the reference Larsen (2017).

The first order wave motion of a moored ship shaped vessel is quite different from other moored structures due to its slender and streamlined shape. When exposed to first order wave loads ship-shaped vessels experience dynamic coupling between surge-heave-pitch, and sway-roll-yaw motions. This dynamic coupling yields that the top end motions will become larger for ship-shaped vessels compared to other moored structures. Figure 3.2 shows the typical elliptic top end motion of a turret moored vessel when the waves are propagating towards its bow.

The dynamic tension in the mooring lines are dependent on the diameter of the elliptic displacement pattern, thus the dynamic line tension is dependent on the first order wave motions. The windward lines will experience a large mean line tension due to the LF forces, however the dynamic line tension due to the WF top end motion will not be that large due to a small elliptic displacement diameter. The leeward

lines will however experience a larger dynamic line tension due to a large elliptic displacement diameter.

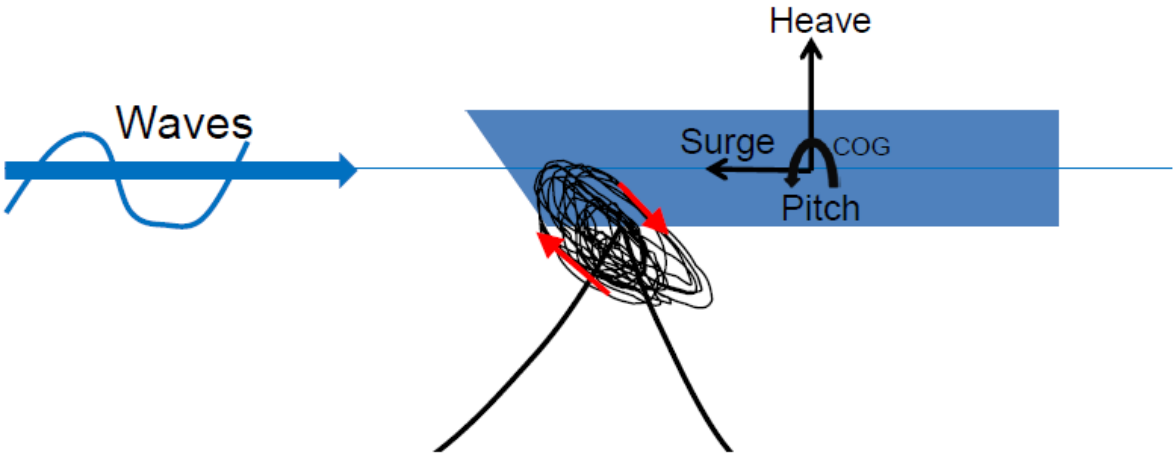

Figure 3.2: First order wave motions at the top end, Larsen (2017).

3.2 Equation of Motion

This section is based on the references Larsen (2017).

The top end motion of a moored FPSO can be described by the equation of motion in all six degrees of freedom:

$$(M + A(\omega)) * \ddot{r} + C(\omega) * \dot{r} + D_l * \dot{r} + D_q * \dot{r}|\dot{r}| + K(r) * r = Q(t, r, \dot{r}) \tag{3.3}$$

Where M is the vessel mass, A(ω) and C(ω) is the frequency dependent added mass and damping, D_l is the linear damping, D_q is the quadratic damping, K(r) represents the non-linear stiffness and r, $\dot{r}$ and $\ddot{r}$ is the position, velocity and acceleration of the vessel. On the right hand side of the equation, are the excitation forces caused by the environmental loads, Q(t,r,$\dot{r}$). All contributions to the equation of motion will be described in the following sections.

3.2.1 Excitation Forces

This section is based on the references Faltinsen (1990), Larsen (2017) and Larsen (2015a).

As mentioned in the previous section, the excitation forces are mainly caused by environmental loads. These can be identified as:

$$Q(t, r, \dot{r}) = \mathrm{q_{wi}} + \mathrm{q_{cu}} + \mathrm{q_{wa}} + \mathrm{q_{thr}} \tag{3.4}$$

, where q_{wi}, q_{cu}, q_{wa} and q_{thr} are the environmental loads caused by wind, current, waves and thrust forces respectively. These environmental loads are as mentioned in section 3.1 the HF, WF, LF and mean loads and the excitation regimes are given in Table 3.1.

Table 3.1: The excitation regimes from waves, wind and current, Larsen (2017).

Weather loads	Mean	HF(2-5s)	WF(5-30s)	LF(30-500s)
Waves	Mean drift force	Sum freq. forces	1st ord. forces	2nd ord. diff. freq.
Wind	Mean speed	-	-	Wind gusts
Current	Mean speed	-	-	-

To investigate the importance of these forces, it is necessary to know the natural oscillation periods of the moored floating vessel. The typical natural period range in all six degrees of freedom for a moored FPSO are listed in Table 3.2.

Table 3.2: The typical range of the natural periods in all six degrees of freedom, for a moored FPSO.

Natural period / Moored structure	Surge	Sway	Heave	Roll	Pitch	Yaw
FPSO	≈> 100s	≈> 100s	10-15s	10-20s	10-15s	»100s

Notice that there are only large natural periods for the moored FPSO, which means that the HF wave forces does not excite a considerable motion of the system, thus the HF loads are omitted. However, the HF loads are important for other structures like a tension leg platform (TLP) where the HF loads excites resonant motions in heave, roll and pitch. The LF forces are however very important for the surge, sway and yaw motions of the vessel. The WF forces are also important to consider because they excite heave, roll and pitch resonant motions.

The dynamic load factor (DLF) is a function of the damping ratio (ξ) and the frequency ratio (β), and is the relation between the dynamic (u_{dyn}) and static response (u_{st}), Larsen (2015a):

$$DLF = |\frac{u_{dyn}}{u_{st}}| = \frac{1}{\sqrt{(1-\beta^2)^2 + (2\xi\beta)^2}} \tag{3.5}$$

Figure 3.3 shows the importance of providing damping in the occurrence of resonant motion response.

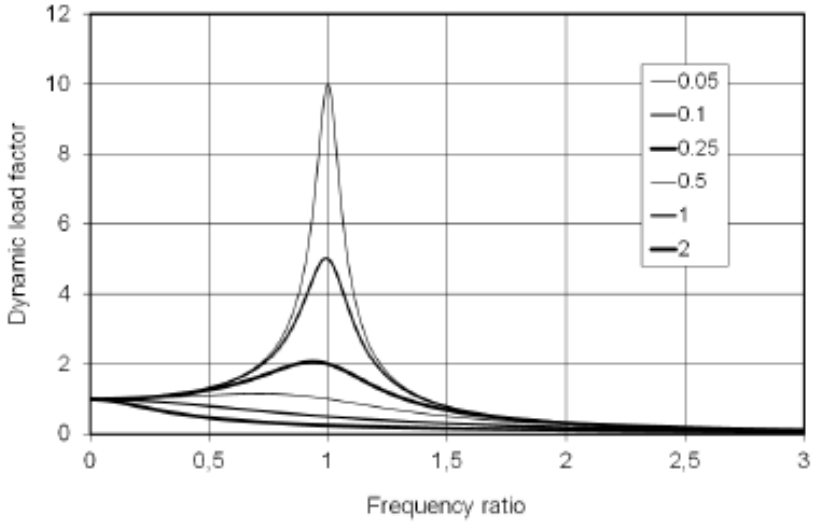

Figure 3.3: Dynamic load factor as a function of the frequency ratio for given values of damping ratio, Larsen (2015a).

Wind Forces

As showed in Table 3.1, the wind excitation loads are divided into mean and LF excitation loads, and the mean and dynamic wind gust velocity is given as $\bar{U}$ and $u(t)$ respectively. However, the wind forces also provide a LF damping force that dampens the LF vessel motions. The total wind excitation force is given in the following equation:

$$\begin{aligned} q_{wi}(t) =& \frac{1}{2}\rho_{air} * C_{D,wi} * A_{wi} * [U(t) - \dot{x}]^2 \\ =& \frac{1}{2}\rho_{air} * C_{D,wi} * A_{wi} * [U(t)^2 - 2U(t)\dot{x} + \dot{x}^2] \\ =& \frac{1}{2}\rho_{air} * C_{D,wi} * A_{wi} * [\bar{U}_{wi}^2 + 2\bar{U}_{wi}u(t) + u(t)^2 - 2(\bar{U}_{wi} + u(t))\dot{x} + \dot{x}^2] \end{aligned} \tag{3.6}$$

, where ρ_{air}, $C_{D,wi}$, A_{wi}, U_{wi}, and $\dot{x}$ are the air density, drag coefficient, vessel's wind

exposed area, mean wind velocity, and the low frequent vessel velocity. The mean wind velocity is very large in comparison with the LF vessel velocity, hence $\bar{U}_{wi} >> \dot{x}$. When only the LF forces are considered the wind excitation force are reduced to:

$$q_{wi}(t) = \frac{1}{2}\rho_{air} * C_{D,wi} * A_{wi} * [\bar{U^2_{wi}} + 2\bar{U_{wi}}u(t) - 2\bar{U}_{wi}\dot{x}] \tag{3.7}$$

Force coefficients are frequently used in describing the environmental loads, and the wind force coefficient is given as:

$$c_{wi} = \frac{1}{2}\rho_{air} * C_{D,wi} * A_{wi} \tag{3.8}$$

Current Forces

The current excitation loads are the mean current forces however like the wind forces, the current will also excite LF damping forces and contributes to a dampened low frequent vessel motion. The total current excitation force is expressed as:

$$q_{cu}(t) = \frac{1}{2}C_{D,cu} * A_{cu} * |\bar{U}_{cu} - \dot{x}|(\bar{U}_{cu} - \dot{x}) = \frac{1}{2}C_{D,cu} * A_{cu} * (\bar{U}^2_{cu} - 2\bar{U}_{cu}\dot{x} + \dot{x}^2) \tag{3.9}$$

,where $\bar{U}_{cu}$, ρ_{water} and $\dot{x}$ are the current velocity, water density and the LF surge velocity. The LF surge velocity is very small in comparison with the current velocity, hence the following can be expressed $\bar{U}_{cu} >> \dot{x}$. The total current excitation force is then reduced to:

$$q_{cu}(t) \approx \frac{1}{2} * C_{D,cu} * A_{cu} * \bar{U}^2_{cu} - \rho_{water} * C_{D,cu} * A_{cu} * \bar{U}_{cu} * \dot{x} \tag{3.10}$$

The current force coefficient is given in the following equation:

$$c_{cu} = \frac{1}{2}\rho_{water} * C_{D,cu} * A_{cu} \tag{3.11}$$

Wave Forces

The wave forces on a floating vessel is divided into first and second order forces. The first order forces are linear wave-structure forces, and can be solved by dividing the wave-structure problem into two loads:

- Wave excitation loads - Are the forces and moments on the floating vessel when it is restrained from oscillating and is exposed to incident regular waves. The hydrodynamic loads consists of the Froude-Kriloff and diffraction forces.
- Wave radiation loads - Are the forces and moments on the vessel when its free to oscillate in all six degree of freedom, and there are no incident waves present. The hydrodynamic loads consists of added mass, damping and restoring terms.

These forces describes the total first order linear forces on a floating vessel, and represents the WF forces. The second order non-linear forces results in mean, HF and LF forces. These forces are very important in mooring design, as mentioned earlier. The second order wave drift force is given by the following equation:

$$\bar{F}_{wf} = 2 * \int_{\infty}^{\infty} S_{\eta}(\omega) * C_{wd}(\omega) d\omega \tag{3.12}$$

,where S_{η} and C_{wd} is the wave spectrum and wave drift force coefficient, respectively, Larsen (2017).

The inertia, damping and stiffness forces of the system are of great importance, because they decide the vessel's motion response. These will be studied in the following sections.

3.2.2 Restoring forces - Stiffness

This subsection is based on the references Larsen (2017), Larsen (2015a), Faltinsen (1990) and Larsen (2015c).

The system's restoring force comes from the stiffness of the mooring lines. The stiffness properties of a mooring line can be categorized into two:

1) Geometric stiffness

2) Elastic stiffness

The total stiffness of a system is given as a combination of both geometric and elastic

stiffness:

$$\frac{1}{k_T} = \frac{1}{k_G} + \frac{1}{k_E} \tag{3.13}$$

Figure 3.4 shows for what frequency region the stiffness forces are dominating, and the system is stiffness dominated when the load frequency is lower than the natural frequency. The excitation loads in this region are balanced by the stiffness forces of the system.

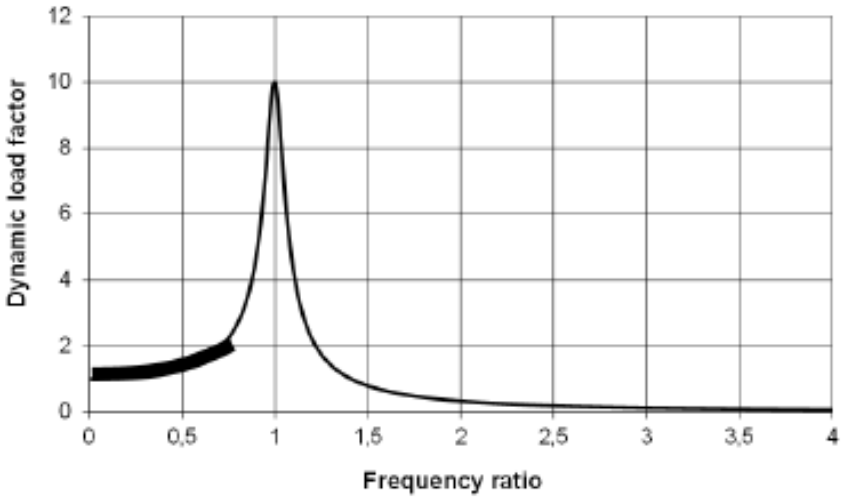

Figure 3.4: Stiffness dominated system, Larsen (2015a).

Geometric Stiffness

The geometric stiffness occurs due to the change in geometry of the mooring line, and is most important for a catenary system with steel and chain lines. The stiffness is mainly provided from the large line weight or by adding clump weights. Figure 3.5 shows the equilibrium position of a catenary system. When the environment excites vessel motions, it is the weight of the line that provides the restoring force. By using the notation in Figure 3.5, the mooring system's restoring force is found from the moment equilibrium of the line and is expressed as:

$$F_h = \frac{W_w * a}{D} \tag{3.14}$$

, where F_h, W_w, a and D is the restoring force, line weight in water, weight moment

arm and the water depth, respectively. It is noteworthy that the relation between restoring force and offset is non-linear.

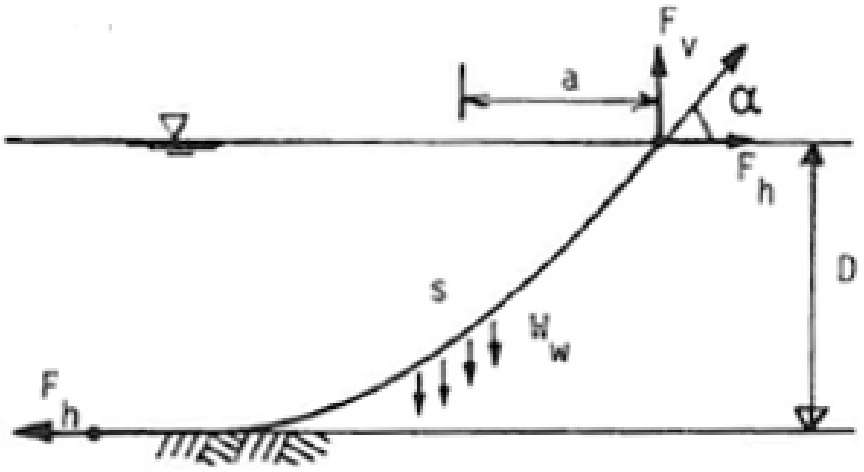

Figure 3.5: Catenary mooring system, Larsen (2017).

The FPSO which is studied in this thesis has a catenary mooring system with a chain-steel line combination. In this case, it is the geometric stiffness that will dominate the restoring force.

Elastic Stiffness

Elastic stiffness is important for taut systems with polyester lines. This stiffness is provided from the elastic elongation of the line. Figure 3.6 shows the equilibrium position of a typical taut moored floating vessel. When vessel motions are excited, the line elongates and the line tension and vessel offset is increasing. The restoring force is found from the moment equilibrium of the line, and is given as:

$$F_h = \frac{F_v * a}{D} \tag{3.15}$$

, where F_h, F_v, a and D is the restoring force, vertical force, horizontal distance from the vessel to the anchor and the water depth, respectively.

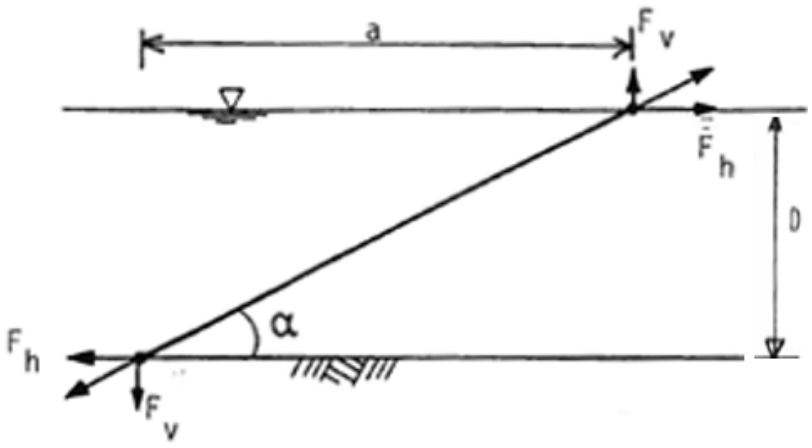

Figure 3.6: Taut mooring system, Larsen (2017).

Static Equilibrium of a Mooring Line

The following figure shows the forces acting on a two-dimensional mooring line with zero bending stiffness. The bending stiffness is neglected for chain mooring lines and wires with large radius of curvature. The line's dynamic effects are also neglected.

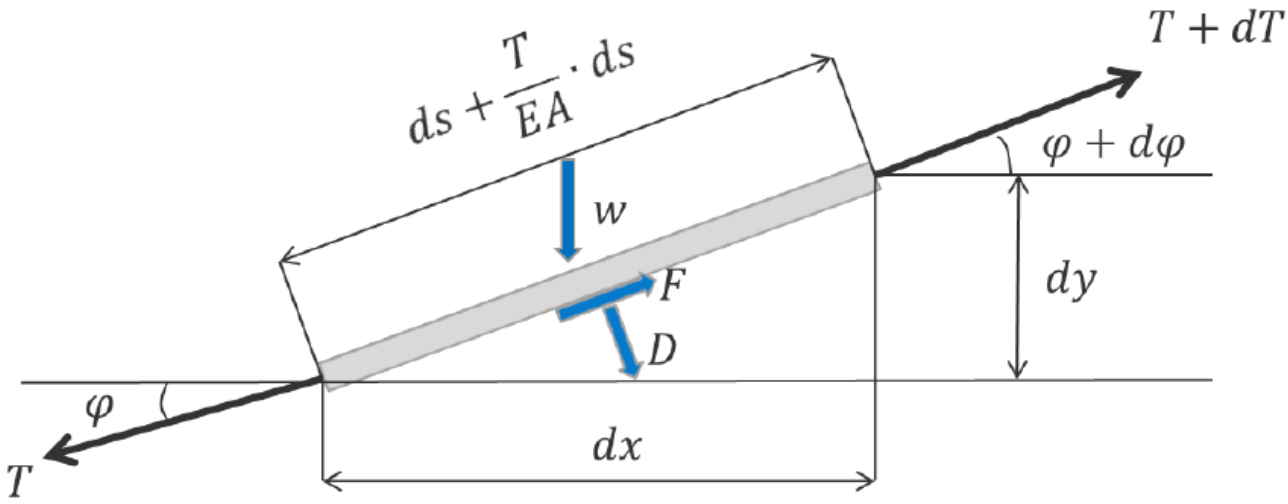

Figure 3.7: Forces acting on a two-dimensional mooring line with zero bending stiffness, Larsen (2015c).

EA, w, T, ϕ, F and D represents the axial stiffness, unit weight in water, tension force, mooring line angle with respect to the x-direction, and the external current forces

in the tangential and normal direction. When decomposing the forces acting on the mooring line into tangential and normal components the equations become:

$$dT = [w * sin\phi - F(1 + \frac{T}{EA})] * ds \tag{3.16}$$

$$T * d\phi = [w * cos\phi + D(1 + \frac{T}{EA})] * ds \tag{3.17}$$

"These equations are non-linear and it is in general not possible to find an explicit solution", Faltinsen (1990). In some locations the current forces are close to zero and can be neglected, thus the equations can be simplified. The normal or radial tension is much smaller than the axial stiffness and the term T/EA can be neglected in equation . The elasticity forces in catenary mooring lines are neglected, cause these lines are considered inelastic. The catenary lines can be described by the catenary equations and is more closely described in the next section.

Catenary Equations for an Inelastic Mooring Line

The catenary equations are derived from equation 3.2.2 and 3.16. The line characteristic is an expression that is frequently used in mooring design. It is the relation between the top pre-tension and the horizontal offset of the floater. The following figure shows the notation that is used in defining the line characteristic of a catenary mooring line.

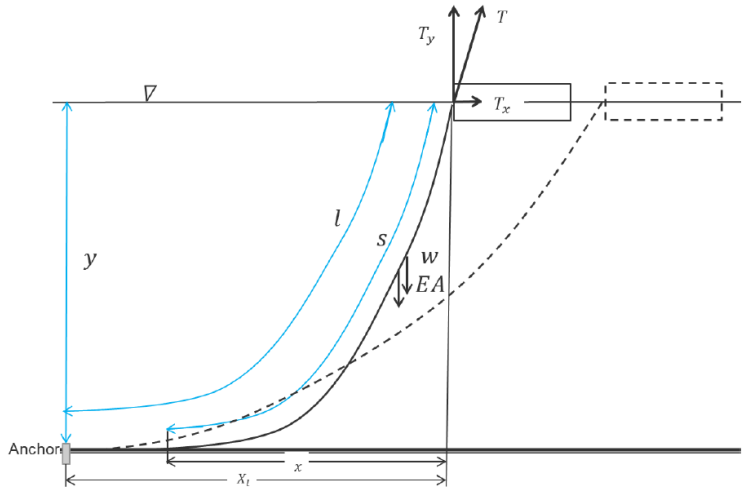

Figure 3.8: The notation that defines the line characteristics of a catenary mooring line, Larsen (2015c).

The horizontal distance between the vessel and the anchor (X_l) is often known, and then it is interesting to find the top end horizontal tension. The following equation expresses the horizontal offset of the floater as a function of the horizontal tension of the mooring line. The equation is called the line characteristic. It is derived from equation 3.2.2 and 3.16, and is applicable for inelastic mooring lines:

$$X_l = l + \frac{T_x}{w} * cosh^{-1}(1 + \frac{wy}{T_x}) - \sqrt{y * (y + \frac{2T_x}{w})} \tag{3.18}$$

Where X_l, l, w, y and T_x are the distance from the vessel to the anchor, length of the line, line unit weight, water depth and the horizontal top tension, respectively. It is also interesting to know the distance from the vessel to where the anchor hits the ground, also called the touch down point (TDP) and is expressed as:

$$x = \frac{T_x}{w} * ln[1 + \frac{wy}{T_x} + \sqrt{(1 + \frac{wy}{T_x})^2 - 1}] \tag{3.19}$$

The equations for the line characteristic and TDP for an elastic mooring line are however quite different, because the elasticity effects must be included. The equations for an elastic mooring line will be described in the next section.

Equations for an Elastic Mooring Line

For taut mooring systems with long elastic lines in high tension levels, the elasticity forces must be included in the two-dimensional mooring equations. The distance between the TDP and the floating vessel for an elastic mooring is now expressed as:

$$x = \frac{T_x}{w} * sinh^{-1}(\frac{T_y}{T_x}) + \frac{T_x * T_y}{w * EA} \tag{3.20}$$

The line characteristic of an elastic mooring line is given as:

$$X_l = (l_0 - \frac{T_y}{w}) * (1 + \frac{T_x}{EA}) + x \tag{3.21}$$

The horizontal top tension is expressed by the following equation:

$$T_x = EA * [\sqrt{(\frac{T}{EA} + 1)^2 - \frac{2wy}{EA}} - 1] \tag{3.22}$$

Mooring System's Restoring Forces

The total restoring in a mooring system is the sum of the restoring force and moment from each mooring line in the system. Figure 3.9 shows a sketch of a spread mooring system for a drilling platform. T_{Hi} and ψ are the horizontal line tension and the angle between the anchor line and the x-axis. The system's horizontal forces and yaw moment are given as F_1^M, F_2^M and F_6^M respectively, and is calculated by the following equations:

$$F_1{}^M = \sum_{i=1}^{n} T_{Hi} * cos\psi \tag{3.23}$$

$$F_2^M = \sum_{i=1}^{n} T_{Hi} * sin\psi \tag{3.24}$$

$$F_6^M = \sum_{i=1}^{n} T_{Hi}(x_i * sin\psi - y_i * cos\psi) \tag{3.25}$$

Where i is the mooring line number and n is the number of mooring lines. The system's restoring forces and yaw moment must be able to equalize the environmental excitation loads to maintain positioning.

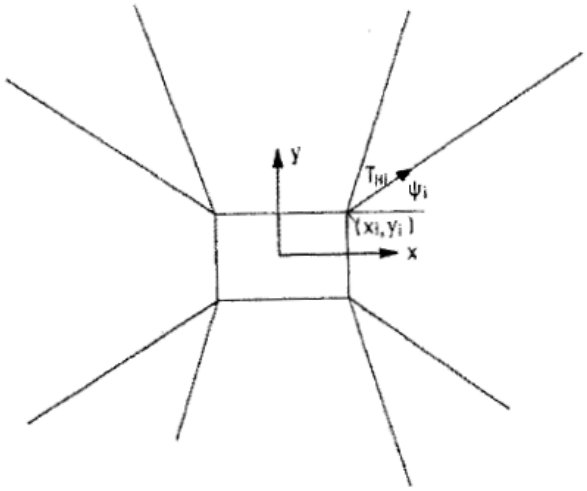

Figure 3.9: Spread mooring system, Faltinsen (1990).

3.2.3 Damping Forces

This section is based on the references Faltinsen (1990), Larsen (2017) and Larsen (2015a).

The damping forces removes energy from the system and reduces the moored vessel's response. Damping is especially important in resonance where the vessel's response is largest, as shown in Figure 3.3. It was shown earlier in Table 3.2, that the natural periods in surge, sway and yaw are large. Hence it is important to provide sufficient damping to reduce the resonant response due to the LF loads from waves, wind and current. The most important LF damping forces for a moored FPSO are the:

- Viscous loads - due to the skin friction and bilge keel effects. The damping from skin friction is very small in comparison with the eddy-making damping from the bilge keels.
- Wave drift damping - the waves provides damping to the vessel, which can be observed by performing a free-decay ship model test in calm water and regular waves.
- Drag forces on the mooring lines and risers - WF loads excites vessel motions, which excites dynamic line and riser motion. Damping occurs from the drag forces due to the dynamic line and riser motions.
- Wave radiation damping - the WF wave loads excite vessel motion, however the vessel generates waves and dampens the vessel's WF motions.
- Wind and current damping - when the wind and current are in contact with the vessel, drag forces occur and LF damping is provided.
- Thrust damping - damping is provided by using automatic thrusters that reduces the vessel motions.

The figure below shows the resonance region where the motion response is at its largest. Here it is very important to provide sufficient damping to balance the excitation loads.

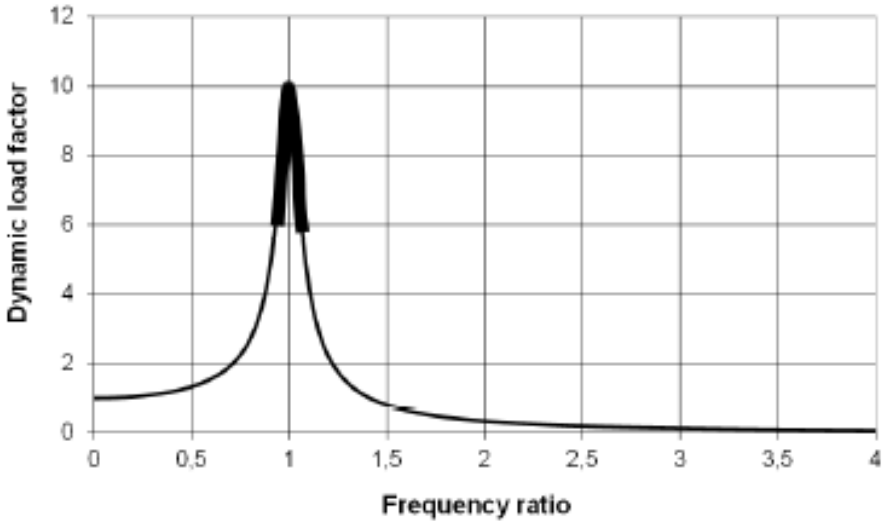

Figure 3.10: The resonance region, Larsen (2015a).

3.2.4 Inertia Forces

This section is based on the references Larsen (2015a) and Larsen (2017).

The system's inertia forces consists of the vessel's mass and added mass which are proportional to the vessel's acceleration. As shown in Figure 3.11, the inertia forces are dominating for load frequencies larger than the natural frequency. This means that the excitation loads in this region are balanced by the inertia forces.

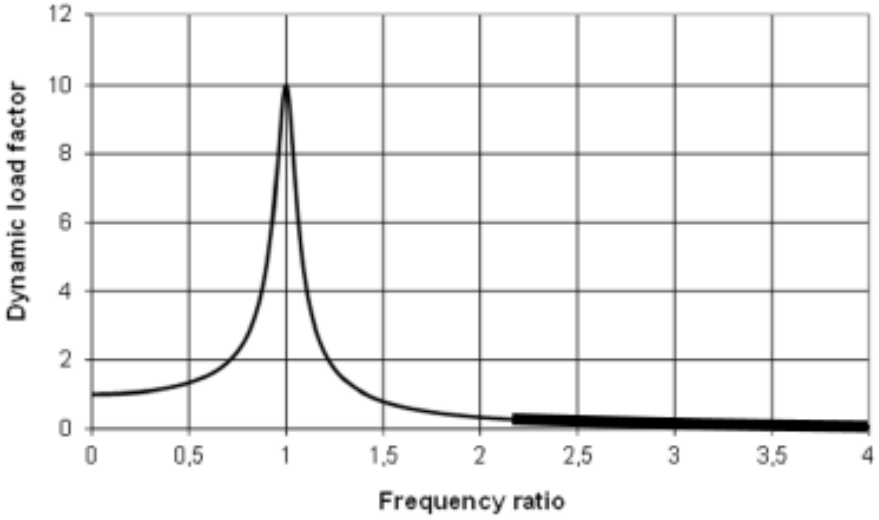

Figure 3.11: Inertia dominated system, Larsen (2015a).

3.3 Time Domain Analysis Methods

This section is based on the references Larsen (2017), ISO (2013), DNV (2013), H. Ormberg (1998) and Klingan (2016).

A time realization of the response of a floating vessel is called a time domain simulation, and is found by numerical integration of the equation of motion in all the degrees of freedom. For this realization, the vessel's response will vary a lot about its expected value, thus the standard deviation will be large. This means that only one realization is not sufficient to provide good response statistics. Several time domain simulations are necessary, and the data from all the simulations can be used to calculate the extreme response statistics. However, it is important that the simulations are long enough to obtain stable statistical properties. According to Section 2.2.9 in the DNV Offshore Standards, DNV (2013) the required simulation length for recording extreme response in a time domain analysis is three hours.

In a time domain analysis, the combined mean, low frequency and wave frequency motions of the vessel are simulated simultaneously. The environmental forces included in the time domain approach, are the mean, wave- and low frequent forces. The behaviour of the vessel, mooring lines and risers (if any) will be described in a time domain analysis. However, how well their behavior is described is dependent on the time domain analysis approach, and there are two different approaches of performing a time domain analysis: separated and coupled approach. These methods will be described in the next sections.

3.3.1 Separated Approach

This section is based on the references H. Ormberg (1998) and Klingan (2016).

The separated approach for a moored vessel is divided into two steps:

1) Vessel motion analysis

2) Dynamic mooring analysis

Step one simulates the top end motion response of a floating vessel (WF and LF motions). The vessel's top end motion due to the dynamic behavior of the mooring lines, is however not simulated and is either neglected or implemented into the model. In the separated approach two simplifications are implemented into the model to describe the vessel's top end motions due to the dynamic behavior of the mooring lines:

a) Additional linear damping forces are implemented to the vessel to account for the damping forces provided by the mooring lines.

b) Additional current forces are implemented to the vessel to account for the current forces acting on the mooring lines that provides stiffness forces to the system.

The additional linear damping and current forces are applied as additional "vessel coefficients", and they must be validated with model tests to ensure correct values. In step two a dynamic mooring analysis is performed with the vessel's top end motions calculated in step one as input.

The shortcomings of this approach are that:

1) The damping effect from the mooring lines must be simplified by additional linear damping forces acting on the floater, which is quite complex to calculate due to the number of parameters that are involved. This requires comprehensive computer power.

2) The mean current loads on mooring lines in deep water are usually not considered which leads to inaccuracies of the stiffness forces to the system, and thus incorrect mean offset. If the mean current loads are included as an additional current force on the vessel, the mean offset will be correct but the mean horizontal forces on the vessel will be incorrect.

This approach is typically used when it is only necessary to investigate one line (which is usually the most loaded one) instead of all the lines. This saves time and computational power but to use this approach, the vessel coefficients must be known and as mentioned it requires comprehensive calculations to find these.

3.3.2 Coupled Approach

This section is based on the references H. Ormberg (1998) and Klingan (2016).

It is called the coupled approach, because the simulation of the vessel's top end motions and the total behavior of the mooring lines are coupled. This means that both the vessel's motions and the mooring line behavior is simulated simultaneously. The coupled approach considers the dynamic behavior of the mooring lines, which will affect the vessel's motion and line tension response. In a coupled approach every force contribution in the equation of motion is solved and accounted for in the time domain.

3.4 Sway-Yaw Stability

This section is based on the reference Larsen (2014b).

The weathervaning ability is a very important property of any turret moored vessel, and there are two motions that contributes to this ability: yaw and sway motions. When the vessel is exposed to wave, wind and current forces it is forced to yaw about the turret in the direction of the environment. However, an opposing moment occur due to the vessel's sway motions. The opposing moment is dependent on the distance between the turret and the COG, which is the "arm" for the sway forces. The total moment about the turret (M_T) is given by the following equation:

$$M_T = M_Z - F_y * x_{GT} \tag{3.26}$$

Where M_Z, F_Y and x_{GT} are the yaw moment, sway force and distance between the COG and turret. The opposing sway moment needs to be larger than the yaw moment for the vessel to be able to weathervane, hence the static sway-yaw stability requirement:

$$\frac{dM_z}{d\psi} + x_{GT}\frac{dF_{sway}}{d\psi} < 0 \tag{3.27}$$

Where $\mathrm{d}M_z/\mathrm{d}\psi$ and $dF_{sway}/\mathrm{d}\psi$ are the change in yaw moment and sway force with respect to change in weather heading. The sway and yaw moments are illustrated in Figure 3.12.

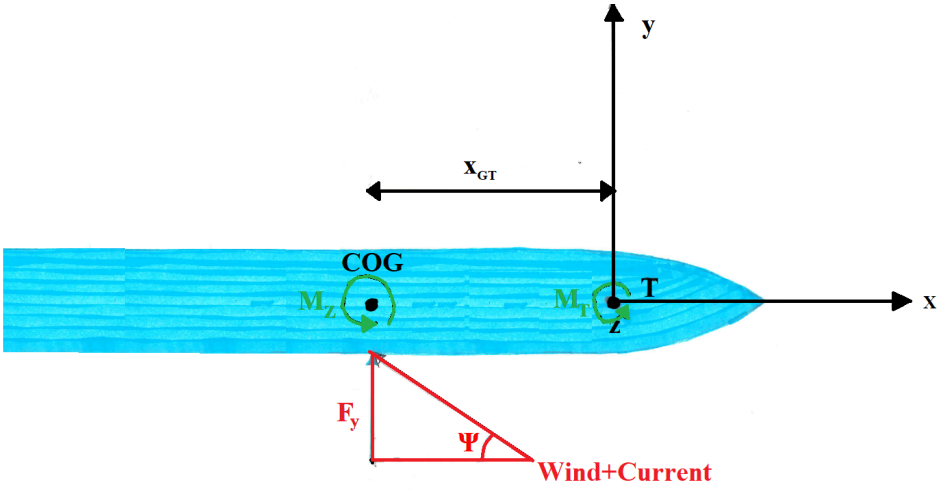

Figure 3.12: Illustration showing the weather moment contributions about the turret.

The positive moment directions are defined as the counterclockwise direction along the axis'. This is shown in Figure 3.13 and is used in the simple sway-yaw stability calculations in section 4.4.

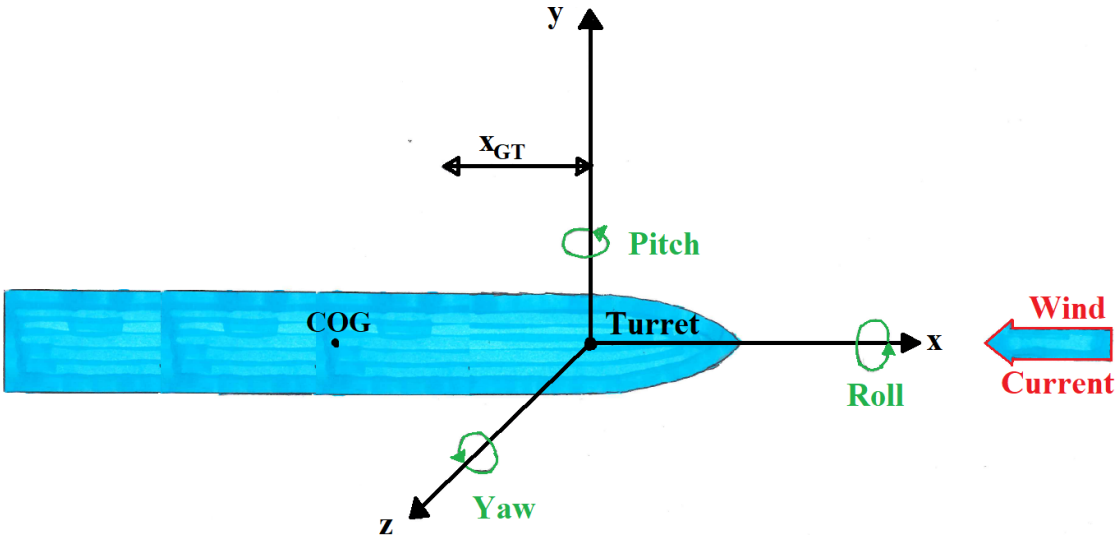

Figure 3.13: An illsustration of the positive moment directions

The modeled FPSO have wind and current force coefficients that describes the wind and current effects on the vessel, in all deegrees of freedom (dof) and in different weather directions. These coefficients have been scaled from wind tunnel tests and are given in Appendix B. When studying the vessel's weathervaning ability, it is important to consider the environmental contributions from waves, wind and current.

However, it is difficult to assess the wave drift forces because it requires integrating over the wave spectrum and the frequency dependent wave drift coefficient, thus for simplicity the wave forces is assumed to have the same values as the wind forces in the simple sway-yaw stability calculations in section 4.4. The weather forces are proportional to the velocity squared, and the total moment (M_T) about the turret is given as:

$$\begin{aligned} M_T &= M_{yaw} - M_{sway} = M_Z - F_y * x_{GT} \\ &= V_{cu}^2(C_{yaw,\psi}^{cu} - x_{GT} * C_{sway,\psi}^{cu}) + V_{wi}^2(C_{yaw,\psi}^{wi} - x_{GT} * C_{sway,\psi}^{wi}) \end{aligned} \tag{3.28}$$

Where M_{yaw} and M_{sway} are the total yaw- and sway moment due to current and wind loads, $C_{yaw,\psi}^{cu}$ and $C_{sway,\psi}^{cu}$ are the yaw and sway current coefficients, $C_{yaw,\psi}^{wi}$ and $C_{sway,\psi}^{wi}$ are the yaw and sway wind coefficients. V_{cu} and V_{wi} are the current and wind speed.

3.5 Damped System Calculations

This section is based on the reference Larsen (2015a), and the calculation of the natural period, damping ratio, critical- and actual damping from a damped system will be described.

The damped natural period (T_d) is found by taking the difference between two damped peaks in the oscillating sample, and is expressed as:

$$T_d = \frac{2\pi}{\omega_d} \tag{3.29}$$

Where ω_d is the damped natural frequency of the system. The logarithmic decrement (Λ) is the ratio between two damped peaks, and is used to find the damping ratio of the system. The damping ratio is the ratio between actual- and critical damping:

$$\Lambda = \frac{1}{n} * ln(\frac{u_i}{u_{i+1}}) \tag{3.30}$$

Where u_i and u_{i+1} are the amplitudes of the peaks, and n is the number of amplitudes between the peaks. As the logarithmic decrement is known, the damping ratio (ξ) can

be calculated by the following equation:

$$\xi = \frac{Actualdamping}{Criticaldamping} = \frac{1}{\sqrt{1+(\frac{2\pi}{\Lambda})^2}} \tag{3.31}$$

The natural frequency (ω_n) of the system is described by:

$$\omega_n = \frac{\omega_d}{\sqrt{1-\xi^2}} = \frac{\frac{2\pi}{T_d}}{\sqrt{1-\xi^2}} \tag{3.32}$$

The natural period can also be calculated by the following equation:

$$T_n = 2\pi\sqrt{\frac{M+A(\omega)}{K(r)}} \tag{3.33}$$

Where M, A(ω) and K(r) is the mass, added mass and stiffness of the system.

As the natural frequency is known the system's critical damping (C_c) is calculated by:

$$C_c = 2m\omega_n \tag{3.34}$$

Where m is the system's mass. For a FPSO m will be the mass and added mass of the vessel. As the critical damping is known, the actual damping (C) can be calculated from equation 3.31. An illustration of a damped system is shown in Figure 3.14.

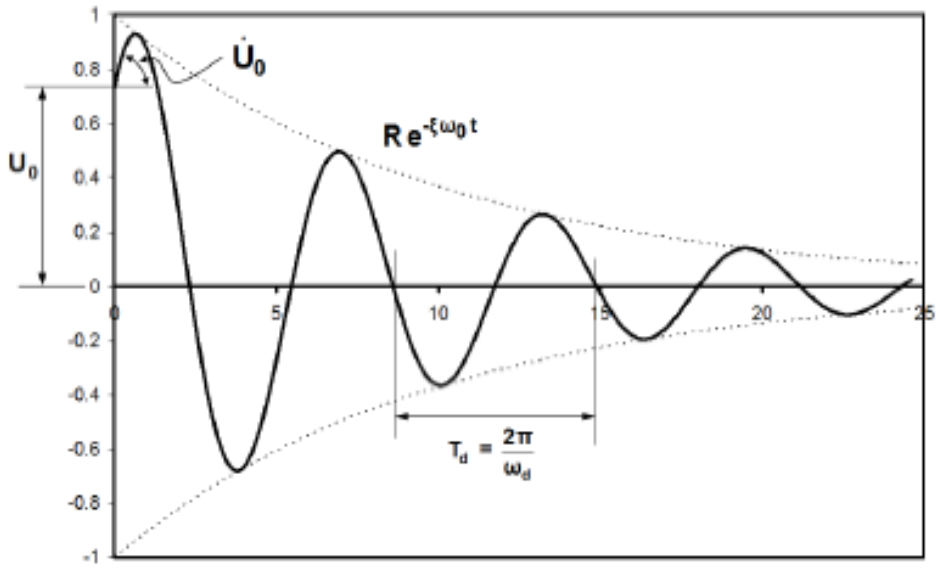

Figure 3.14: Free oscillation of sub-critically damped system, Larsen (2015a).

3.6 Dynamic Equilibrium of a Turret

This section is based on the reference Larsen (2014a).

The dynamic forces and moments from the mooring lines, dynamic pressure from the waves, and the turret's weight and inertia, are absorbed by boogies and radial wheels located around the turret. The boogies and radial wheels are supports that absorb the vertical and the horizontal forces that occur in the turret, respectively. The turret's weight rests on the boogies, thus both the moments and vertical forces are absorbed by these. Figure 3.15 shows a simple description of the turret supports and the forces and moments.

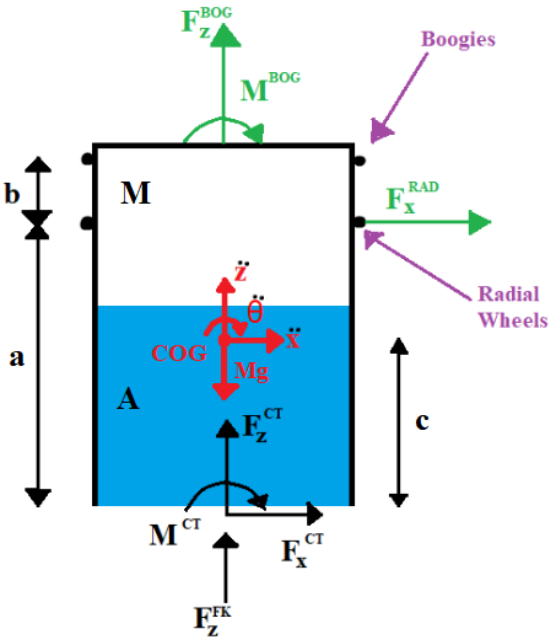

Figure 3.15: Illustration of the turret and its forces and moments

By decomposing the forces in x- and z-direction and by taking the moment about the $COG_{T.W.}$ (COG of the turret with entrapped water), three easy equations of equilibrium can be made to express the total forces and moments in the turret's boogies and radial wheels. These are given as:

$$\begin{aligned} \sum F_x = ma \Longrightarrow & F_x^{CT} + F_x^{RAD} + Mg * sin\theta = (M+A)\ddot{x} \\ & F_x^{RAD} = (M+A)\ddot{x} - F_x^{CT} - Mg * sin\theta \end{aligned} \tag{3.35}$$

$$\begin{aligned} \sum F_z = ma \Longrightarrow & F_z^{CT} + F_z^{BOG} + F_z^{FK} - Mg * cos\theta = (M+A)\ddot{z} \\ & F_z^{BOG} = (M+A)\ddot{z} + Mg * cos\theta - F_z^{CT} \end{aligned} \tag{3.36}$$

$$\begin{aligned} \sum M_{COG} = Ia_\theta \Longrightarrow & M^{CT} + M^{BOG} - F_x^{CT} * c + F_x^{RAD} * (a-c) = I_\theta \ddot{\theta} \\ & M^{BOG} = I_\theta \ddot{\theta} + F_x^{CT} * c - F_x^{RAD} * (a-c) - M^{CT} \end{aligned} \tag{3.37}$$

A more detailed description of the notation is written in the Nomenclature. These

simple but important equations will be used to calculate the force and moment time series in the boogies and radial wheels. The equations will be simplified by neglecting the dynamic pressure and the mooring moment at the top end fixing point. The former force contribution is neglected because these pressure forces are small in comparison with the other forces. The mooring moment at the fixing point is equal to zero because all mooring lines are connected to the same top end point, which will result in no moment arm. This will be more closely described in section 4.1.4.

3.6.1 Turret Up-Lift

Figure 3.16 shows an illustration of a turret that experience uplift. The turret lies on several boogies, and the turret gravity force prevents the turret from lifting. In extreme weather conditions the boogies experience a varying vertical force and moment, which in combination can get larger than the turret gravity force and uplift occur. The turret is a critical component in both the mooring and oil&gas production, and a turret uplift will destroy components that processes oil and gas. The FPSO and turret must thus be designed to prevent uplift.

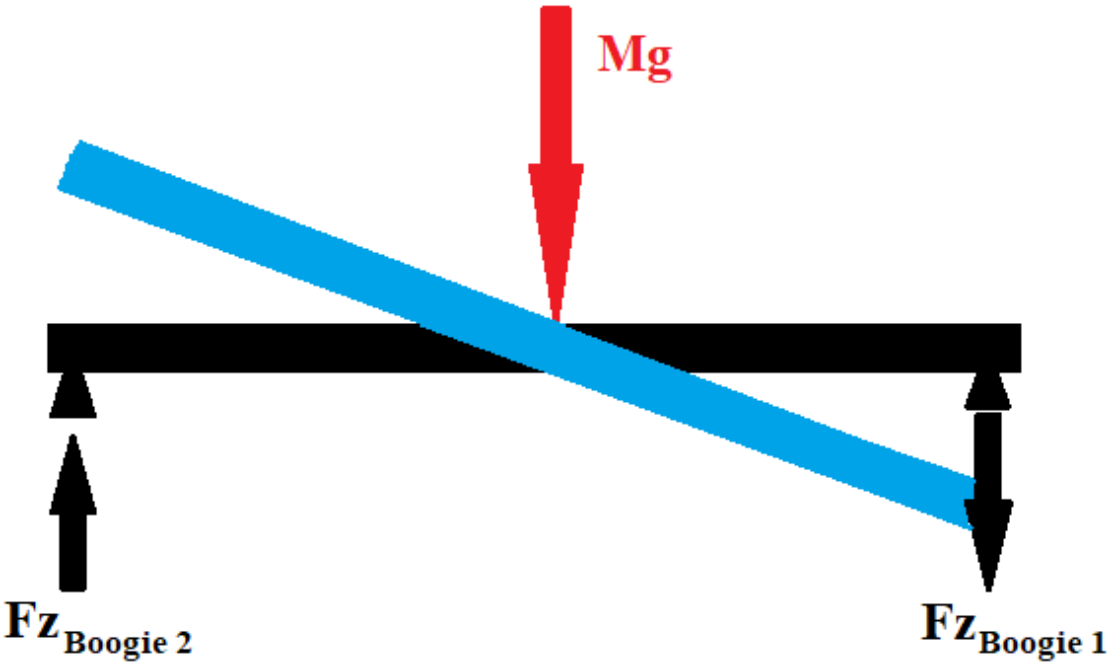

Figure 3.16: Illustration of the turret uplift.

3.7 Probability Distributions

This section will provide basic knowledge about the probability distribution of wave processes, and is based on the reference Tor Vinje (2004) and Leira (2010). In this thesis the focus will be around the Gumbel probability density function, because this is a good distribution to describe the extreme loads that occur in the mooring lines and the turret, which are to be investigated.

A wave process is irregular/random (stochastic) and it is hard to predict. By making certain assumptions it is possible to make a probability density function (pdf) for the wave elevation, thus it is possible to predict the wave elevation. The assumptions states that the surface elevation is a stationary, narrow banded and normally distributed stochastic process. This means that the mean and variance of the surface elevation is constant (where the mean is zero), the incoming wave frequencies are within a narrow interval of frequencies (which practically means that the incoming waves have approximately the same frequency), and that the wave elevation will be equally distributed over and under the mean surface. Such a wave process is showed in Figure 3.17. The figure also shows the peaks and the extreme peak in the time serie.

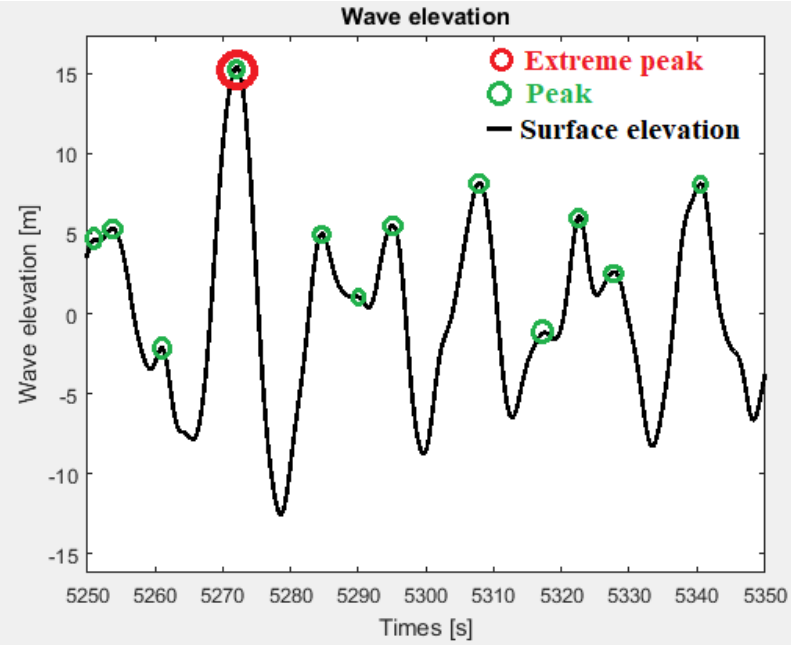

Figure 3.17: Time serie of the wave elevation in ULS weather conditions taken from Sima.

Based on the assumptions stated above, the surface elevation can be described and

predicted by a Gaussian pdf. It is also useful to describe the peaks or the wave amplitudes of a wave process. Based on the assumption that each wave is stationary, statistically independent and normally distributed, the wave amplitudes can be described by a Rayleigh distribution.

In each time serie there exist one maximum or extreme wave amplitude. By performing N number of simulations or measurements there exist N number of maximum/extreme wave amplitudes. By satisfying the assumptions for the Gaussian and Rayleigh distribution, Gumbel's probability density function can be used to indicate the most probable extreme wave amplitude. The Gaussian, Rayleigh and Gumbel probability density function is showed in Figure 3.18.

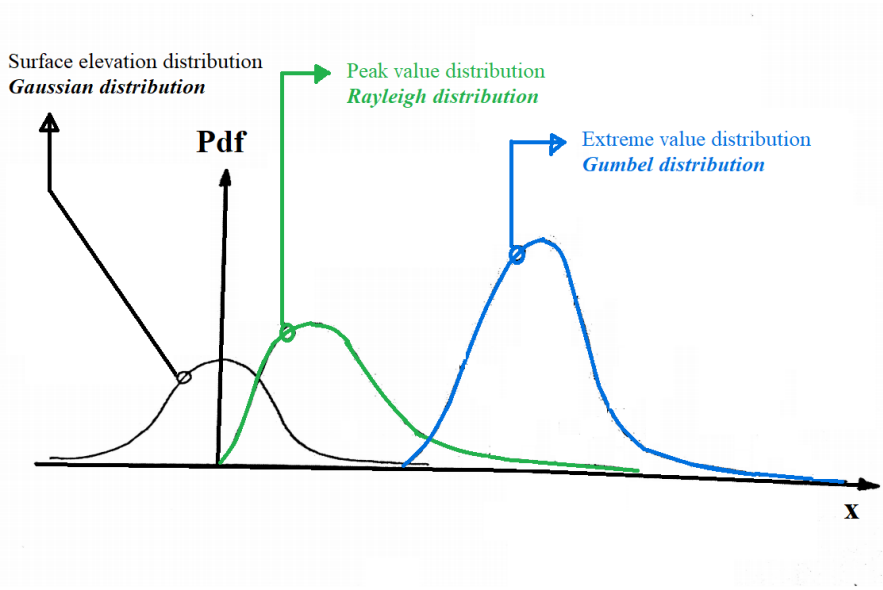

Figure 3.18: Probability density function of the surface elevation, peaks and the extreme/maximum peaks from N time series.

Gumbel's probability density function gives an indication of the most expected extreme value and is expressed as:

$$f(x) = \frac{1}{\beta} e^{-(\frac{x-u}{\beta} + e^{-(\frac{x-u}{\beta})})} \tag{3.38}$$

, while the Gumbel cumulative density function shows the probability of X to be less or equal to a value of X:

$$F(x) = e^{-e^{(\frac{x-u}{\beta})}} \tag{3.39}$$

Where β and u are moment estimators and these are given as:

$$\beta = \frac{\sigma * \sqrt{6}}{\pi} \tag{3.40}$$

$$u = \mu - \beta * \gamma \tag{3.41}$$

Where $\sigma$and μ are the variance and mean respectively, which are calculated from the sample of extreme values. γ is the Euler-Mascheroni constant.

The Gumbel distribution is not only used to describe extreme wave heights, but also extreme responses, and to find the characteristic design response. The characteristic design response of the vessel's horizontal offset and the line tension is given as the most probable maximum (MPM), while the characteristic design loads of the turret is given as the 90% fractile value from the probability distribution. The 90% fractile value corresponds to a probability of exceedance by 10%. These characteristic design responses will be investigated in chapter 7.

3.8 Sima Introduction

This section is based on the references Larsen (2017), ISO (2013), Larsen (2015b) and DNV (2017a).

Sima is a module within the Sesam software that can model and simulate marine operations. Within Sima there are two features that are important to know of:

1) Simo - is a tool which performs numerical integrations and simulations of the motions and station keeping behaviour of a floating vessel in the time domain. Simo performs quasi-static analysis which means that top end tension is calculated from the vessel's WF and LF motions, whereas all the six degree of freedom top end motions of a floating vessel is captured. However, if the vessel is moored only the restoring forces from the mooring stiffness is considered in a quasi-static analysis. This means that the mooring lines are thereby only functioning as springs that provide restoring, which means that *"The elastic elongation of the line is determined quasistatically"*, DNV (2017a). Thus the mass forces on the lines are ne-

glected, which in other words means that the dynamic line tension behavior due to added mass and damping of the mooring lines is not considered. "Only the tangential component of the top end motion is assumed to have any effect on the dynamic tension", DNV (2017a). This approach is sufficient when the dynamic behavior of the mooring lines can be neglected. The mooring lines are modelled by the catenary equations and are assumed to form catenaries.

2) Riflex - is another tool which performs a non-linear time domain finite element analysis (FEM) of slender structures. Riflex is used to perform simulations and FEM-analysis of risers and mooring lines, which describes their total static and dynamic behaviour. *"The basic principle in this approach is to accumulate the external loading in a number of small load increments."*, DNV (2017b), and to find the static configuration at each load step by using the displacement from the previous load increment as the initial solution. Riflex performs a step-by-step numerical integration of the dynamic equilibrium equations, which is a proper way to treat the non-linear behaviour according to DNV (2017a).

A Simo-Riflex coupled simulation will describe the fully mooring system behaviour including the vessel's response due to the dynamic motions of the mooring lines. In this thesis, there will be performed modelling of mooring systems and simulations of the turret moored FPSO in Simo and Riflex. The system that is modeled in Riflex describes both the total vessel and mooring line response simultaneously, which means that the model in Riflex is performing Simo-Riflex coupled simulations. From here on and out this thesis, the simulations from the model in Riflex will be called *Riflex* and not *Simo-Riflex coupled*. The results between the model in Simo and Riflex will be compared to investigate the vessel motions and line tension during ultimate and accidental limit state conditions. The vessel's hydrostatic and -dynamic properties is configured in Wamit and is provided by Prof. II Kjell Larsen and Equinor, but the mooring system has been modeled in both Simo and Riflex.

3.8.1 Coordinate Systems

This section is based on the reference DNV (2017a).

Different coordinate systems are used in SIMO and it is important to know the difference between them:

1) Global coordinate system ($_{GL}$) - is a fixed coordinate system in the domain where the vessel's position is referred from.

2) Local coordinate system ($_L$) - is the coordinate system of the FPSO. The coordinate system follows the vessel's motions.

3) Body-related coordinate system ($_R$) - is a local coordinate system that follows the vessel's horizontal motion.

4) Initial coordinate system ($_I$) - is the coordinate system of the vessel's initial position before the simulation starts. This coordinate system remains fixed during the simulation.

The weather direction and mooring line direction in Riflex is always chosen with respect to the global coordinate system. The direction of the mooring lines in SIMO is defined with respect to the initial coordinate system. The global ($_{GL}$), local ($_L$), and initial ($_I$) coordinate systems are illustrated in Figure 3.19.

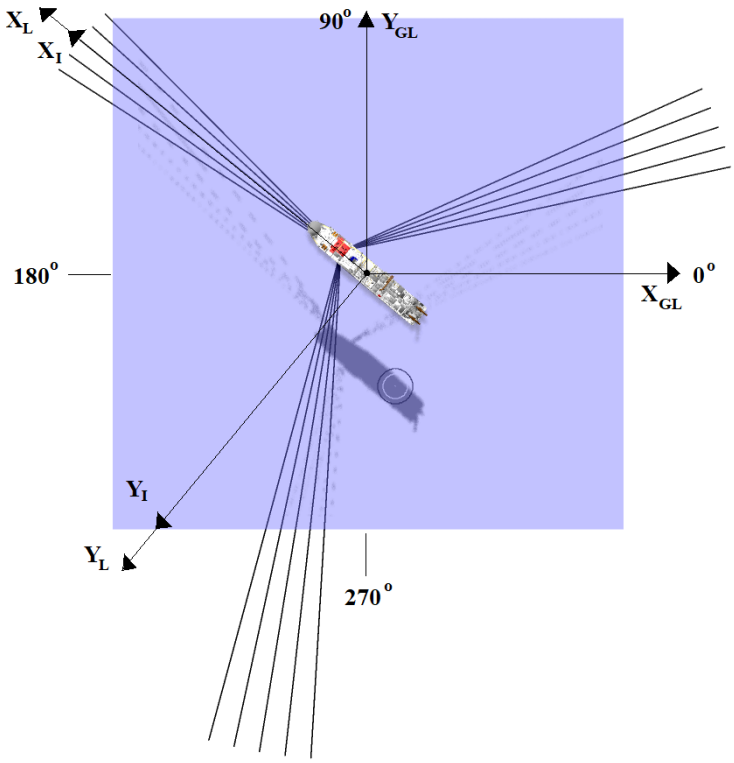

Figure 3.19: An illustration of the global ($_{GL}$), local ($_L$), and initial ($_I$) coordinate systems. The degrees (0, 90, 180 and 270) are with respect to the global coordinate system.

Chapter 4

The FPSO, Mooring System and Environmental Conditions

This chapter will describe and provide the fundamental information about the FPSO's Response Amplitude Operators (RAO), weathervaning abilities, and the mooring system that is to be numerically simulated. The system description of the turret moored FPSO, the vessel's RAOs and the environmental conditions (from a metocean design basis of the field), are provided by Equinor and Prof. II Kjell Larsen.

4.1 System Description

The FPSO is turret moored with 15 lines in total. These lines are divided into three clusters, where there are 5 lines in each cluster. Each cluster got a specific line length and a chain-wire segment configuration, where the pre-tension in all lines are 2097kN. The lines are anchored with suction anchors on the seabed, 371.6 meters below the calm water surface. It is assumed that there are no pipelines on the seabed within the anchoring region.

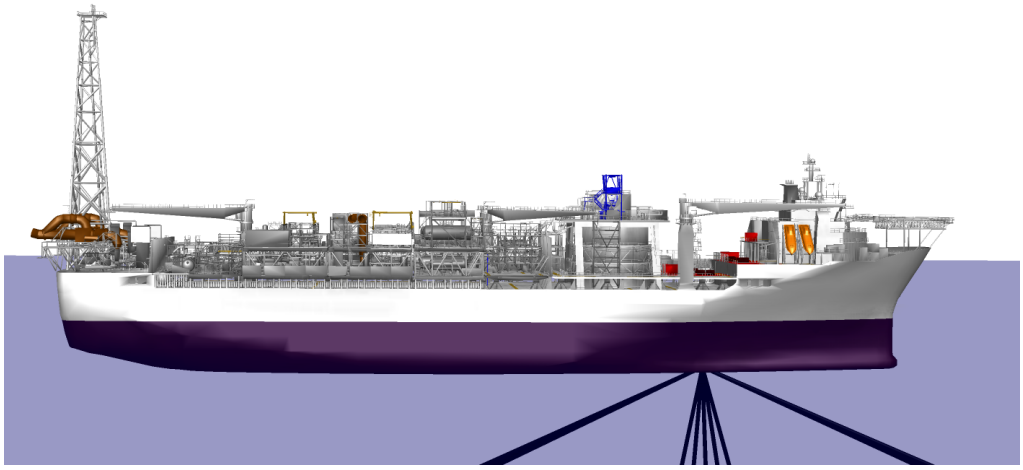

Figure 4.1: Illustration of the example FPSO in Sima

4.1.1 Ship Dimensions

The FPSO's main dimensions and particulars are presented in Table 4.1.

Table 4.1: The main dimensions and particulars of the FPSO.

Parameters	Symbol	Unit	Value
Length between perpendiculars	L_{PP}	m	273.2
Depth	D	m	30.0
Breadth	B	m	54.8
Draft ballast	T_B	m	16.6
Draft full load	T_L	m	21.3
Draft model in SIMA	T_S	m	17.1
Turret Weight	W_{TUR}	tonnes	6 000
Lightship weight	Δ_{LW}	tonnes	91 000
Displacement ballast	Δ_B	tonnes	208 000
Displacement full load	Δ_L	tonnes	273 000
Displacement model in SIMA	Δ_S	tonnes	218 800
Turret location (x,y,z) relative to $_{GL}$	Fairlead	m	(70, 0, -17.1)
Model's center of gravity (x,y,z) relative to $_{GL}$	COG	m	(0, 0, 3.136)

4.1.2 Mooring System

The FPSO is as mentioned earlier turret moored with 15 lines, which are divided into three clusters with 5 lines in each cluster. This configuration makes it possible for the vessel to weathervane while maintaining position keeping and beneficial production. Each cluster have different line lengths and segment configuration of top studless chain, spiral strand steel wire and bottom studless chain. The main characteristics and properties of the three line configurations are given in Table 4.2. The data of the line length, pre-tension, direction and fastening point of every line is given in Table 4.3, and is based on a Mimosa file provided by Prof. II Kjell Larsen and Equinor, which is given in Appendix A. The Mimosa file is based on assessments by Equinor of how long and how large the line length, pre-tension and breaking strength should be. Figure 4.2 shows the turret mooring system of the vessel.

Table 4.2: The main properties of the mooring lines: segment length (l_{seg}), segment diameter (d_{seg}), weight in air (w_{air}), Young's modulus (E) and breaking strength (T^{BS}).

	Cluster 1, Line Longer i				
Line segment	l_{seg} [m]	d_{seg} [m]	w_{air} [kN/m]	E [MPa]	T^{BS} [kN]
R4 studless chain	50	0.17	5.7276	47700	24073
Spiral strand wire	355	0.151	1.11321	20200	22000
R3S studless chain	520	0.17	5.7276	47200	21876
	Cluster 2, Line Long i				
R4 studless chain	50	0.17	5.7276	47700	24073
Spiral strand wire	355	0.151	1.11321	20200	22000
R3S studless chain	420	0.17	5.7276	47200	19592
	Cluster 3, Line Longest i				
R4 studless chain	50	0.17	5.7276	47700	24073
Spiral strand wire	355	0.151	1.11321	20200	22000
R3S studless chain	720	0.17	5.7276	47700	24073

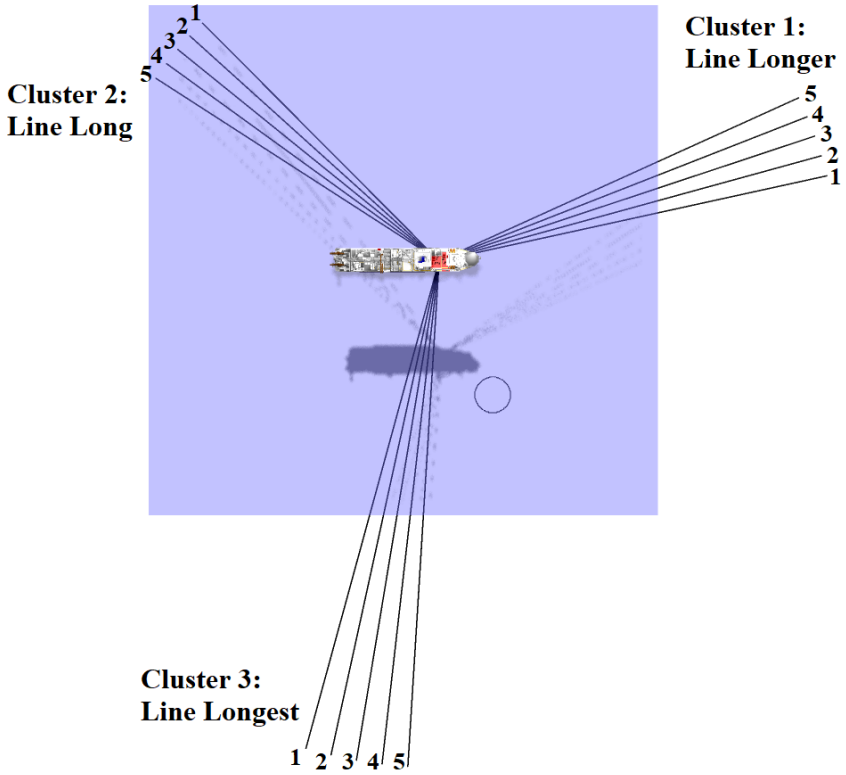

Figure 4.2: Illustration of the mooring line set-up taken from Simo.

Table 4.3: The table shows the line direction (relative to the initial coordinate system), pretension and the fastening point of every line. Table taken from SIMO.

Name	Line Type	Attachment Point	X	Y	Z	Pretension	Direction
Line_Longerr1	Type_longer	Fairlead	70.0	0.0	-17.1	2.097e+06	14.0
Line_Longerr2	Type_longer	Fairlead	70.0	0.0	-17.1	2.097e+06	17.0
Line_Longerr3	Type_longer	Fairlead	70.0	0.0	-17.1	2.097e+06	20.0
Line_Longerr4	Type_longer	Fairlead	70.0	0.0	-17.1	2.097e+06	23.0
Line_Longerr5	Type_longer	Fairlead	70.0	0.0	-17.1	2.097e+06	26.0
Line_Long1	Type_long	Fairlead	70.0	0.0	-17.1	2.097e+06	134.0
Line_Long2	Type_long	Fairlead	70.0	0.0	-17.1	2.097e+06	137.0
Line_Long3	Type_long	Fairlead	70.0	0.0	-17.1	2.097e+06	140.0
Line_Long4	Type_long	Fairlead	70.0	0.0	-17.1	2.097e+06	143.0
Line_Long5	Type_long	Fairlead	70.0	0.0	-17.1	2.097e+06	146.0
Line_Longest1	Type_longest	Fairlead	70.0	0.0	-17.1	2.097e+06	254.0
Line_Longest2	Type_longest	Fairlead	70.0	0.0	-17.1	2.097e+06	257.0
Line_Longest3	Type_longest	Fairlead	70.0	0.0	-17.1	2.097e+06	260.0
Line_Longest4	Type_longest	Fairlead	70.0	0.0	-17.1	2.097e+06	263.0
Line_Longest5	Type_longest	Fairlead	70.0	0.0	-17.1	2.097e+06	266.0

4.1.3 Modeling in Simo

The mooring lines are modeled in Simo by giving them a weight, length, stiffness, pretension and direction. The anchor positions are then found by solving the catenary equations in a static analysis. These anchor positions in Simo are used to define the anchor positions in Riflex. The different calculations methods in Simo and Riflex's static analysis might lead to discrepancy in the line stiffness. This will be more closely discussed in section 6.1.

4.1.4 Modeling in Riflex

As mentioned earlier, Riflex uses the FEM to solve the equation of motion of slender elements, for instance mooring lines. It is thus important to have enough elements in the lines to properly describe their behaviour. However, by increasing the number of elements in the lines, the simulation time also increases because of more nodal point calculations. The elements should be small where the line dynamic behaviour is large so that it can be captured, while large elements where the dynamic behaviour is smaller. As showed in Table 4.2, the mooring lines are divided into three segments: R4 studless chain (top end section), spiral strand wire (mid section) and R3S studless chain (bottom section). The top end and mid section behaviour of the mooring lines are experiencing large dynamic behaviour, and thus the elements here should be smaller than the bottom segment. The mooring lines' are modelled with a top end, mid and bottom section element length of 5.0, 25.5 and 30.0 meters respectively.

Figure 4.3a below shows that all the mooring lines are connected to a joint top end fixing point, which as mentioned in section 3.6 neglects the mooring moment at the fixing point. Figure 4.3b shows that the mooring lines are connected around the turret which is the correct way to model. However, due to numerical difficulties the system was simplified by modeling a joint fixing point as in Figure 4.3a.

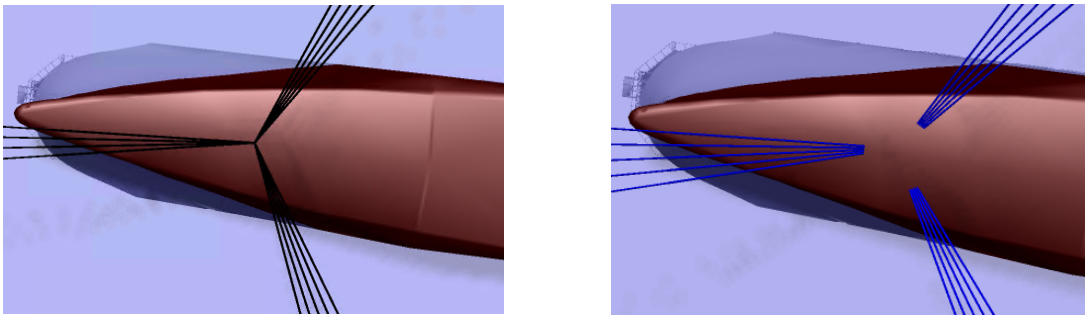

(a) Joint top end fastening *(b) Different top end fastening*

Figure 4.3: The simplified modeling in Riflex (left) and the correct modeling in Riflex (right)

The FPSO with the mooring configuration shown in Table 4.2, Figure 4.2 and Table 4.3, will be analyzed in this thesis using Simo and Riflex.

4.2 Environmental Conditions in the Oil Field.

This section describes the extreme environmental data of the waves, wind and current from the oil field where the FPSO is located. These extreme values will be used in the numerical simulations in Simo and Riflex.

4.2.1 Waves

The waves are generated from the Joint North Sea Wave Project (JONSWAP) double peaked spectrum, and the contour plots of the significant wave height and peak period is showed in Figure 4.4. The largest 100 year return period corresponds to a significant wave height (H_S) of 15.5 meters and a peak period (T_P) of 18.5 seconds. A sensitivity analysis around the peak of the 100 year return period is performed in order to investigate which combination of H_S and T_P that creates the largest tension response. The results will be presented later in this thesis.

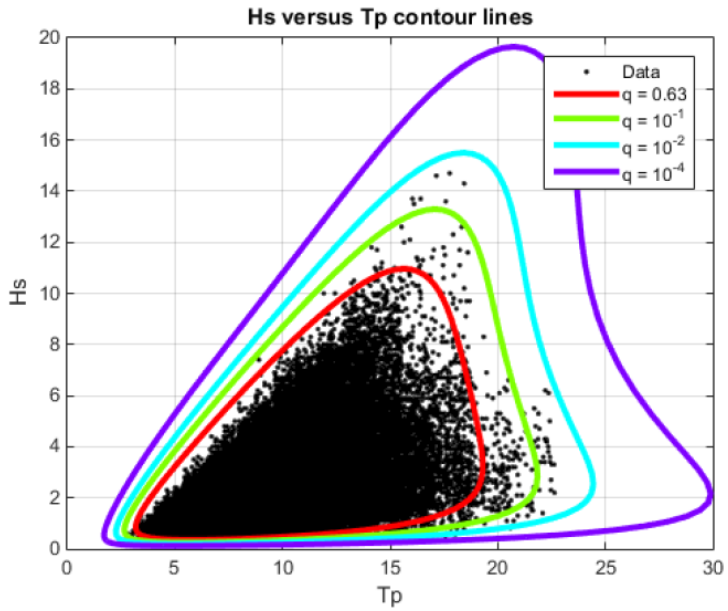

Figure 4.4: Contour plot of the significant H_S and T_P for different values of annual probability of exceedance, where the duration of extreme event is 3 hours.

4.2.2 Wind

The table below shows the oil field's maximum omni directional wind speed, reference height and direction in a 100 year return period. This wind speed will be used in the simulations. The vessel's motion response due to wind is given by the wind coefficients. Due to the vessel's non-symmetric superstructure, the vessel achieves some sway and yaw motions when the wind is propagating towards the bow, which corresponds to wind direction of 180 degrees in the wind coefficients. The sway and yaw motions in 180 degrees are marked with red in wind coefficients attached in Appendix B. Also notice that the wind only excite motion response in surge, sway, roll and yaw.

Table 4.4: The maximum wind speed from a return period of 100 years where the duration of extreme event is 1 hour.

Wind speed [$\frac{m}{s}$]	Reference height [m]	Direction [^{o}]
32.5	10	0-360

4.2.3 Current

The table below shows the oil field's maximum omni directional current speed, reference height and direction in a 10 year return period which will be used in the numerical simulations. The vessel's motion response due to current is similar to the wind given by coefficients, and these can be found in the Appendix B. The vessel below the sea surface is streamlined and symmetric about the longitudinal axis, thus the current coefficients in Appendix B are given in the interval [0 180] degrees. Similar to the wind, the current excite vessel motions in surge, sway, roll and yaw. It is noteworthy that the current excites sway motions when the current is headed towards the bow, which may be a result of unevenly distributed mass in the FPSO. However, the vessel is symmetric thus no yaw motions occur in this current direction.

Table 4.5: The maximum current speed from a return period of 10 years where the duration of extreme event is 10 minutes.

Current speed $[\frac{m}{s}]$	Reference height $[m]$	Direction $[^o]$
1.23	0	0-360

4.3 Motion Response Amplitude Operators

This section will present the surge, sway, heave, roll and pitch RAOs of the unmoored FPSO in regular waves. The RAOs are shown for waves propagating towards the bow (180^o) and starboard or port side (90^o) of the vessel as showed in Figure 4.5. The COG is the reference point in every RAO figure showed in the following sections.

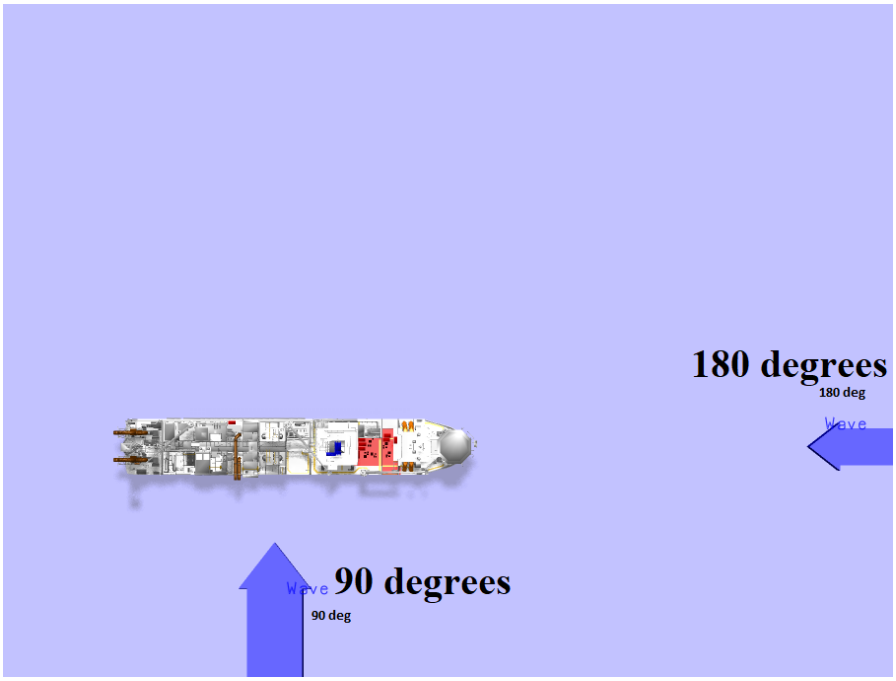

Figure 4.5: The wave direction which the RAO plots are based upon.

4.3.1 Surge

Studying Figure 4.6, the surge motion response decreases at wave periods of 12.5-13 seconds which is a result of cancellation effect when the wavelength is approximately the same as the vessel's length. The vessel's response is then increasing towards a response of 1 where the vessel follow the waves.

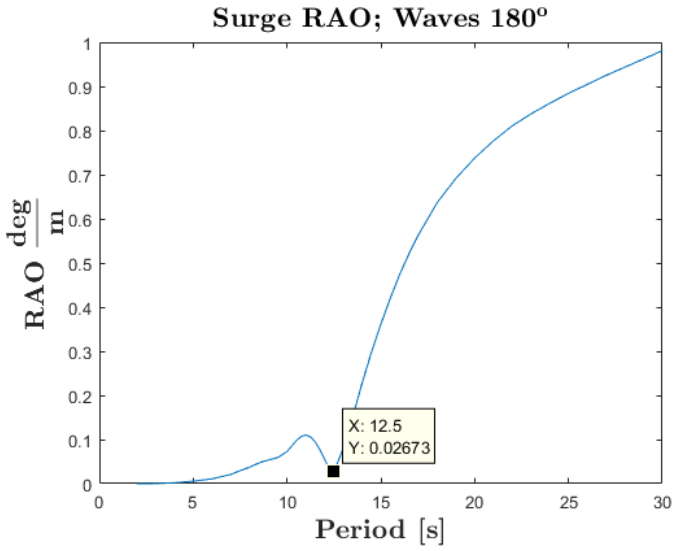

Figure 4.6: Model's surge RAO with incoming wave direction of 180 degrees

No surge motions is expected when waves are coming from a 90^o angle, however due to non-symmetry about the vessel's longitudinal axis, a pressure difference between the fore- and aft of the vessel will occur. A result of this is a surge motion response peak at 11 seconds.

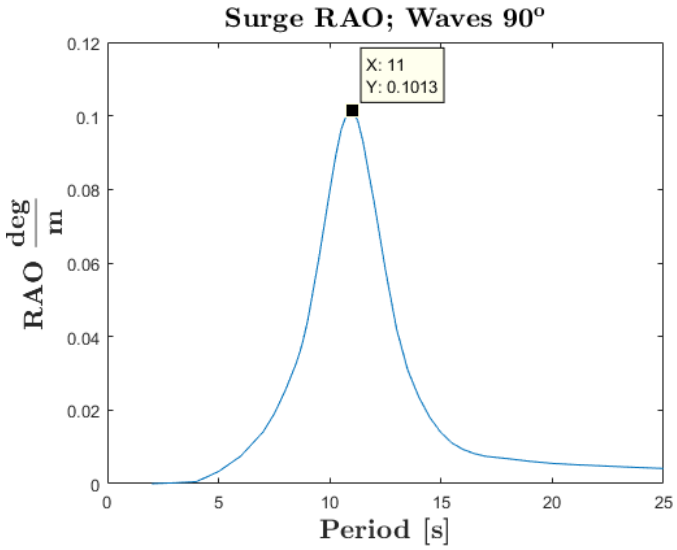

Figure 4.7: Model's surge RAO with incoming wave direction of 90 degrees

4.3.2 Sway

When studying the FPSO's sway motion response in 90^o waves in Figure 4.8, a jump in response occur at wave periods approximately 25.8 seconds. The FPSO achieves a maximum sway response of 1.14 for this wave period. This is a result of a sway-roll coupling effect which is discussed more closely in section 4.3.4. The sway response in head waves (180^o) are however negligible.

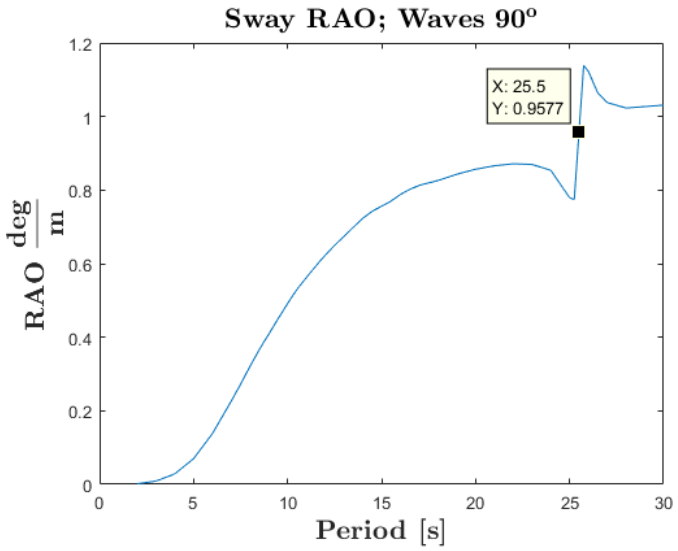

Figure 4.8: Model's sway RAO with incoming wave direction of 90 degrees

4.3.3 Heave

The FPSO's heave motion response in 90^o waves is showed in Figure 4.9. The largest heave response appear for wave periods of 12 seconds, thus the FPSO's natural period in heave is 12 seconds. The vessel have a maximum response of 1.5 in resonance motions. A wave amplitude of 10 meters then corresponds to a heave response of 15 meters.

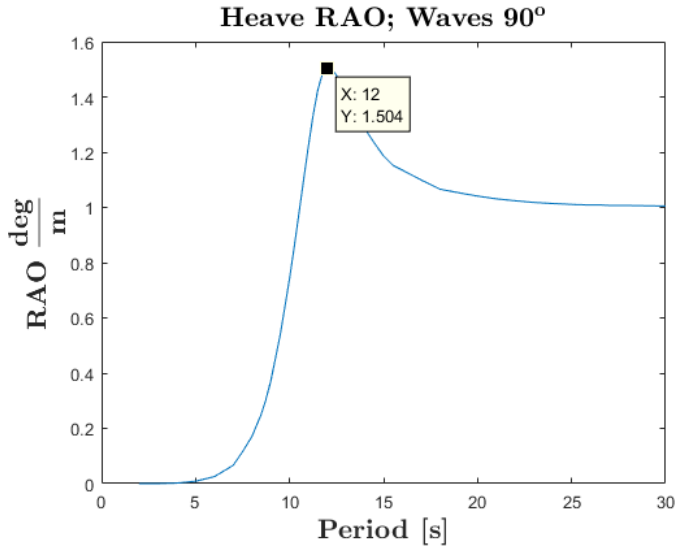

Figure 4.9: Model's heave RAO with incoming wave direction of 90 degrees

The FPSO's length between the perpendiculars is 273.2m. When the wave length equals the vessel's length, the wave period is according to linear wave theory 13.2 seconds, and based on basic ship hydrodynamics, the vessel achieves a smaller motions response due to cancelling wave effects. This is observed in the heave motion response between 11.5 and 13.5 seconds in the figure below.

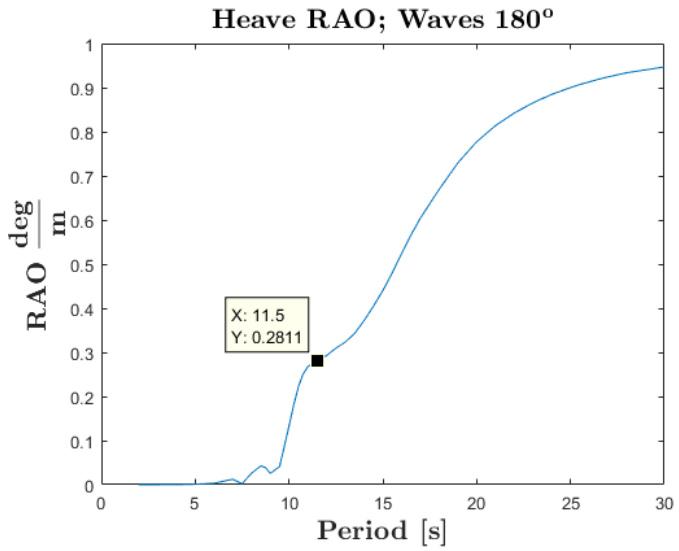

Figure 4.10: Model's heave RAO with incoming wave direction of 180 degrees

4.3.4 Roll

The roll motion for a ship is the most critical degree of freedom with respect to response. Figure 4.11 shows the FPSO's roll motion response in 90^o waves, and the maximum response is 9.9 deg/m at wave period 25.5 seconds. This is the natural period in roll, and a wave amplitude of 2 meters in resonance, will give a roll response of 20^o. This shows how important it is to weathervane the vessel. Recall Figure 4.8, which shows a jump in the sway response at 25.8 seconds. This is due to the resonance motions in roll, which due to coupling excites sway motion. The roll motion in head waves are however negligible

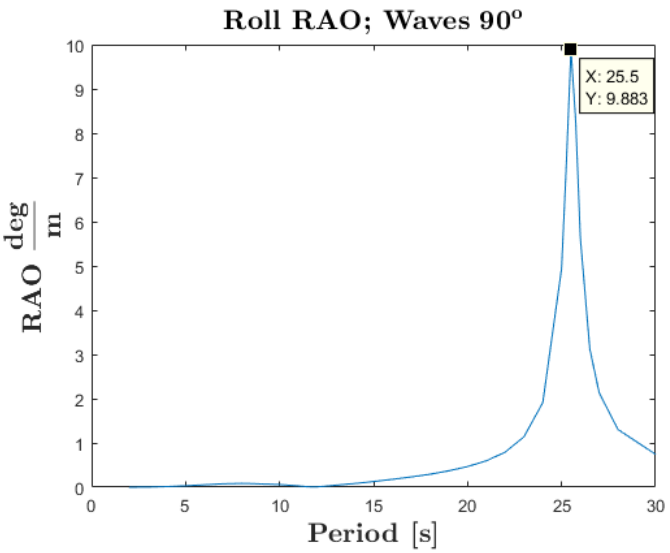

Figure 4.11: Model's roll RAO with incoming wave direction of 90 degrees

4.3.5 Pitch

The maximum pitch motion response in Figure 4.12 is 0.34 deg/m, and the maximum pitch response occurs for wave periods of 11.3. The waves are propagating towards the vessel's side, and similar to the surge response, the non-symmetry pressure effects is what excites the pitch motion. The maximum pitch and surge response in 90 degrees waves occur at 11 seconds and thus surge-pitch coupled motions occur.

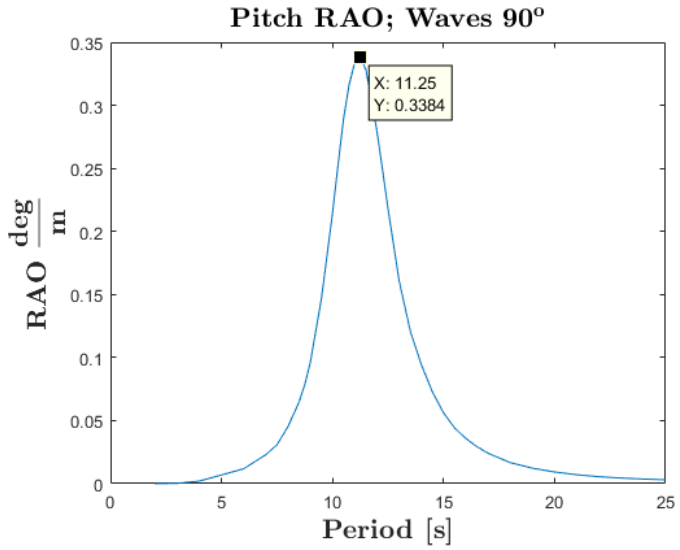

Figure 4.12: Model's pitch RAO with incoming wave direction of 90 degrees

The following figure shows the pitch motion response in 180^o waves, and the maximum response is 0.71deg/m for wave periods of 15 seconds, which is the pitch natural period in head sea. Studying Figure 4.13, a cancelling effect occurs at approximately 11 seconds.

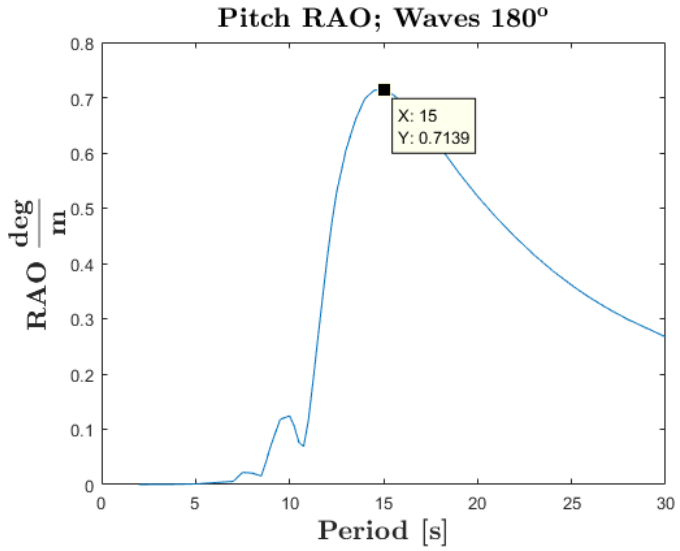

Figure 4.13: Model's pitch RAO with incoming wave direction of 180 degrees

4.4 FPSO's Sway-Yaw Stability

The following figures shows the total turret moment in co-linear ULS weather conditions for different distances between the COG and turret (x_{GT}). When x_{GT} is 120 and 70 meters (Figure 4.14 and 4.15) the opposing sway moment is larger than the yaw moment, and the vessel is within the stability requirement thus it is able to weathervane.

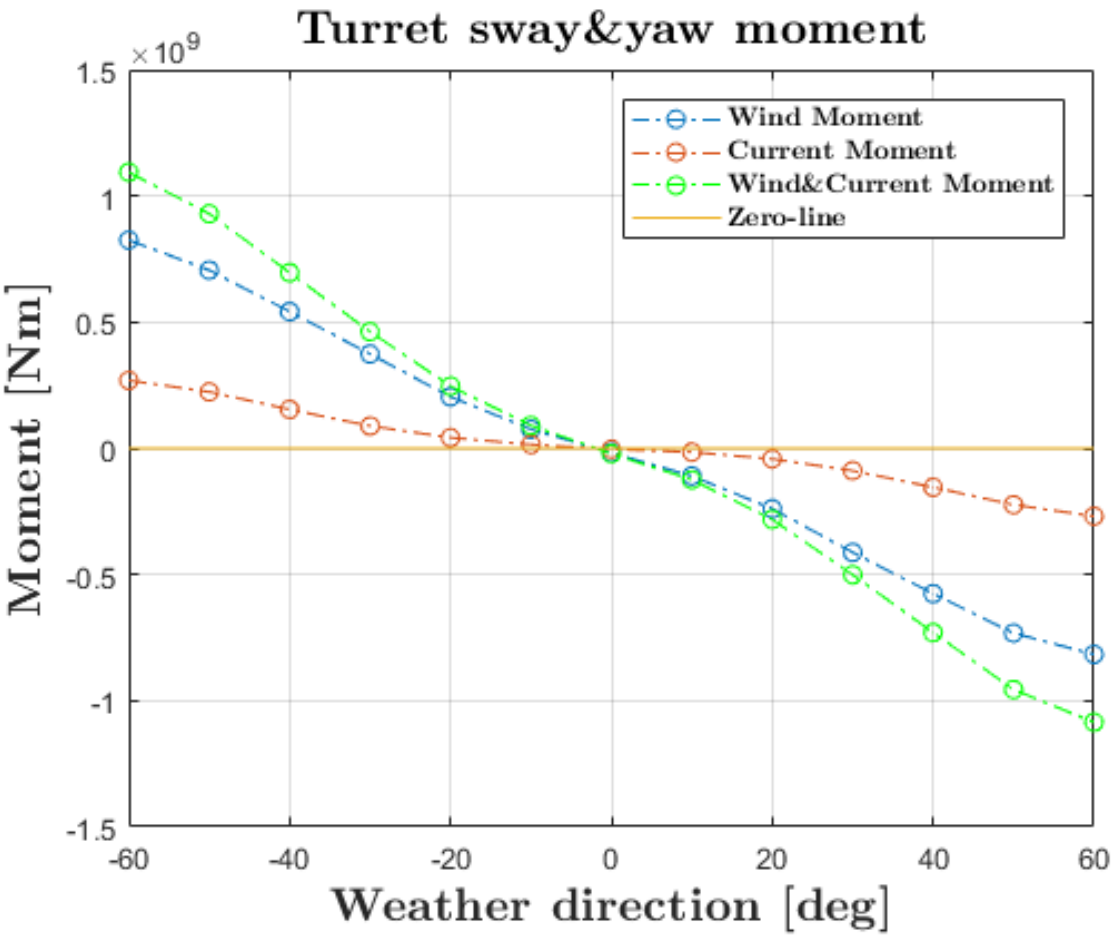

Figure 4.14: Turret moment when X_{GT} = 120m. The incoming weather direction is -60^o to 60^o relative to the bow.

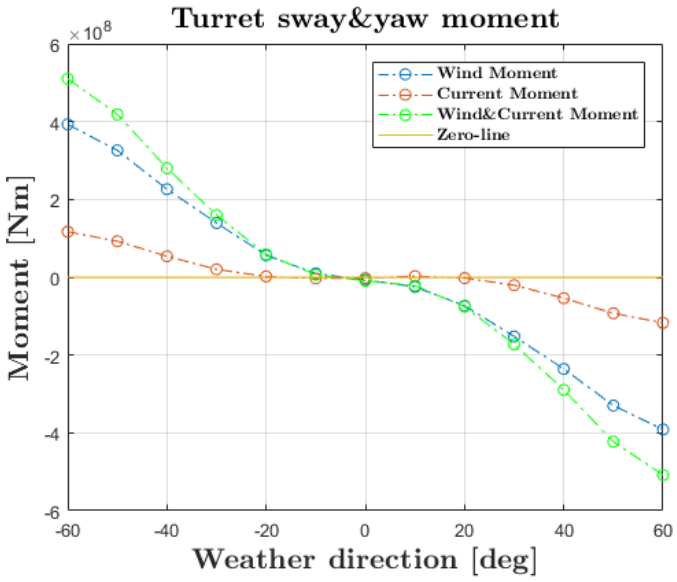

Figure 4.15: Turret moment when X_{GT} = 70m. The incoming weather direction is -60^o to 60^o relative to the bow.

Figure 4.16 shows the total moment when x_{GT} is 30 meters. In this case the yaw moment is larger than the sway moment, thus the vessel is not within the stability requirement. The sway moment does not get larger than the yaw moment until the vessel has turned -50^o and 60^o, and then it start to weathervane. These yaw motions creates large line tensions which can be devastating for the mooring system.

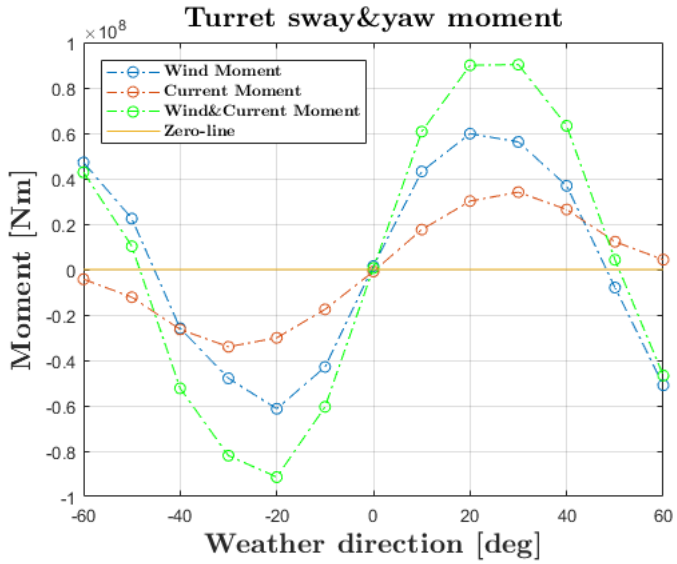

Figure 4.16: Turret moment when X_{GT} = 30m. The incoming weather direction is -60^o to 60^o relative to the bow.

Chapter 5

Numerical Simulations in SIMA

This chapter will describe the procedure of the numerical simulations performed within Simo and Riflex. Four simulation analyzes are performed:

1) Surge Decay & System Characteristic

2) Wave Contour in co-linear- and spread weather

3) 50 ULS simulations in co-linear- and spread weather

4) 50 ALS simulations in co-linear- and spread weather

, where the simulations in 2, 3 and 4 are conducted with environmental conditions corresponding to 100 year waves and wind, and 10 year current return period. 1, 3, and 4 are conducted in both Simo and Riflex, and the results from these tests are presented and discussed in chapter 7. The spread and co-linear weather simulations are performed similar as described in the end of section 2.3 with one exception: the initial direction of the co-linear weather is 0^o and not 15^o relative to vessels bow. However, these two weather analyzes are based on the fact that the site specific data is not available, but in this case the meta-ocean data is known.

5.1 Surge Decay & System Characteristic Test

A surge decay test is performed in order to calculate the damping and natural period of the system in surge. The surge decay is conducted in Simo and Riflex and is performed by applying a large specified force in the COG of the vessel, and then releasing it. The vessel starts to decay and after a while the decay motion is stops.

It is interesting to investigate if there exist any stiffness discrepancies between the system modeled in Simo and Riflex, thus a system characteristic is performed. In order to get a good estimation of the system characteristics, stepwise specified forces with increasing magnitude are applied at the vessel's COG in order to have multiple reference points in the characteristic. Figure 5.1 shows how the the system characteristic and decay test are conducted. The largest specified force is calculated to be

2*F_{ULS} = 6871015.5 N which corresponds to 100 year wind and 10 year current return period, where the wave forces are simplified to be equal the 100 year wind forces. Six points in the system characteristic is found sufficient, thus the specified force step is ΔF = 1145169.3 N.

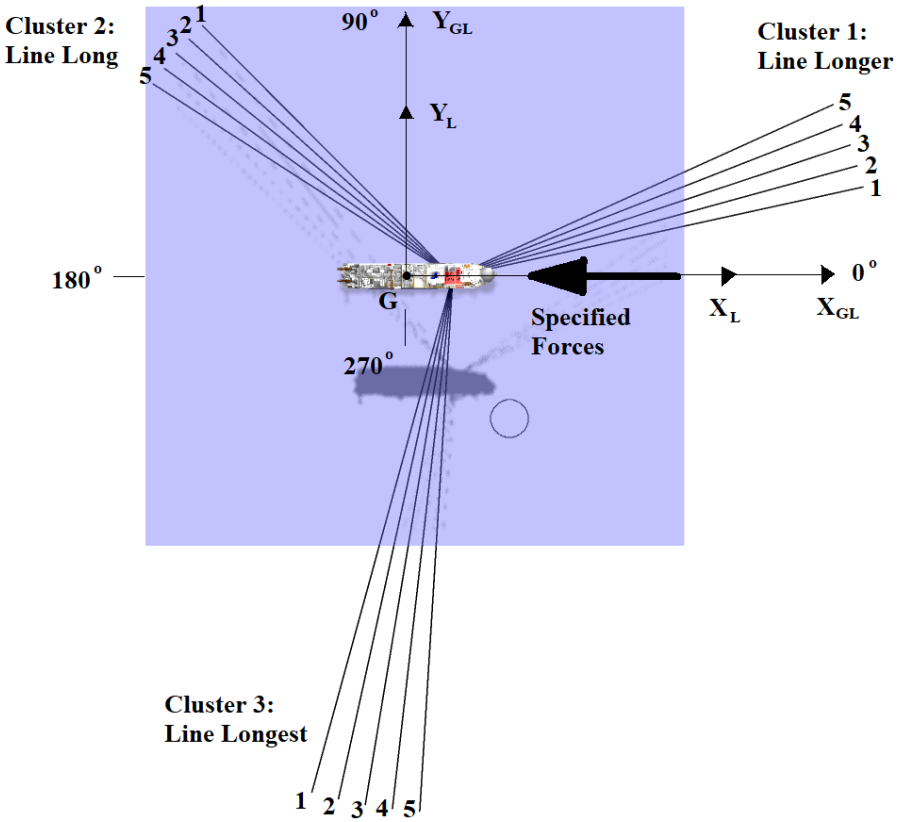

Figure 5.1: The mooring and vessel configuration and the applied forces during the system characteristic and decay test.

5.2 Wave Contour Simulations

Wave contour simulations are performed in Riflex in order to find out which H_S and T_P combination that results in the largest line tensions. The H_S and T_P values generated in the simulations are based on the 100 year wave contour peak in Figure 4.4. Six different combinations of H_S and T_P have been simulated in both spread and co-linear weather conditions, and these are listed in Table 5.1.

Table 5.1: The H_S and T_P values generated in the wave contour simulations.

	Countour Check	
	$H_S[m]$	$T_P[s]$
Simul. 1	15.5	18.5
Simul. 2	15.0	19.0
Simul. 3	14.5	20.0
Simul. 4	15.0	17.0
Simul. 5	14.5	16.0
Simul. 6	14.0	15.0

5.3 Co-linear Weather Simulations in ULS and ALS

Figure 5.2 shows the initial position of the FPSO in ULS co-linear weather simulations. The weather is co-linear when the wind, waves and current is acting in the same direction, DNV (2013). The vessel is rotated 140^o with respect to the global coordinate system, and the weather is propagating in 320^o relative to the global coordinate system. The co-linear weather is propagating towards the bow which is in-line with line Long 3. In the ALS simulations, Line Long 5 in cluster 2 is removed from the mooring system, because that line achieves the second greatest loads in the ULS co-linear weather simulations. This will be discussed later in chapter 7.

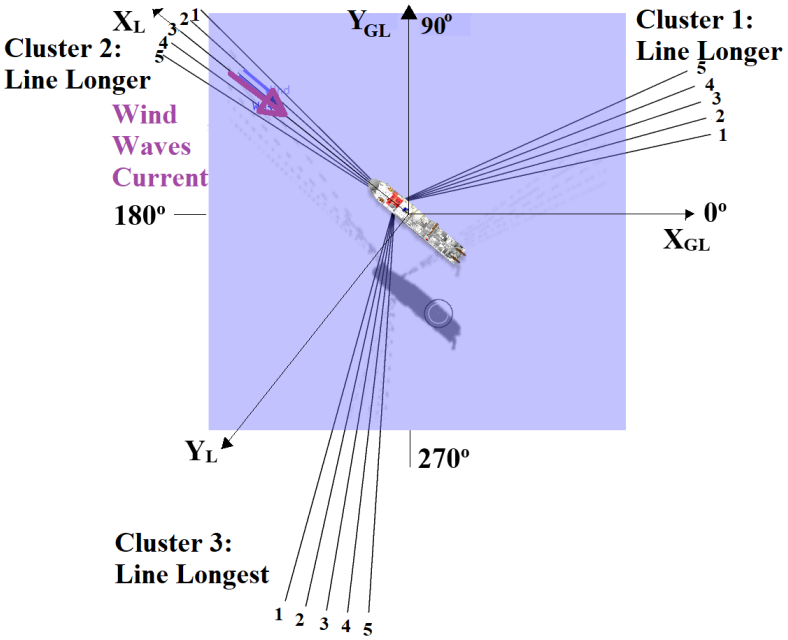

Figure 5.2: The ULS mooring configuration and vessel's initial heading in the co-linear weather simulations.

5.4 Spread Weather Simulations in ULS and ALS

Numerical simulations are performed with bow heading waves, and a wind and current heading with 30^o and 45^o relative to the waves. Similar as in the co-linear weather the wave direction is in-line with Line Long 3, and the vessel is initially rotated such that the bow is heading towards the waves which are propagating in 320^o relative to the global coordinate system. Figure 5.3 shows the initial position of the FPSO during an ULS spread weather simulation. Line Longest 3 in cluster 3 has been removed from the mooring system, because that line achieves the second greatest loads in the spread weather simulations.

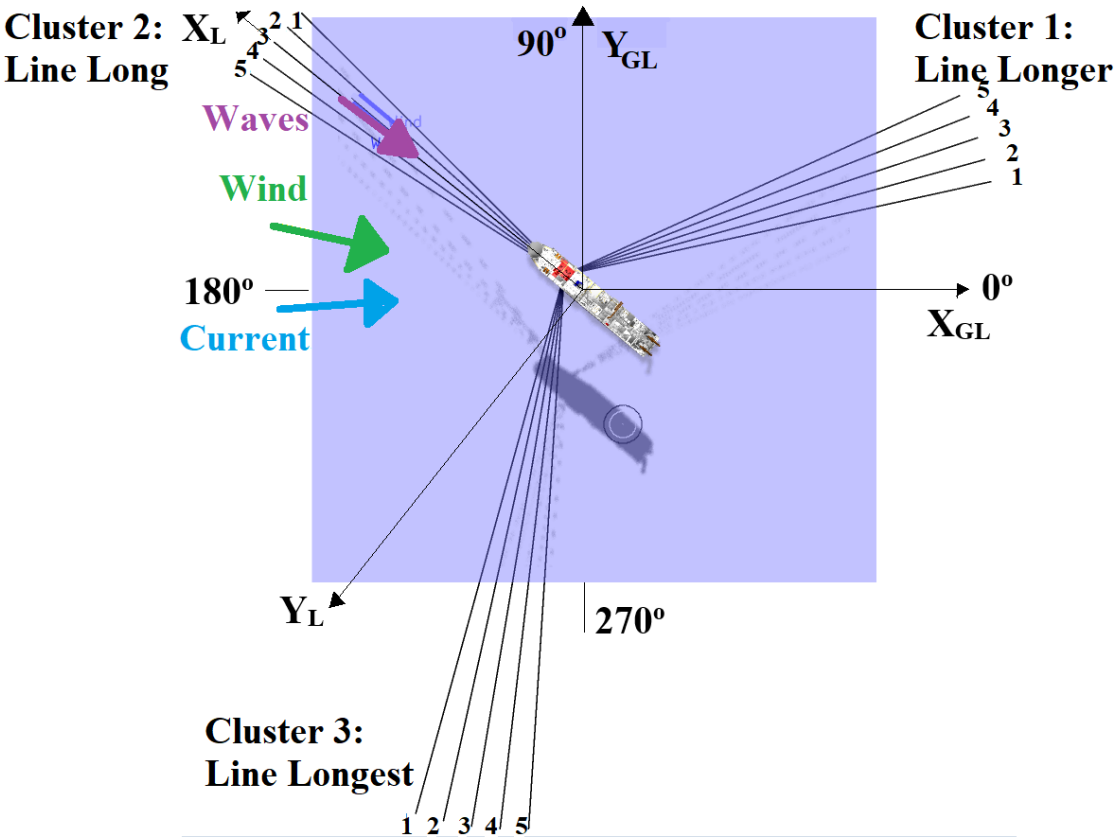

Figure 5.3: The ULS mooring configuration and vessel's initial heading in the spread weather simulations.

Chapter 6

Quality Analysis and Discussion

To ensure that the mooring system is correctly modeled, it is important to perform simulation analyzes. In the following sections, the results from the static, surge decay and system characteristic are are presented and discussed to show the quality of the simulations. In addition the LF damping from the mooring lines and the mean turret shear force have been estimated. Finally a convergence test of the line tension standard deviation of leeward line Long 4 have been investigated.

6.1 Static Pre-Tension Analysis

A static analysis of Line Long 1 is performed to study if there is a discrepancy in the top-end pre-tension between the system in Riflex and Simo. The initial given pre-tension value was as mentioned earlier given in Simo to be 2097kN in all lines. Figure 6.1 show the top-end tension of Line Long 1 in Simo and the tension in all line elements in Riflex. The results show that the pre-tension in Simo and Riflex are 2098kN and 2072kN respectively. The deviation between the initial given pre-tension and the pre-tension in Simo and Riflex is 1kN and 25kN, which equals a percentage difference of approximately 0.05% and 1.2%. The difference between the initial pre-tension and the pre-tension in Simo is so small that it is negligible. The difference between the initial pre-tension and the one in Riflex is also small, but as it will show later in the surge decay test there is a possibility for a system stiffness discrepancy between Simo and Riflex that will have an impact on the pre-tension and other results.

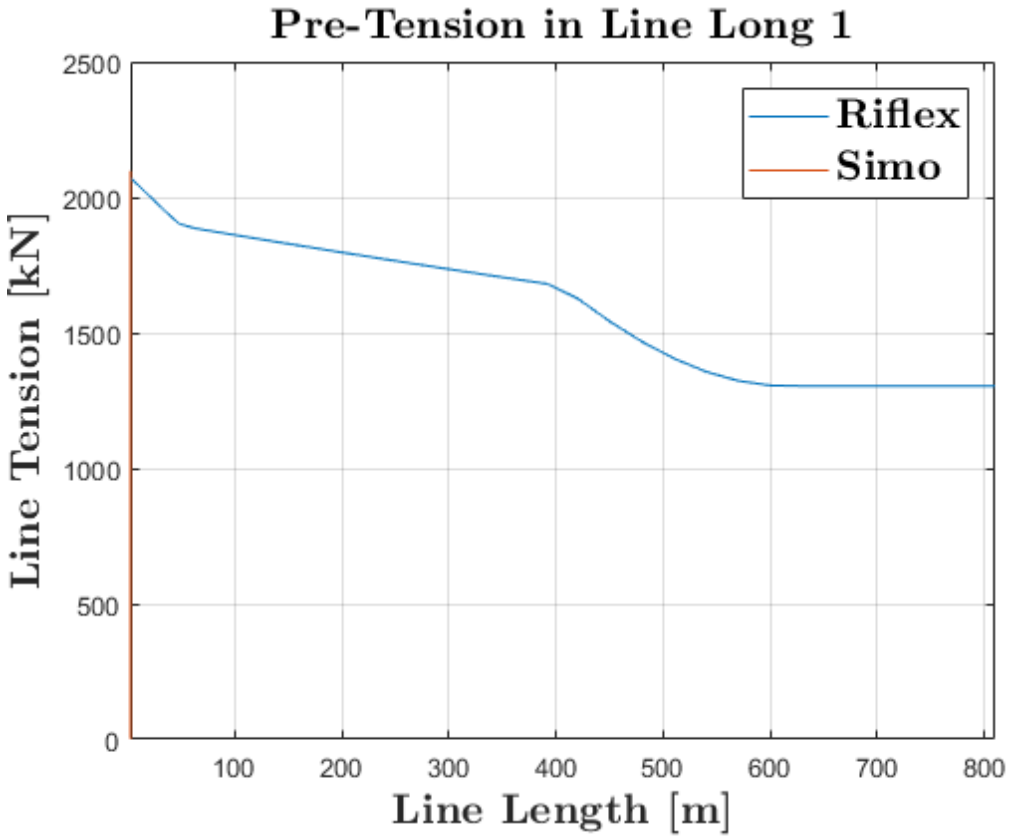

Figure 6.1: The line tension along Line Long 1 in Riflex and the top tension of the line in Simo.

The difference in pre-tension is probably a result of many reasons. One reason might be because of the line stiffness properties in Simo and Riflex are calculated with two different methods from two different sets of input data, which may have lead to different stiffness properties. Simo requires the line diameter, E-modulus, emfac number and line weight to calculate the line stiffness. The emfac number describes the geometry of the line, for example the emfac number of a chain mooring line and a steel wire is 2 and 1 respectively. Now Simo got all the information it needs to calculate the line stiffness by solving the catenary equations as mentioned in section 3.8. Riflex however, requires the line weight, buoyancy area and the axial stiffness(EA), and uses the FEM to calculate the static mooring configuration. The axial stiffness is calculated by E-modulus*cross-section, where the cross section of the chain is calculated as $\pi * r^2 * emfac$ where r is the radius of the chain. The two different sets of input data and calculation methods have most likely led to discrepancy in the system's stiffness between Riflex and Simo, thus the small difference in the pre-tension.

6.2 Surge Decay

The FPSO's averaged surge decay in Riflex and Simo is shown in Figure 6.2. The surge amplitudes in the decay are significantly lower in Riflex than in Simo, which is due to the damping from the dynamic motions of the mooring lines which is considered in Riflex. From just a glance at Figure 6.2 it looks like the surge natural period is the same in both Riflex and Simo, however there is a difference. By using the equations in section 3.5 it shows that the surge natural period in Riflex is slightly lower than in Simo, which is unexpected. The surge natural period in Riflex and Simo is 185.6s and 187.9s respectively, with a difference of 1.2%. It would make sense if the surge natural period in Riflex was slightly larger than in Simo as a result of the added mass contribution from the dynamic line motion in Riflex, however this is not the case which means that either the system's mass or stiffness is different between the model in Riflex and Simo. The mass is the same thus the stiffness must be different. The discrepancy in natural period is probably due to that the line stiffness properties in Simo and Riflex are calculated in two different ways with two different sets of input data, which was mentioned in the previous section. Another possible reason for the stiffness discrepancy can be a result of the bottom friction differences in Riflex and Simo. The bottom friction can be defined in Riflex, however this is not an option in Simo. If the bottom friction is to be defined in Simo, the catenary lines must be modeled as slender elements where a friction value can be implemented into the elements modeled at the sea bottom. However, by modelling the mooring lines like slender elements, consequences in the line behavior and catenary calculations will have lead to a completely different system. In other words the bottom friction can not be defined in Simo, and if there exist a default value it is unknown. The bottom friction will affect the location of the mooring line's touch down point (TDP), and thus affect the line length from the top end to the TDP. The elastic stiffness is dependent on the line length, and it seems like the elastic stiffness is larger in Riflex as a result of a shorter line length due to the larger bottom friction. It will be seen from the system characteristics in the next section that there exists a discrepancy in the line stiffness between the model in Simo and Riflex.

The damping terms, natural period and frequency are calculated by the equations in section 3.5 and are presented in Table 6.1. The damping coefficients are estimated by assuming that the added mass in surge is 10% of the vessel's mass, and is calculated as $C = C_C * \zeta = 2 * m * \omega_n * \zeta$. The estimated damping coefficient in the Riflex surge decay is 39.3% larger than the damping in the Simo surge decay, which is a result

of the mooring line damping. The large surge natural periods in Simo and Riflex indicates that the system is underdamped, which coincides with the calculated surge damping ratios. Large low frequent resonant surge motions are expected.

	ζ [-]	C_c [$\frac{Ns}{m}$]	C [$\frac{Ns}{m}$]	T_n [s]	ω_n [$\frac{rad}{s}$]
Simo	0.039	1.61*10^7	6.3308*10^5	187.9	0.03345
Riflex	0.064	1.63*10^7	1.0428*10^6	185.6	0.03385

Table 6.1: Calculated parameters from the surge decay: damping ratio(ζ), critical damping(C_c), damping(C), natural period(T_n) and natural frequency(ω_n).

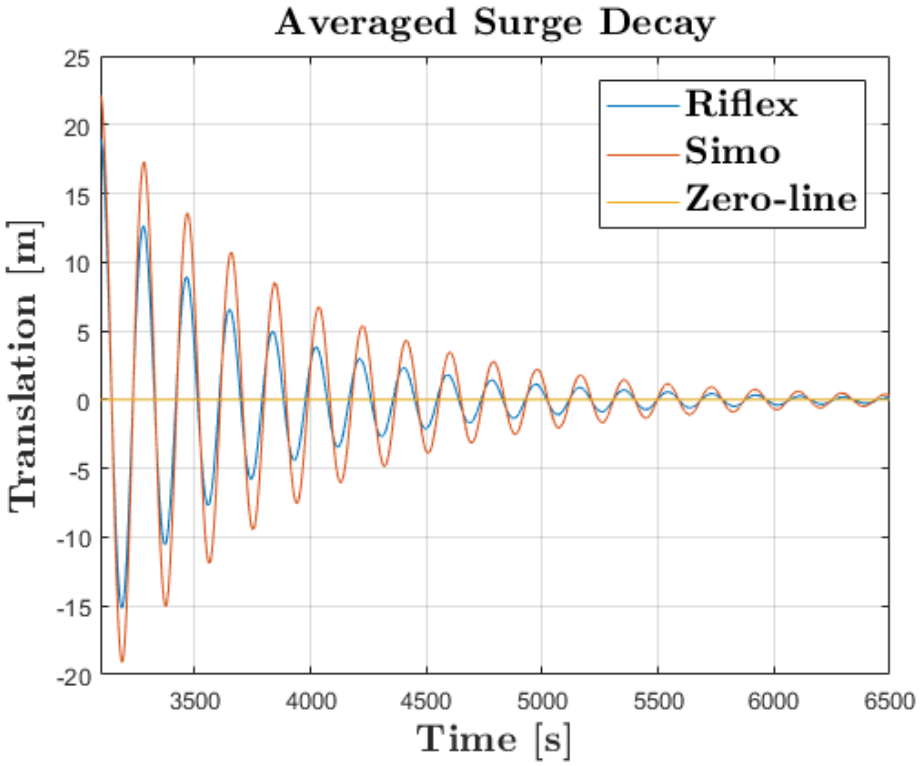

Figure 6.2: Averaged surge decay in Riflex and Simo.

Power Spectral Density of the Surge Decay

To quality check the surge decay and the natural period, a power spectral density (PSD) plot has been made. According to the PSD in Figure 6.3, the surge natural frequency is 0.005282 for both Riflex and Simo which corresponds to a natural period of 189s. The spectrum's accuracy can be discussed, but it clearly shows that the energy is concentrated in the low frequency area. The spectrum shows that the surge decay

in Riflex obtains less energy than in Simo due to the mooring line damping which, as mentioned earlier, is included in Riflex.

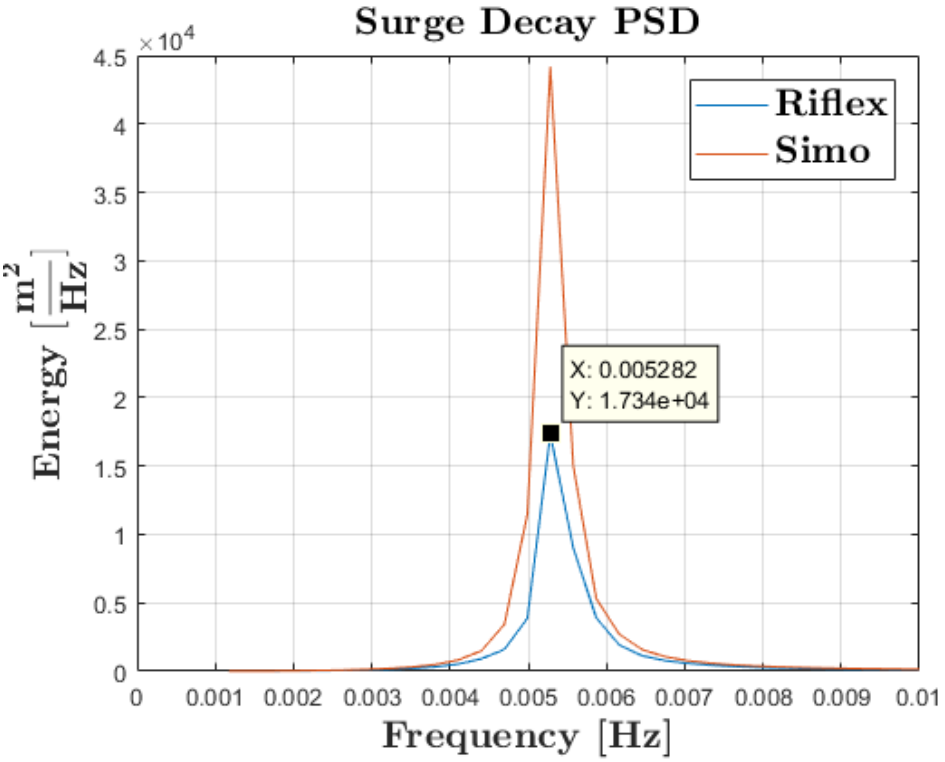

Figure 6.3: PSD plot of the surge decay (small smoothing factor) in Riflex and Simo.

6.3 System Characteristic

The system characteristics in Figure 6.4 are found when the FPSO is exposed to stepwise increasing loads, and the corresponding surge translation of the COG is measured. The question if there is a stiffness difference between the mooring system in Riflex and Simo, is answered by looking at the system characteristic. The mooring configuration in Riflex is stiffer than in Simo when looking at Figure 6.4. The system characteristics are slightly non-linear and the discrepancy in stiffness between Simo and Riflex is slighty varying with increasing loads. The stiffness coefficient in Simo and Riflex is 281145.7 and 290659.9$\frac{N}{m}$ respectively, where the system in Riflex, according to the system characteristic, is at most 3.3% larger than Simo. This will affect the results such that the FPSO's motions and line tension response in Riflex will become slightly underestimated when compared with Simo.

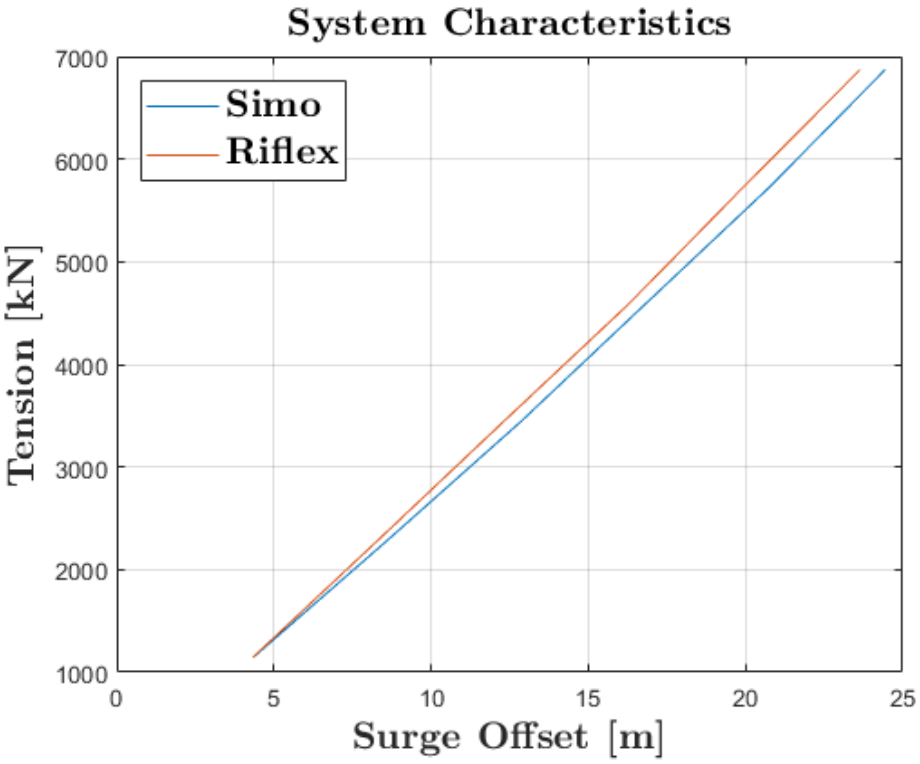

Figure 6.4: System characteristic in Riflex and Simo.

6.4 Low Frequent Mooring Damping

Section 3.2.3 described the most important LF damping forces for a moored FPSO and the damping from mooring lines are very important, because they provide a large amount of damping to the low frequent motions. It is interesting to see how much LF damping that is provided by the line dynamics versus the linear vessel and quadratic environmental damping. The mooring lines provided a damping of 39.3% in the surge decay, however it would be interesting to investigate how large damping the system would get in ULS weather conditions.

The focus will be around the surge LF damping. The FPSO's linear surge damping is given as $B_L = 5.236 * 10^5 \frac{Ns}{m}$. The wind and current provides linear damping in addition to the linear vessel damping, and is given as $B^L_{Q,wi} = 1.9136 * 10^5 \frac{Ns}{m}$ and $B^L_{Q,cu} = 3.9163 * 10^5 \frac{Ns}{m}$. Simo does not include the dynamic motion of the mooring line, thus the mooring damping is neglected and the total damping in Simo is provided by linear vessel and environmental damping: $B^{Tot}_{Simo} = B_L + B^L_{Q,wi} + B^L_{Q,cu} = 1106590 \frac{Ns}{m}$. Additional damping which are included in the simulations are not included in this sim-

ple damping estimation, because they are not necessary when only studying the line damping magnitude. The standard deviation of the LF surge translation, assuming that the damping is small, is according to Faltinsen (1990) given as:

$$\sigma_{x,LF} = \sqrt{\frac{\pi * S_{F,LF}(\omega, LF)}{2 * B_{LF} C_{LF}}} \tag{6.1}$$

, where the $S_{F,LF}(\omega, LF)$, B_{LF} and C_{LF} are the LF spectral density, LF damping and stiffness respectively. If the spectral density and stiffness is assumed to be the same between Simo and Riflex, then the total damping in Riflex can be expressed by the total damping in Simo:

$$\begin{aligned} \frac{\sigma^{Simo}_{x,LF}}{\sigma^{Riflex}_{x,LF}} &= \sqrt{\frac{B^{Tot}_{Riflex}}{B^{Tot}_{Simo}}} \\ B^{Tot}_{Riflex} &= (\frac{\sigma^{Simo}_{x,LF}}{\sigma^{Riflex}_{x,LF}})^2 * B^{Tot}_{Simo} \end{aligned} \tag{6.2}$$

The LF surge standard deviation was found from an ULS co-linear simulation to be 3.5 and 5.8 meters in Riflex and Simo respectively. The total damping in Riflex is then calculated to be 2872352.4 $\frac{Ns}{m}$ where the mooring line damping is responsible for 61.5% of the total damping included in the estimation. This is a lot of damping provided by the mooring lines, however it is not unreasonable. The lines experience a large loads during ULS simulations and large dynamic line motions will produce drag, and thus large damping is provided to the system.

6.5 Mean Turret Shear Force

It is possible to compare the turret forces with the environmental loads to check if the turret forces are reasonable. The easiest way to compare these forces is to investigate the mean forces in co-linear weather. The mean forces from waves, wind and current should approximately be the same as the mean turret shear force. The wind and current coefficients are known, thus these forces are easy to calculate. The mean wave drift force ($\bar{F}_{wf}$) is however unknown and can be calculated by equation 3.12. To simplify the mean wave drift force equation it can be assumed that the integral

over the wave drift coefficient can be described as a constant, $C_{wd}(\omega) = C_{wd}$. The variance of the wave spectrum is given as the integral over the wave spectrum, assumed that the wave elevation is normally distributed, and it can be shown that the variance becomes $(\frac{H_s}{4})^2$, Larsen (2015a). The simplified equation of the mean wave force is expressed as:

$$\bar{F}_{wf} = 2 * C_{wd} * (\frac{H_s}{4})^2 \tag{6.3}$$

The wave drift coefficient is however frequency dependent, and to find a reasonable constant the wave spectrum must also be included in the decision. Figure 6.5 shows the wave drift coefficient plotted against the scaled wave spectrum with the intention of choosing a constant for the wave drift coefficient. The wave drift and the wave spectrum intersect at $C_{wd} = 53870\frac{N}{m^2}$, however this is the maximal value of the wave drift coefficient within the wave spectrum's area. A reasonable wave drift coefficient is then found to be $C_{wd} = \frac{53870}{2} = 26935\frac{N}{m^2}$. By calculating the mean wave drift force and adding on the mean wind and current forces, the total mean weather force is $\bar{F}_{weather} = 3.62 * 10^6 N$. This corresponds very good with the mean turret shear force calculated from one of the co-linear simulations which was found to be $\bar{F}_{Shear}^{Turret} = 3.59 * 10^6 N$. This gives a good indication that the turret forces are reasonable.

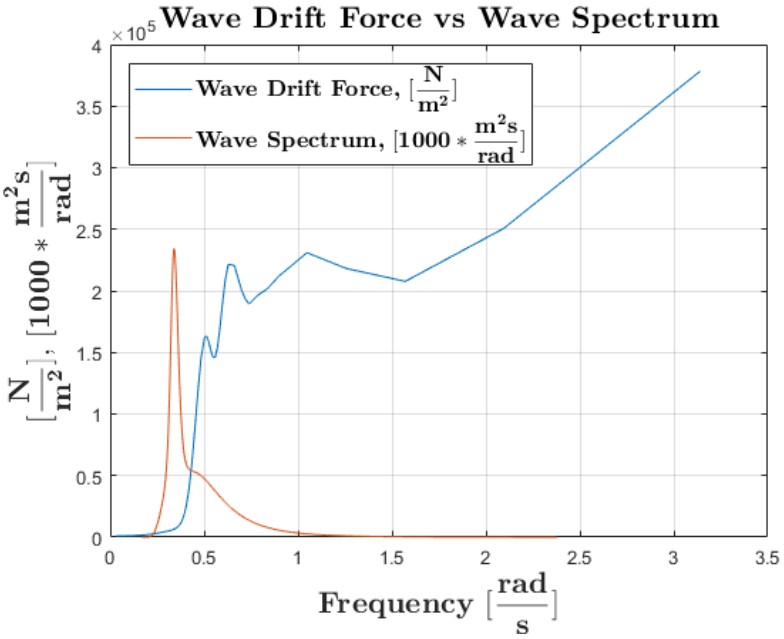

Figure 6.5: The wave drift coefficient plotted up against a scaled wave spectrum.

6.6 Convergence Test

The number of simulations that is necessary to obtain valid response results is a difficult question to answer. To figure out how many simulations it takes to properly describe the line tension, a standard deviation convergence test of the line tension in Long 4 have been performed and the results are shown in Figure 6.6. 50 simulations have been performed in both weather conditions in Riflex and Simo, and the figure shows how the tension standard deviation is converging towards a constant value. The standard deviation in Riflex is converging in both weather conditions, while the convergence graph in Simo is slightly declining. Notice that the convergence in Simo is approximately the same in both weather conditions, while Riflex converges towards a higher standard deviation in spread weather. The tension variation is thus larger in spread compared to co-linear weather. It is also noteworthy that the tension standard deviation is larger in Riflex compared to Simo, thus the line tension varies more in Riflex. The convergence graphs are quite stable and thus 50 simulations is found to be sufficient to provide valid tension response results.

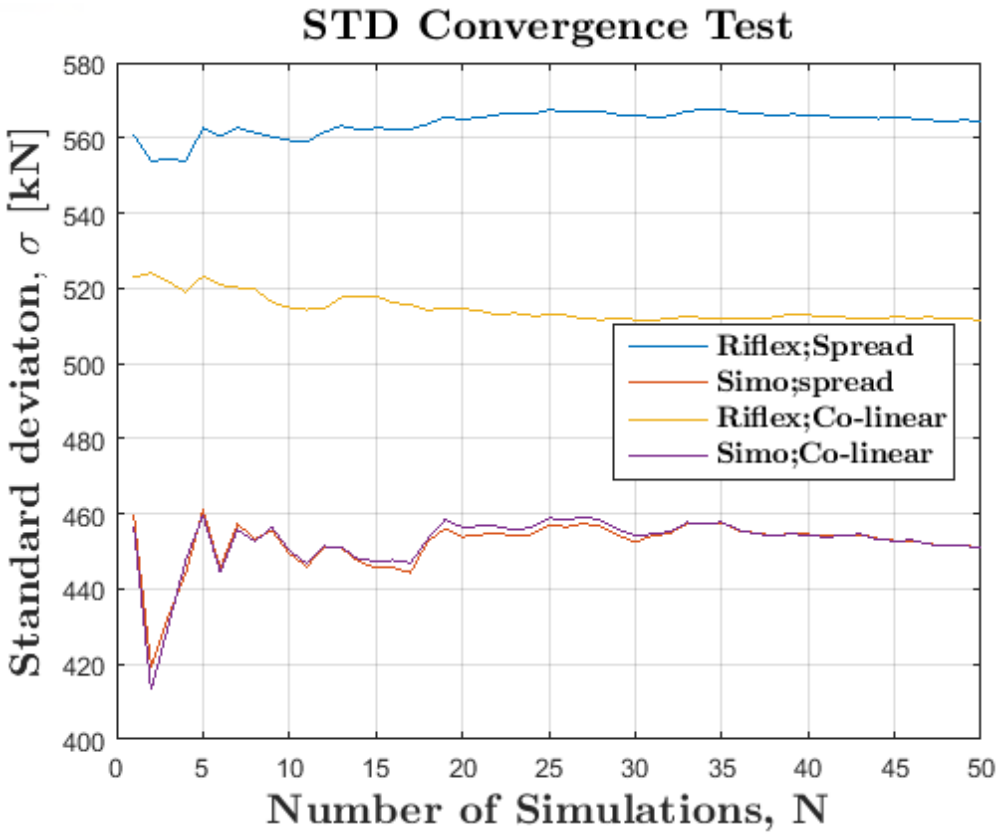

Figure 6.6: The standard deviation convergence of the line tension in Long 4 in ULS.

Chapter 7

Results and Discussion

In this chapter the vessel motion, line tension and turret load responses will be presented and discussed. The extreme vessel motions, line tensions and turret loads statistics are presented for all ULS and ALS simulations. The time series, its statistics and PSDs of the vessel's six dof motions, line tensions and turret loads are however only presented for the ULS simulations. The ALS time series, statistics and PSDs of the vessel's motions, line tensions and turret loads are placed in Appendix C, D and F respectively. The 6 dof motions and the line tensions response are compared between Simo and Riflex. All simulations and analyzes are performed for both spread and co-linear weather, and the results from both weather conditions are presented and discussed.

7.1 Wave Contour Analysis

The wave contour simulations have been performed in Riflex in both co-linear and spread ULS weather conditions. The line tension results from the co-linear and spread wave contour simulations are given in Figure 7.1 and Figure 7.2 respectively, and will be discussed in this section.

7.1.1 Co-linear Weather

The Long lines are the ones who achieves the largest line tension in the co-linear simulations in Figure 7.1. This is as expected because the waves, wind and current is propagating in-line with line Long 3. The leeward Longest lines achieves a slightly larger tension than the Longer lines, which is probably a result of a larger elliptic surge-heave-pitch motion that results in a larger dynamic tension. This phenomenon will be investigated more closely later in the report. The results show that a H_S = 15.5m and T_P = 18.5s results in largest line tension, and is thus further used in the ULS and ALS co-linear simulations.

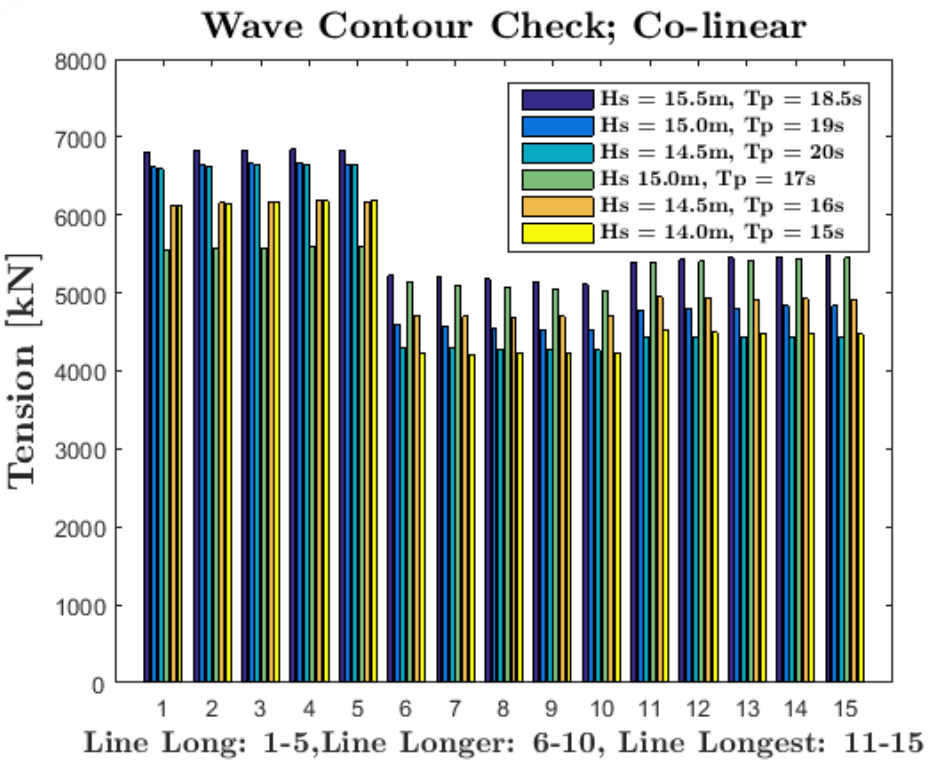

Figure 7.1: The line tension in each line during ULS co-linear weather with different H_S and T_P values.

7.1.2 Spread Weather

In the ULS spread weather simulations, it is the simulation with $H_S = 15.5m$ and $T_P = 18.5s$ which achieves the largest line tension response in the Long and Longest lines, and the second largest tension response in the Longer lines. The simulation with $H_S = 15.0m$ and $T_P = 17.0s$ achieves the largest tension response in the Longer lines, however the Longer lines' tension response are sufficiently lower than the Long and Longest lines's response, and thus not that important. It is reasonable to further use a H_S and T_P of 15.5m and 18.5s in the ULS and ALS spread weather simulations.

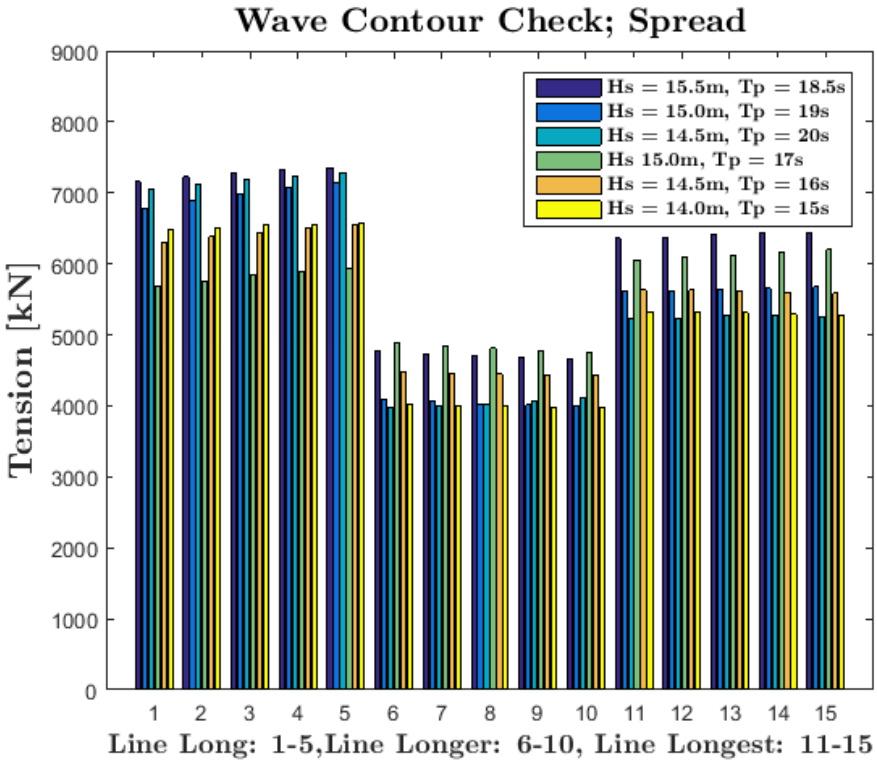

Figure 7.2: The line tension in each line during ULS spread weather with different H_S and T_P values.

7.2 Ultimate Limit State Motion Analyzes

This section will present and discuss the FPSO's motion response during ULS co-linear and spread weather conditions. The results will be presented in form of figures and tables. The presented motions time series shows the largest motion response based on the 50 simulations. The presented motion time series consists of a total, low frequency and wave frequency filtered time series. These are compared to investigate the vessel's motion contributions. The motion time series are with respect to the the global coordinate system.

7.2.1 Surge-Sway Translation

Figure 7.3 shows the vessel's offset in the global horizontal plane during ULS co-linear and spread weather conditions. The initial position of the vessel's COG is at origo, however as mentioned earlier the first 200 seconds of the time series are not considered due to transient motions. The vessel's offset in Riflex is lower than in Simo

for both weather conditions which is due to the dynamic line motion in Riflex which provides damping. In both softwares the FPSO is in co-linear weather initially translating towards port-side and aftwards, and then forward and aftwards in a straight line. In spread weather however the vessel covers a larger offset area in the positive y-axis, thus the vessel is translating towards the starboard side. Keep in mind that the first 200 seconds of the time series are deleted due to transient motions. This have been done with all the results except for the yaw results, because it is interesting to see how quickly the vessel weathervanes.

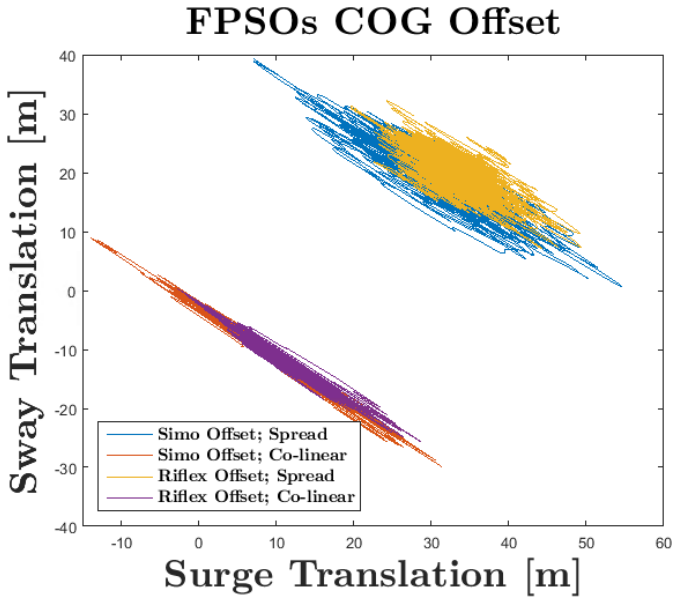

Figure 7.3: The FPSO's surge-sway translation of the COG in the global axis system in ULS co-linear and spread weather conditions.

7.2.2 Surge Translation

Time Series

Figure 7.4 shows the total, LF and WF filtered surge time series. The LF surge translation is much larger in comparison with the WF surge translation in both Riflex and Simo, thus the LF loads are dominating the surge motion. From the figure it looks like the surge WF translation is approximately the same between Riflex and Simo, however the time series statistics in Table 7.1 shows that the WF surge response is slightly larger in Simo compared to Riflex. The surge LF translation is also larger in Simo compared to Riflex for both weather conditions. This is due to the damping

from the mooring lines which reduces vessel's LF resonant motions in Riflex but not in Simo, thus the surge translation is overrated in Simo. The slowly varying motions have in this cutted time serie a period of approximately 165s. This is not close to the surge natural period, however the period is large and thus resonant surge motions can occur during the whole simulation. It is noticeable that the surge translation is larger in the spread weather compared to the co-linear weather condition.

As mentioned above, the statistics from the surge time series are presented in Table 7.1. The max and min surge translation are larger in Simo than in Riflex, which is expected due to the mooring damping considered in Riflex. The difference in max values are 1.9% and 9.2% in respectively spread and co-linear weather, thus the surge line damping in Riflex is larger in co-linear weather. The standard deviation is also larger in Simo due to the larger surge variations. The mean surge translation is however larger in Riflex. It is also noticeable that the surge translation is significantly larger in spread than co-linear weather.

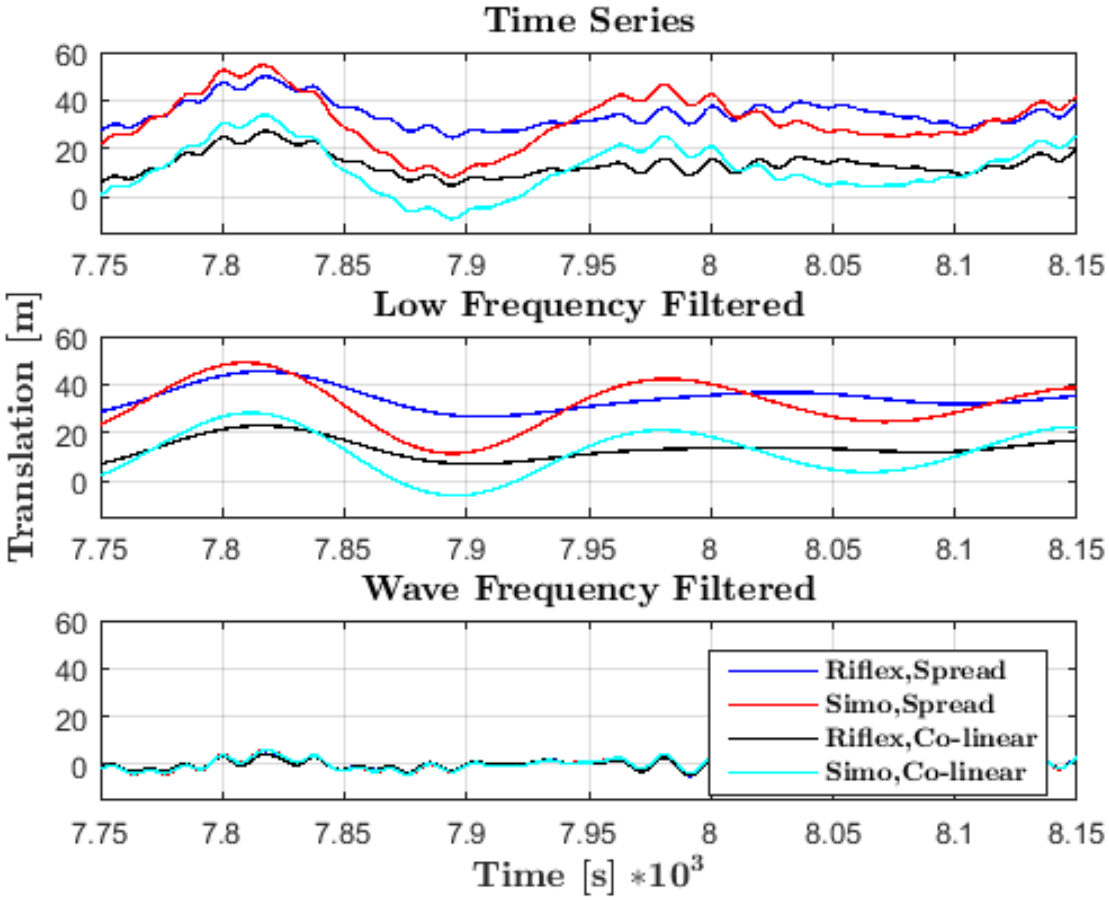

Figure 7.4: Total, LF and WF surge time series of the vessel's COG.

Table 7.1: The max, min, mean (μ), standard deviation (σ) of the vessel's COG surge translation.

	Spread							
	Riflex				**Simo**			
Surge	MAX	MIN	μ	σ	MAX	MIN	μ	σ
Total [m]	55.6	20.3	32.6	4.2	56.7	6.0	30.1	6.2
LF [m]	49.2	20.8	32.6	3.6	50.2	7.6	30.1	5.6
WF [m]	7.1	-6.6	0.0	1.7	8.7	-6.8	0.0	1.8
	Co-linear							
	Riflex				**Simo**			
Surge	MAX	MIN	μ	σ	MAX	MIN	μ	σ
Total [m]	30.7	-1.1	11.3	3.8	33.8	-13.4	9.9	6.0
LF [m]	25.1	0.7	11.3	3.3	28.1	-9.9	9.9	5.4
WF [m]	6.4	-6.4	0.0	1.7	7.4	-6.7	0.0	1.8

PSD

The surge translation PSD in Figure 7.5 verifies that the LF translation energy is much larger in Simo than in Riflex. It shows that the LF surge translation is larger in spread weather, and that the surge translation is mostly a result of the LF motions. The WF energy translation is approximately the same between Riflex and Simo in both weather conditions, which is expected. The LF and WF energy peaks are concentrated at $f_{LF} = 0.005472 s^{-1}$ and $f_{WF} = 0.05396 s^{-1}$ which corresponds to a period of 183s and 18.5s. The LF period is close to the surge natural period and resonance occur. The WF period coincides with the generated wave period of 18.5s, thus the waves excite some wave frequent surge motions.

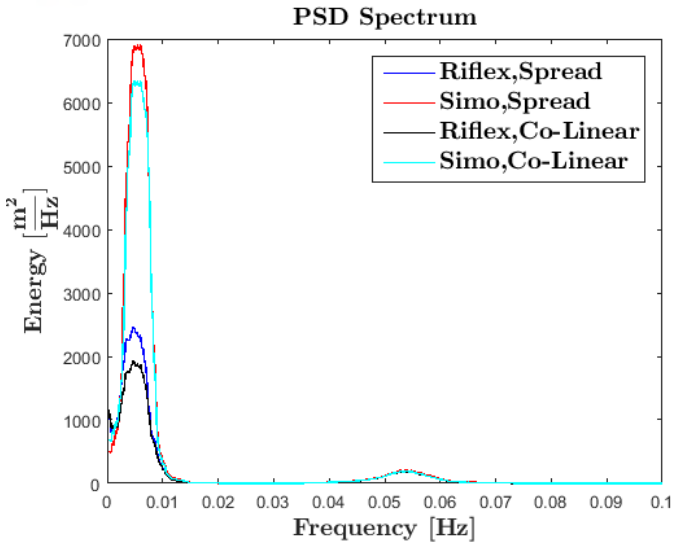

Figure 7.5: Surge energy spectrum.

7.2.3 Sway Translation

Time Series

Similar to the vessel's surge translation, Figure 7.6 shows that the sway translation is dominated by the LF loads. The LF sway translations in Riflex are as expected less than in Simo in both spread and co-linear weather conditions due to the mooring line damping. The WF sway translation however is approximately the same for Riflex and Simo in both weather conditions. Notice that the FPSO is translating in the negative and positive y-axis in respectively co-linear and spread weather, respectively. The slowly varying sway period is in the time series approximately 170s, which may cause resonance.

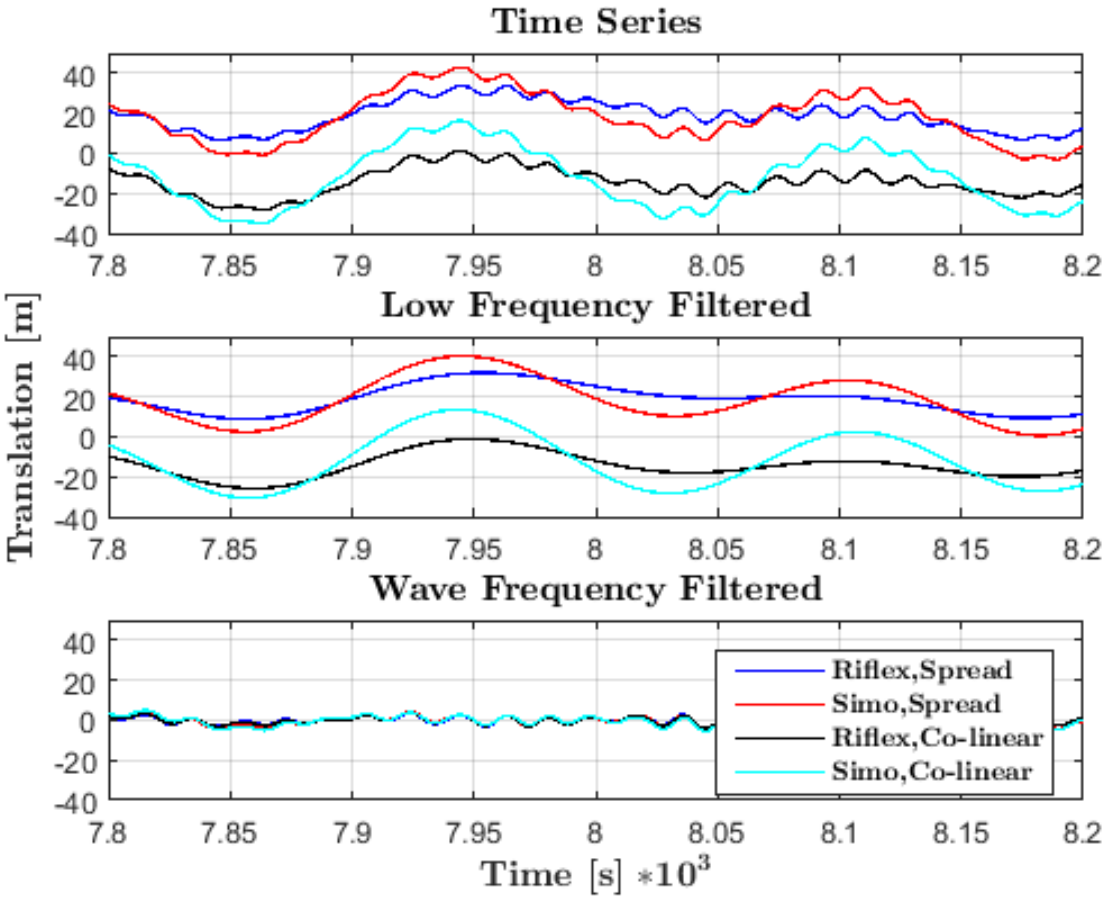

Figure 7.6: Total, LF and WF sway time series of the vessel's COG.

The sway time series statistics is presented in Table 7.2. When comparing the statistics, it tells us that the sway translation is larger in the spread weather compared to

co-linear. The system in Riflex has a smaller maximum sway motion in both weather conditions compared to Simo, which is due to mooring damping. The mean sway translation is however larger in Riflex, and the sway standard deviation is larger in Simo due to larger sway motion variations. The differences in the max values between Riflex and Simo are 21.6& and 92.6% in spread and co-linear weather respectively. The maximum sway motions are much smaller in Riflex and thus the dynamic line effects have a significant affect on the sway motions.

Table 7.2: The max, min, μ and σ of the vessel's COG sway translation.

	Spread							
	Riflex				**Simo**			
Sway	MAX	MIN	μ	σ	MAX	MIN	μ	σ
Total [m]	33.7	6.7	20.0	4.0	43.0	-3.1	19.4	5.5
LF [m]	31.9	8.9	20.0	3.7	40.3	0.6	19.4	5.0
WF [m]	4.6	-4.4	0.0	1.4	5.2	-5.0	0.0	1.5
	Co-linear							
	Riflex				**Simo**			
Sway	MAX	MIN	μ	σ	MAX	MIN	μ	σ
Total [m]	1.2	-28.4	-12.5	3.1	16.2	-35.0	-11.4	5.5
LF [m]	-1.2	-25.8	-12.6	2.6	13.5	-30.6	-11.5	4.9
WF [m]	4.2	-4.3	0.0	1.4	5.3	-5.4	0.0	1.5

PSD

The energy spectrum in Figure 7.7 verifies that the system in Simo achives a larger LF sway response than Riflex for both spread and co-linear weather conditions. It is also seen that the LF motions is considerably larger than the WF sway motions. The LF and WF energy peaks are concentrated at $f_{LF} = 0.005283 s^{-1}$ and $f_{WF} = 0.05396 s^{-1}$ which corresponds to a period of 189s and 18.5s, respectively. The surge and sway natural period of a moored FPSO typically have, as mentioned earlier in section 3.2, a period larger than 100s which means that the large LF sway motions can excite resonant sway motions. For spread weather the energy in the PSD seems to increase when the frequency goes towards zero for both Riflex and Simo. It is assumed that this LF sway energy behaviour is due to the wind gusts that excites extremely LF sway motions of the FPSO.

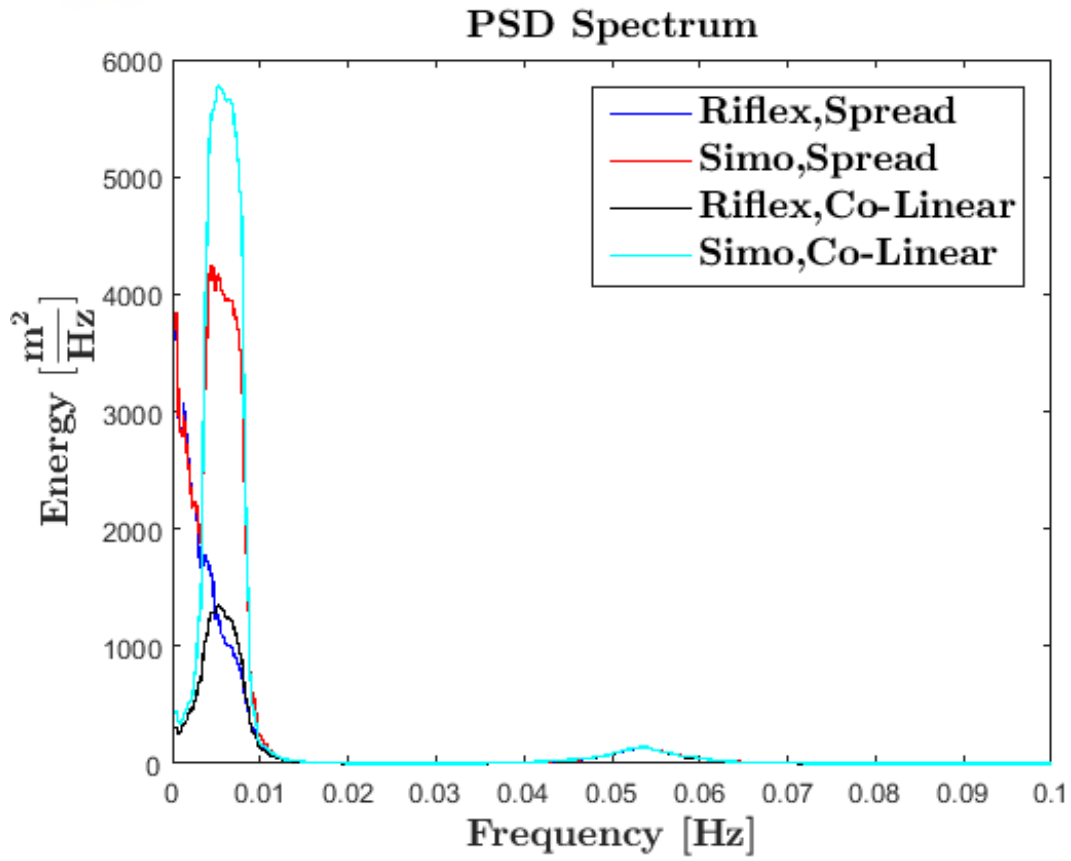

Figure 7.7: Sway energy spectrum.

7.2.4 Heave Motion

Time Series

The heave motion time series in Simo and Riflex are presented in Figure 7.8 for both spread and co-linear weather conditions. The figure shows that the total, LF and WF filtered time series of the heave motion are approximately the same for both Riflex and Simo. This means that the vessel's heave motion is not considerably affected by the dynamic motions of the mooring lines. The heave motion is completely dominated by the WF motions of the vessel. In other words, the first order waves control the FPSO's heave motions, which is expected because it follows the waves.

The heave time series' statistics are shown in Table 7.3. The statistics verifies that the max, min, mean, and standard deviation of the heave motion is approximately the same between Riflex and Simo in spread and co-linear weather conditions, thus the vessel's heave motion is not affected by the dynamic line behavior.

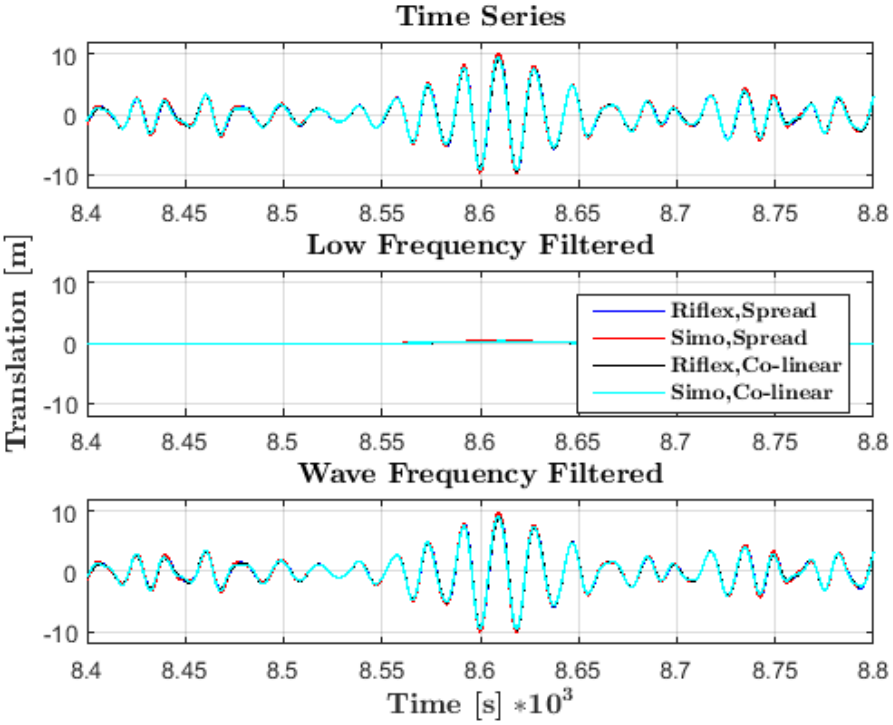

Figure 7.8: Total, LF and WF heave time series of the vessel's COG.

Table 7.3: The max, min, μ and σ of the vessel's COG heave translation.

	Spread							
	Riflex				**Simo**			
Heave	MAX	MIN	μ	σ	MAX	MIN	μ	σ
Total [m]	9.9	-9.7	-0.2	2.1	10.2	-9.7	-0.2	2.1
LF [m]	1.6	-0.4	-0.2	0.1	1.6	-0,4	-0.2	0.11
WF [m]	9.6	-10.0	0.0	2.1	9.9	-10.0	0.0	2.1
	Co-linear							
	Riflex				**Simo**			
Heave	MAX	MIN	μ	σ	MAX	MIN	μ	σ
Total [m]	9.2	-9.4	-0.2	2.0	9.3	-9.3	-0.2	2.1
LF [m]	1.5	-0.4	-0.2	0.1	1.5	-0,4	-0.2	0.1
WF [m]	9.0	-9.6	0.0	2.0	9.1	-9.5	0.0	2.1

PSD

Studying the heave motion energy spectrum in Figure 7.9, the energy peak occurs at a frequency of f_{WF} = 0.05274s^{-1}. This frequency corresponds with a period of 19s which is close to the generated wave period, thus the total heave energy comes from the WF first order wave loads. The heave energy is slightly larger in the spread

weather compared to the co-linear weather, thus spread weather excites larger WF heave motions which may be a result of a greater surge-heave-pitch coupling. The FPSO's heave RAOs shows that the heave natural period is 12s which corresponds to a frequency of f = 0.0833. There exist some heave energy at the natural frequency but there is no energy peak which indicates that resonance occur. The generated waves have a period of 18.5 seconds which is 6.5 seconds away from the heave natural period, thus resonance is not expected.

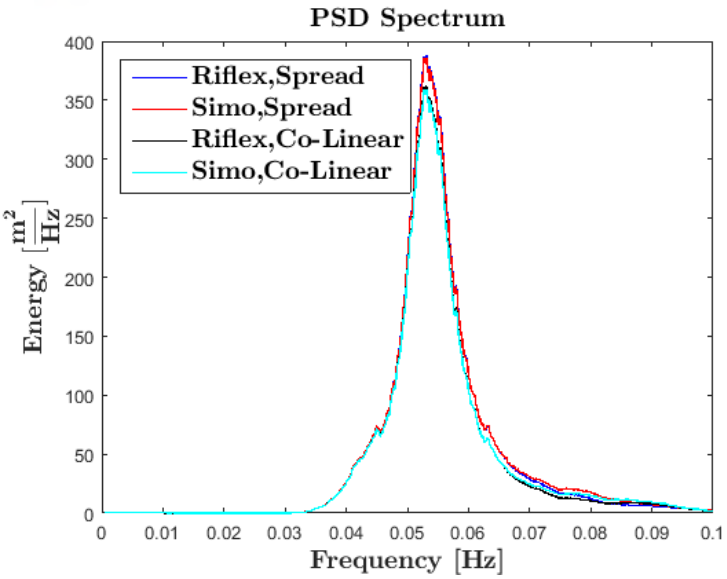

Figure 7.9: Heave energy spectrum.

7.2.5 Roll Motion

Time Series

Figure 7.10 shows the roll time series of the FPSO, and the roll motions are dominated by the WF loads. The LF loads are close to zero and does not excite any significant roll motions. The vessel's roll motion is larger in the spread weather condition, which is expected because the weather is propagating with an angle relative to the bow thus will lead to environmental forces from the side. The time series shows that the system in Riflex experiences a larger roll peak than in Simo during spread weather condition, which is interesting. This might be a result of a roll resonance occurrence in both Simo and Riflex in combination with dynamic line effects that is captured in Riflex. The roll motion between Simo and Riflex in co-linear weather is however approximately the same, and in this environment there is almost no rolling.

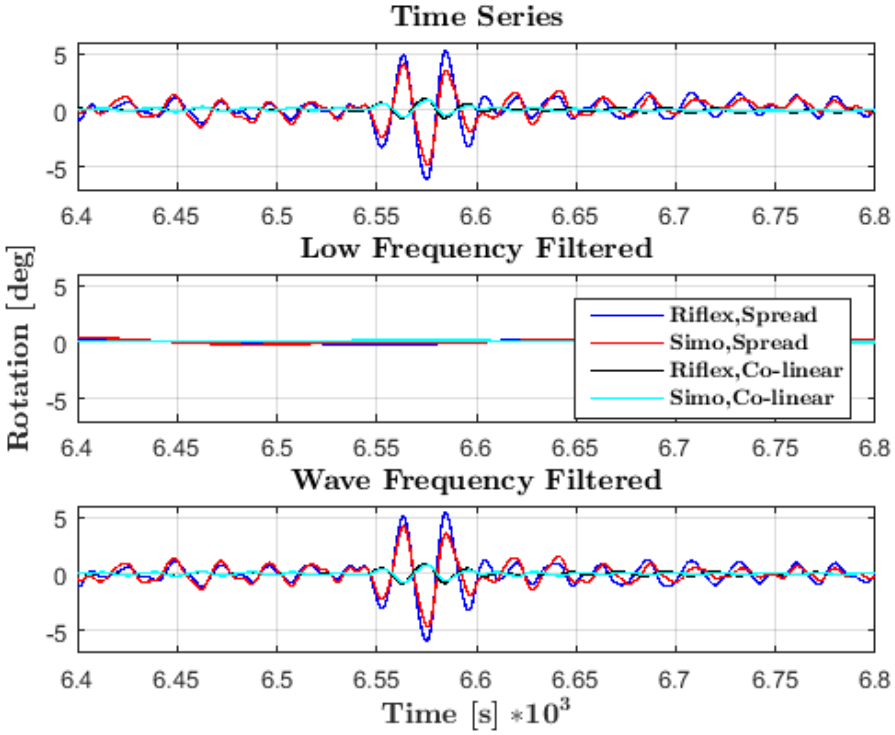

Figure 7.10: Total, LF and WF roll time series of the vessel's COG.

The statistics in Table 7.4 show that the spread weather condition achieves a greater roll maximum, minimum and σ. As mentioned above, Riflex experiences larger roll peaks than Simo in spread weather and that is verified in the table below. Riflex achieves larger WF roll motions, but less LF roll motions than Simo during spread weather. The maximum, minimum, μ and σ are the same between Simo and Riflex in co-linear condition, and the roll motion significantly smaller than in spread weather.

Table 7.4: The max, min, μ and σ of the vessel's COG roll rotation.

	Spread							
	Riflex				**Simo**			
Roll	MAX	MIN	μ	σ	MAX	MIN	μ	σ
Total [deg]	5.3	-6.2	0.2	1.0	4.1	-4.8	0.2	1.0
LF [deg]	0.8	-0.7	0.2	0.2	1.1	-1.3	0.2	0.3
WF [deg]	5.4	-6.0	0.0	0.9	4.2	-4.7	0.0	0.9
	Co-linear							
	Riflex				**Simo**			
Roll	MAX	MIN	μ	σ	MAX	MIN	μ	σ
Total [deg]	1.0	-0.7	0.1	0.2	1.0	-0.7	0.1	0.2
LF [deg]	0.2	-0.1	0.1	0.1	0.2	-0.1	0.1	0.1
WF [deg]	0.9	-0.8	0.0	0.2	0.8	-0.8	0.0	0.2

PSD

The roll energy spectrum in Figure 7.11 show that Simo achieves a larger amount of LF roll motions than Riflex in spread weather, while there are no LF roll energy in the co-linear environment. Large interesting WF energy peaks occur in the spectrum at f = 0.04104s^{-1}. This frequency corresponds to a period of 24.4s which is 1.1s away from the vessel's roll natural period of 25.5s, thus resonant roll motions occur in spread weather. Riflex experiences a smaller resonant roll motion and smaller LF energy than Simo, however Riflex experiences larger WF energy from the first order waves outside the resonance range which might be because of the dynamic line effects.

Studying the co-linear energy spectrum there are almost no energy related to roll motion, which makes sense because all environmental forces is propagating towards the bow. However, there is a tendency of a small energy peak at the roll natural frequency and some, almost unnoticeable LF energy close to f = 0, which might be a hint from the LF wind gusts.

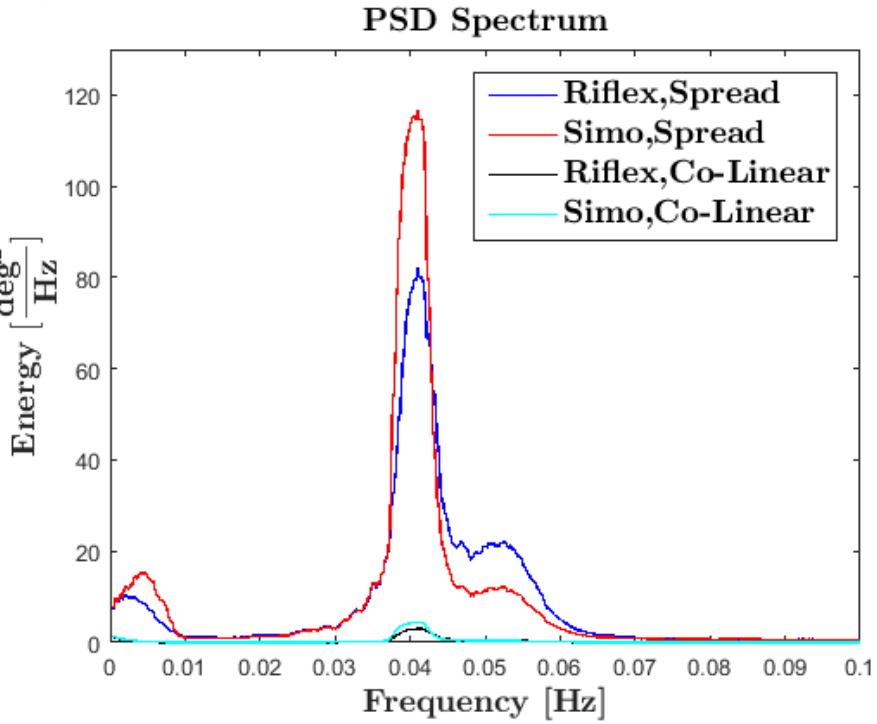

Figure 7.11: Roll energy spectrum.

7.2.6 Pitch Motion

Time Series

In this section, the FPSO's pitch motion will be studied. Figure 7.12 shows the total, LF and WF filtered pitch time series, and there are no visual differences in the vessel's pitch motions between Riflex and Simo in both spread and co-linear weather conditions. Similarly as the FPSO's heave motion, the vessel's pitch motion in Riflex is not considerably affected by the dynamic motions of the mooring lines. The pitch motion is fully dominated by the WF first order waves, where the slowly varying motions are close to zero.

The pitch time series' statistics are shown in Table 7.5. The statistics verifies that the maximum, minimum and σ of the pitch is approximately the same between Simo and Riflex in both weather conditions, however Riflex achieves slightly smaller maximum and minimum pitch response which may be a result from the dynamic mooring behaviour that dampens the pitch responses.

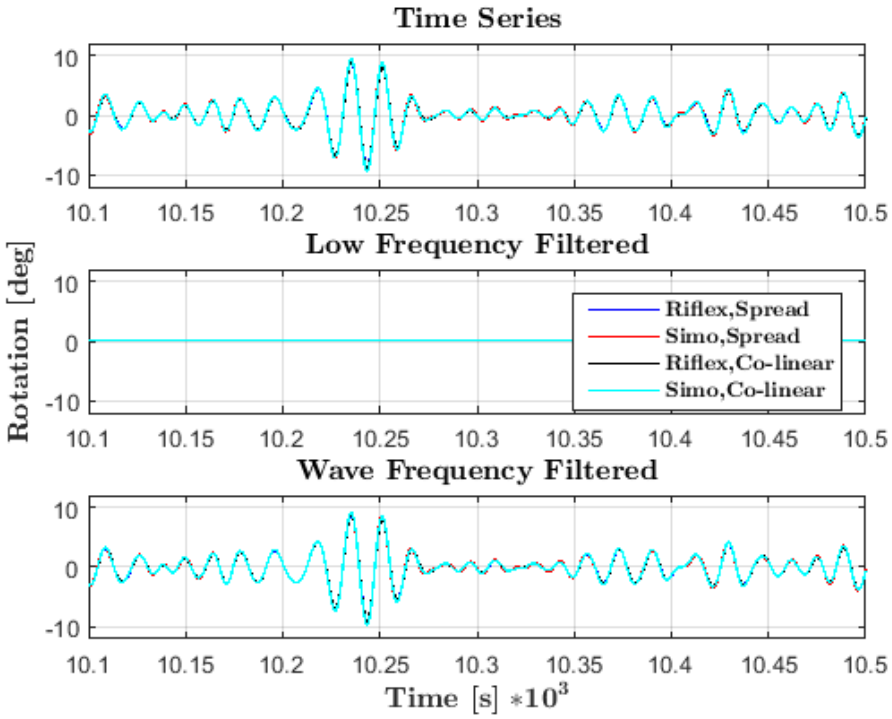

Figure 7.12: Total, LF and WF pitch time series of the vessel's COG.

Table 7.5: The max, min, μ and σ of the vessel's COG pitch rotation.

	Spread							
	Riflex				**Simo**			
Pitch	MAX	MIN	μ	σ	MAX	MIN	μ	σ
Total [deg]	8.9	-8.8	0.2	1.9	9.4	-9.4	0.2	2.0
LF [deg]	0.7	0.1	0.2	0.0	0.7	0.0	0.2	0.0
WF [deg]	8.7	-9.0	0.0	1.9	9.2	-9.6	0.0	2.0
	Co-linear							
	Riflex				**Simo**			
Pitch	MAX	MIN	μ	σ	MAX	MIN	μ	σ
Total [deg]	9.0	-8.9	0.2	1.9	9.4	-9.4	0.2	2.0
LF [deg]	0.6	0.1	0.2	0.0	0.6	0.1	0.2	0.0
WF [deg]	8.8	-9.1	0.0	1.9	9.3	-9.6	0.0	2.0

PSD

The pitch energy spectrum is showed in the figure below. It verifies that the pitch motion is completely dominated by the WF loads, and there is no pitch motion due to LF loads in the energy spectrum. The spectrum shows two peaks within the WF range with a frequency of 0.05481^{-1} and 0.07094^{-1}. These corresponds to a period of 18.3s and 14.1s. The period of 18.3s, is as mentioned earlier in section 7.2.4 approximately the same as the generated wave period of 18.5s, thus the waves excites large pitch motions. The pitch energy peak at 14.1s is in the area of the pitch resonance period of 15s, thus resonant pitch motions occur. The heave natural frequency is $0.083s^{-1}$ which is also within the energy interval, thus a pitch-heave coupling is possible. It is worth to mention that the spread environment excites larger pitch energy in the resonance region, while the co-linear environment excites larger pitch energy outside the resonance region. The spectrum also shows that Simo achieves a slightly larger pitch energy compared to Riflex in the energy spectrum, which can also be seen in the statistics, thus the dynamic behaviour of the mooring lines have a slightly effect on the vessel's pitch motions.

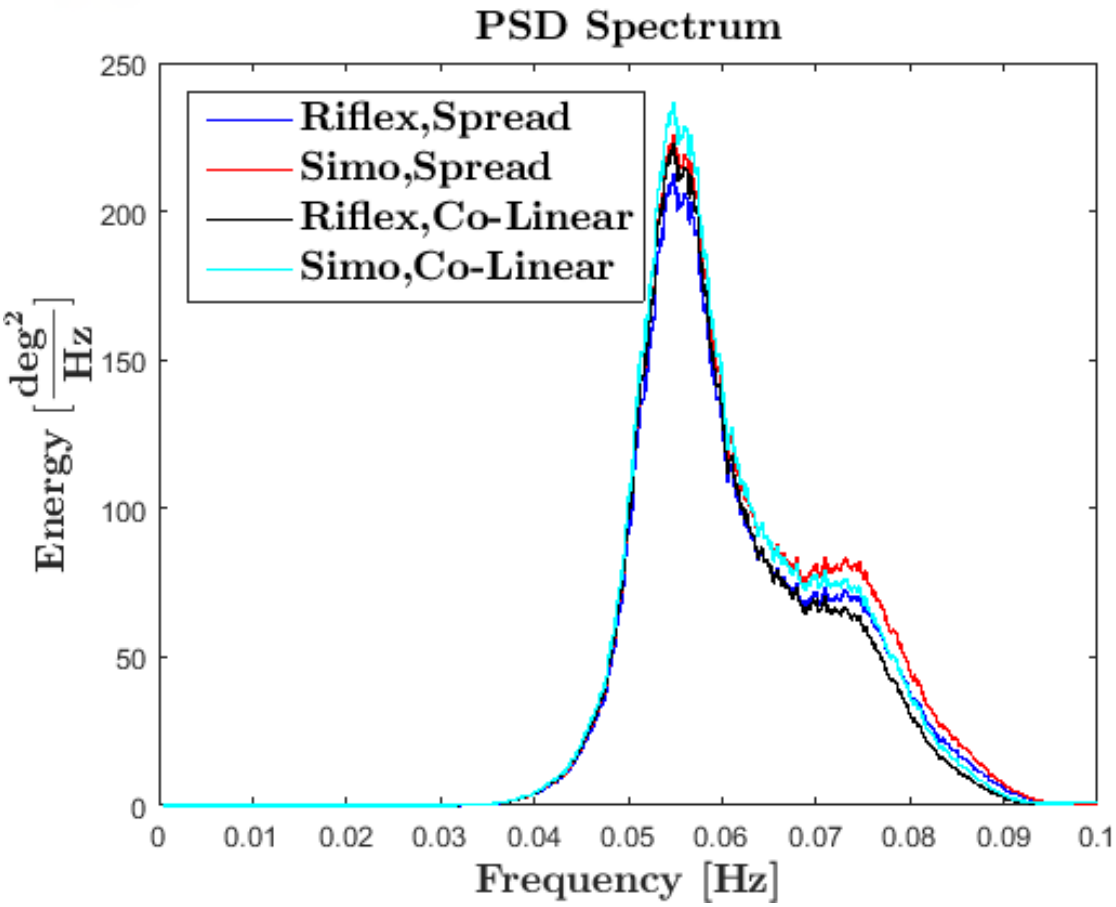

Figure 7.13: Pitch energy spectrum.

7.2.7 Yaw Motion

Time Series

When studying the yaw motion time series in Figure 7.14, it is easy to see that the yaw motion varies more in spread weather compared with co-linear weather. The vessel's initial heading in spread weather is 140 deg and then the vessel starts to weather-vane by yawing towards the wind direction. However in co-linear weather the vessel's heading is more or less stays the same. The vessel's yaw motion in spread environment is dominated by the LF loads. Having said that, the yaw motion is also excited by dynamic WF loads which is likely to be a result of the waves that propagates with an angle relative to the vessel's bow. On the other hand, the vessel's yaw motion in co-linear weather visually stays the same with a hint of small LF yaw excitation, while there are no WF yaw motions present in this environment. It is also noticeable that

Simo achieves larger yaw motions than Riflex in spread environment.

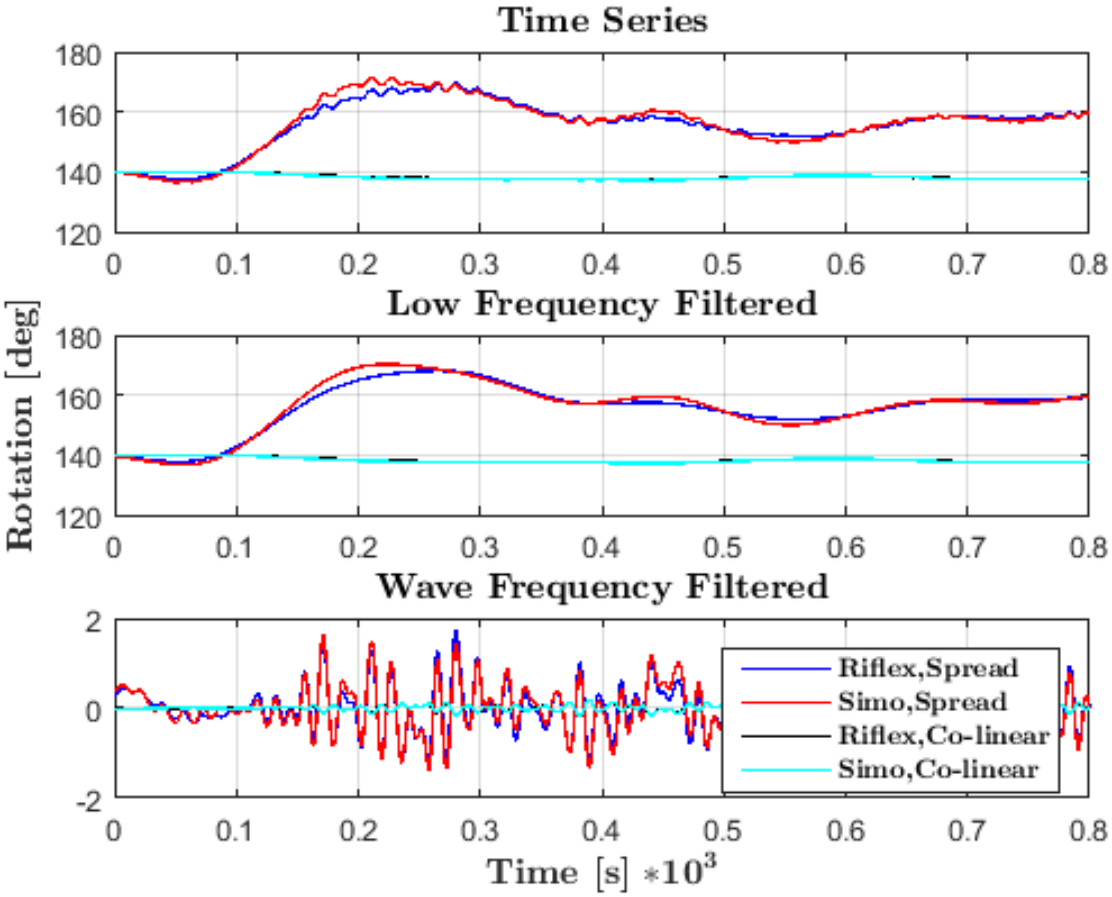

Figure 7.14: Total, LF and WF yaw time series.

The time series' statistics are shown in Table 7.6. Statistics show that the vessel weathervanes and achieves a mean heading of 157.0 deg, which is a heading between the wind and wave direction in spread weather in both Riflex and Simo. The mean heading in co-linear weather is however approximately 137.6 deg in both Riflex and Simo. All weather is propagating in 320 deg which is towards the vessel's initial heading, but the vessel seems to achieve a mean heading of 137.6 degrees. This is a result from the wind gusts which excites yaw motion due to the non-symmetry of the FPSO's superstructure. The vessel's wind coefficients presented in Table B.1 in Appendix B shows that the vessel starts to yaw when the wind is coming in towards the bow. Notice that the maximum yaw motions in spread weather are smaller in Riflex compared to Simo, which most probable is due LF damping from the mooring lines.

Table 7.6: The max, min, μ and σ of the vessel's COG yaw translation.

	Spread							
	Riflex				**Simo**			
Yaw	MAX	MIN	μ	σ	MAX	MIN	μ	σ
Total [deg]	169.6	137.5	157	3.2	171.5	136.5	157.0	3.7
LF [deg]	168.1	137.7	157.0	3.2	170.3	136.8	157.0	3.6
WF [deg]	2.5	-1.6	0.0	0.5	2.3	-1.6	0.0	0.5
	Co-linear							
	Riflex				**Simo**			
Yaw	MAX	MIN	μ	σ	MAX	MIN	μ	σ
Total [deg]	140.1	136.1	137.6	0.6	140.1	135.9	137.5	0.7
LF [deg]	140.1	136.3	137.6	0.6	140.1	136.1	137.5	0.7
WF [deg]	0.3	-0.4	0.0	0.1	0.3	-0.3	0.0	0.1

PSD

The yaw PSD spectrum in Figure 7.15 verifies that the vessel's yaw motion is dominated by the LF loads in both spread and co-linear weather, where the WF yaw energy is almost negligible in comparison. The LF yaw energy in spread weather has an energy peak at frequency 0.001296 which corresponds to a period of 771.6 seconds, which means that environmental loads with extremely large periods are causing the yawing. The wind gusts have such large periods and is likely to excite these LF motions. The LF energy in the co-linear environment has no clear peak, but the yaw energy is increasing for decreasing frequencies towards zero, thus wind gusts excite these LF motions too. It is noteworthy that the yaw motion in spread weather conditions is slightly smaller in Riflex compared to Simo, which may be a result from the dynamic line damping.

Small yaw WF motions in spread weather are observed in the time series and a small energy peak is observed at $f_{WF} = 0.054 s^{-1}$ which corresponds with the generated wave period of 18.5s. The WF motions in spread weather is approximately the same in Simo and Riflex. There exist no WF yaw energy in the co-linear environment, thus only the LF wind gusts excite LF yaw motions in this environment.

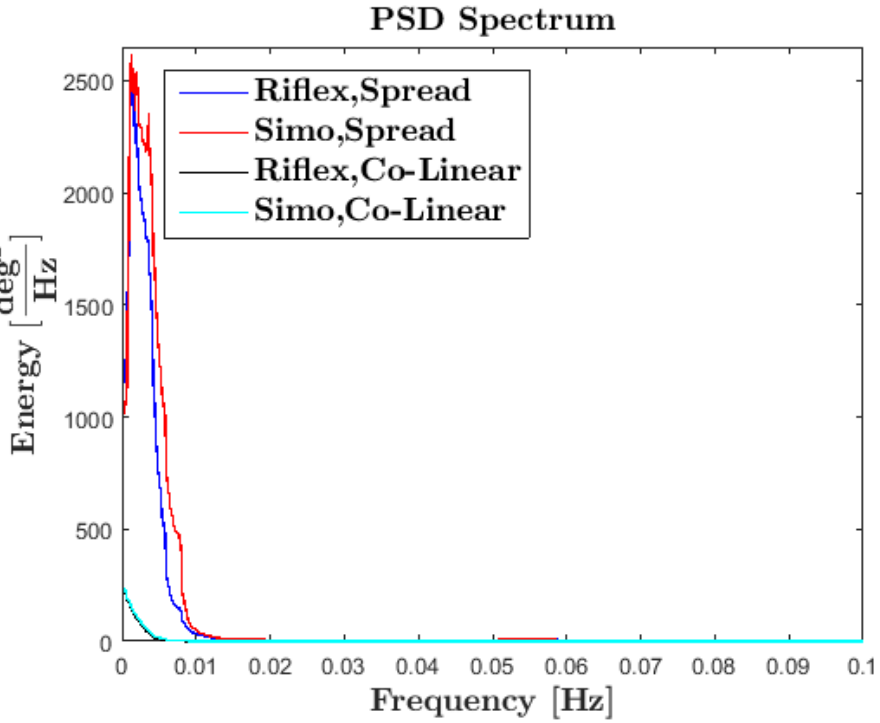

Figure 7.15: Yaw energy spectrum.

7.2.8 Most Probable Maximum, Minimum and 90% Fractile Motions

This subsection will present the most probable maximum, minimum and 90% fractile motion response in all six dof in ULS conditions. The characteristic design value of the vessel's offset is given as the most probable maximum, and is found from the Gumbel probability distributions that are based on all simulations in all dof in both weather conditions in Simo and Riflex. Figure 7.16 shows an example of two gumbel probability density function illustrations in surge (Figure 7.16a) and in sway (Figure 7.16b). The MPM and 90% fractile values are calculated from these distributions. Simo seems to achieve larger maximum and minimum surge and sway response compared to Riflex. It is also noteworthy that the Riflex gumbel distributions are much slender and more closely distributed towards the MPM than in Simo, thus the standard deviation is larger in Simo compared to Riflex.

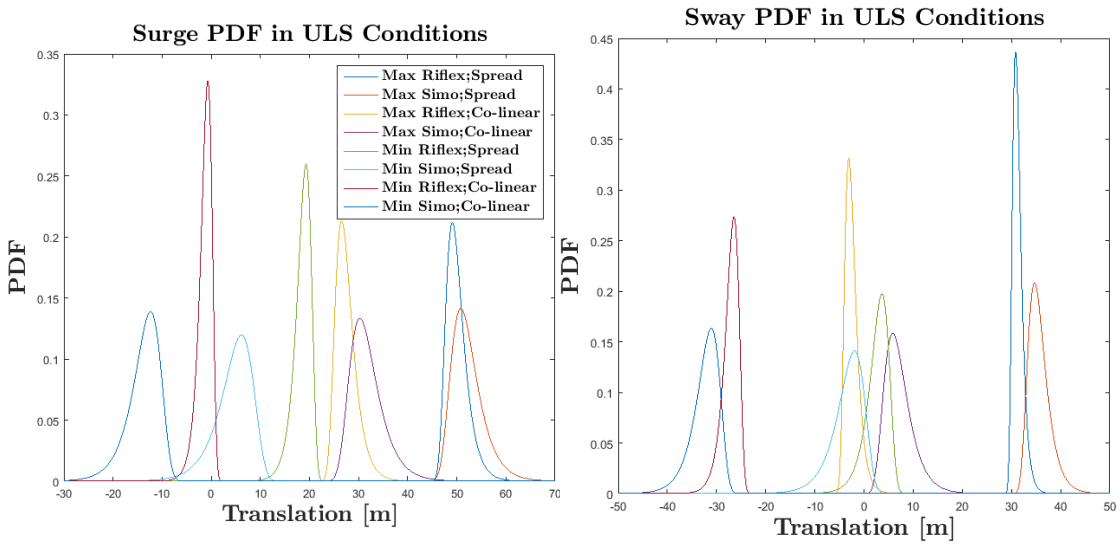

(a) Max.&Min. Surge PDF

(b) Max.&Min. Sway PDF

Figure 7.16: Max.&Min. Gumbel pdf of the surge (7.16a) and sway (7.16b) translation in Riflex and Simo for both spread & co-linear weather in ULS conditions.

Table 7.7 presents the MPM and 90% fractile values of the vessel's six dof motions in both weather conditions in Simo and Riflex. Based on these extreme motion statistics the MPM surge, sway, roll and yaw motions are considerably larger in the spread weather compared to the co-linear weather. This is expected because spread weather excites larger motion response in these dof as previously seen in the motion time series and PSDs. To give an illustration, the MPM of the vessel's surge motion have been compared in Riflex, and the surge MPM is 46.1% larger in spread weather. The MPM of the vessel's heave and pitch motions are however approximately the same between spread and co-linear weather, and are not significantly affected by the different numerical softwares, thus not considerably affected by the dynamic line behaviour. It is noticeable that the MPM surge, sway and yaw motions in Riflex are smaller than in Simo for both weather conditions, which is as mentioned earlier a result from the dampened maximum values due to the dynamic line damping.

Table 7.7: The most probable and 90% fractile max, min, and μ and σ of the vessel's motions based on the 50 ULS spread simulations.

	Spread Weather ULS Condition											
	Riflex						**Simo**					
	Max		**Min**		**Stat**		**Max**		**Min**		**Stat**	
	MPM	90%	MPM	90%	μ	σ	MPM	90%	MPM	90%	μ	σ
Surge [m]	48.8	53.9	19.1	15.0	32.7	4.0	50.4	57.9	5.7	-3.1	30.3	6.1
Sway [m]	30.7	33.2	3.4	-2	20.1	3.9	34.4	39.5	-2.4	-9.8	19.5	5.3
Heave [m]	7.5	9.4	-8.3	-10	-0.2	2.1	7.7	9.6	-8.4	-10.1	-0.2	2.2
Roll [deg]	3.8	5.1	-5	-6.7	0.2	1.0	3.7	4.8	-5.2	-7.2	0.2	1.0
Pitch [deg]	6.9	8.5	-7.3	-8.8	0.2	1.9	7.3	8.9	-7.8	-9.4	0.2	2.0
Yaw [deg]	165.5	168.7	136.6	136.0	157.0	3.4	168.1	173.4	135.8	135	157.0	3.7
	Co-linear Weather ULS Condition											
	Riflex						**Simo**					
	Max		**Min**		**Stat**		**Max**		**Min**		**Stat**	
	MPM	90%	MPM	90%	μ	σ	MPM	90%	MPM	90%	μ	σ
Surge [m]	26.3	31.3	-0.9	-4.1	11.5	3.8	29.8	37.8	-12.8	-20.4	10.1	6.1
Sway [m]	-3.3	0.0	-26.7	-30.5	-12.5	3.2	5.5	12.2	-31.4	-37.9	-11.5	5.3
Heave [m]	7.2	8.9	-8	-9.6	-0.2	2.1	7.3	9.1	-8,1	-9.6	-0.2	2.1
Roll [deg]	0.8	1.1	-0.6	-0.7	0.1	0.2	0.8	1.2	-0.6	-0.8	0.1	0.2
Pitch [deg]	6.9	8.5	-7.3	-8.8	0.2	1.9	7.2	8.9	-7.8	-9.4	0.2	2.0
Yaw [deg]	140.1	140.2	135.2	134.2	137.6	0.7	140.1	140.4	135.0	133.8	137.6	0.8

7.3 Accidental Limit State Motion Analyzes

This section will present and discuss the MPM and 90% fractile statistics based on Gumbel distributed maximum motions from the 50 ALS simulations in spread and co-linear weather. The ALS time series, its statistics and PSDs of the six dof motions are not presented in the report, but can be found in Appendix C.

7.3.1 Surge-Sway Translation

Figure 7.17 illustrates the vessel's offset in the horizontal plane in ALS co-linear and spread weather conditions. The offset is similar as in the ULS conditions, however the offset is more chaotic and covers a larger area. The illustration clearly shows the LF mooring damping effect on the sway and surge motions of the Riflex system.

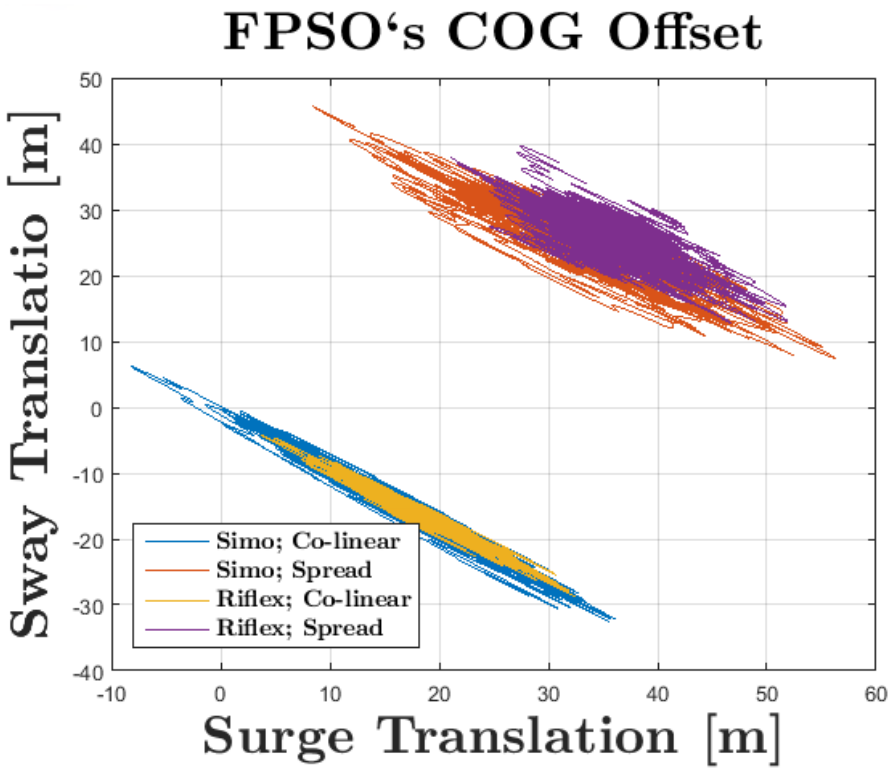

Figure 7.17: The FPSO's surge-sway translation of the COG in the global axis system in ALS co-linear and spread weather conditions.

7.3.2 Most Probable Maximum, Minimum and 90% Fractile Motions

This subsection will present and discuss the extreme six dof motions in ALS co-linear and spread weather conditions. The extreme six dof motion statistics are calculated from the Gumbel probability density distributions. Figure 7.18 below shows the Gumbel distributions of the surge (Figure 7.18a) and sway (Figure 7.18b) translation in ALS conditions.

By studying the surge and sway Gumbel distributions, the largest most probable maximum and minimum translations occurs in spread and co-linear weather respectively. The most probable maximum or minimum is located as the maximum or peak value in the pdf distributions, while the motion's 90% fractile value corresponds to the 90% area below the Gumbel distribution. Similar to the ULS Gumbel distributions in section 7.2.8, the ALS Riflex Gumbel distributions are much slender and more are closely distributed towards the MPM than the Simo distributions, thus the standard deviation is larger in Simo compared to Riflex.

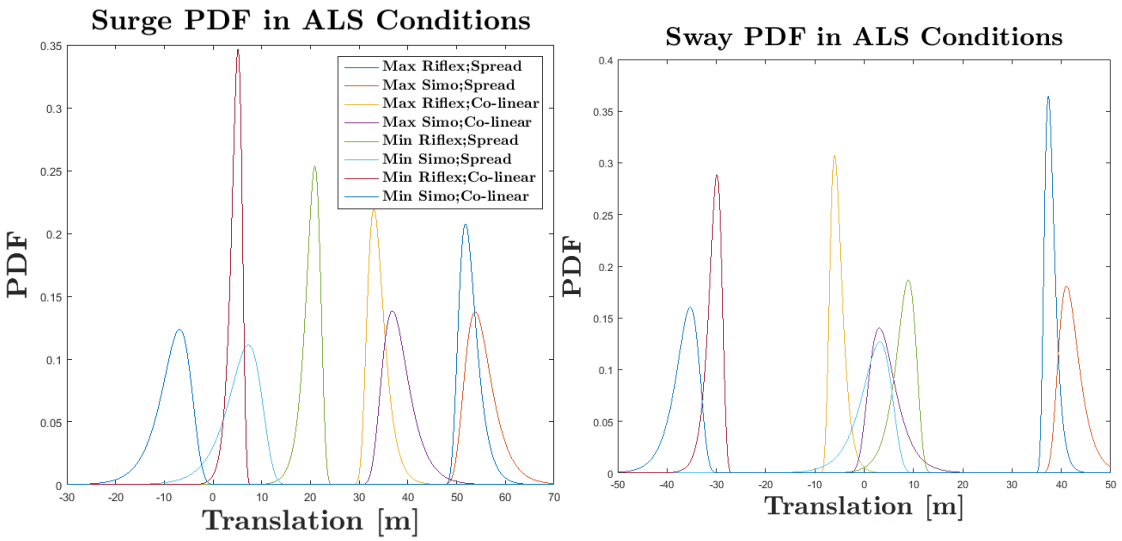

(a) Max.& Min. Surge PDF

(b) Max.& Min. Sway PDF

Figure 7.18: Max.& Min. Gumbel pdf of the surge (7.16a) and sway (7.16b) translation in Riflex and Simo for both spread & co-linear weather in ALS conditions.

The MPM and 90% fractile values of the vessel's extreme six dof motions in both ALS weather conditions in Simo and Riflex are presented in Table 7.8. Similar to the ULS extreme motion statistics, the ALS MPM surge, sway, roll and yaw motions are considerably larger in the spread weather compared to the co-linear weather. As observed from the ULS yaw motions in section 7.2.7, the vessel has larger difficulties to weathervane in spread weather due to the different weather directions, which is also the case in the ALS simulations and can be observed in Appendix C. As a result of this the vessel achieves larger sway, surge, roll and yaw motion response. These dof's extreme motions are also as expected larger in ALS compared to the extreme ULS motion responses, which is because of the one line failure. For comparison, the spread MPM surge value in Riflex in ALS is 5.2% larger than in ULS. A line break will lead to larger tensions and dynamic behaviour in the adjacent lines, which will thus lead to larger MPM surge, sway, roll and yaw motions.

The MPM heave and pitch motions are exactly the same between ALS and ULS, which means that a line break does not affect these vessel motions. As observed in the ULS heave and pitch motion time series, they are approximately the same between Riflex and Simo, thus these motions are not considerably affected by the dynamic behaviour of the lines. A line break will increase the line tensions and dynamic behaviour of the adjacent lines, but it apparently does not affect the vessel's maximum

heave and pitch motions.

Similar to the ULS MPM values, the ALS MPM surge, sway and yaw motions in Riflex are smaller than in Simo for both weather conditions as a result of the dynamic line damping in Riflex. The standard deviation in Simo is thus much larger than in Riflex, which means that the surge and sway variation are larger and thus the vessel covers a larger range in Simo.

The vessel yaws freely about the turret, but the turrets MPM yaw motion is larger after a line break. The vessel's mean heading based on the 50 simulations is however the same between the ULS and ALS simulations.

Table 7.8: The most probable and 90% fractile max, min, and μ and σ of the vessel's motions based on the 50 ALS spread and co-linear simulations.

	Spread Weather ALS Condition											
	Riflex						**Simo**					
	Max		**Min**		**Stat**		**Max**		**Min**		**Stat**	
	MPM	90%	MPM	90%	μ	σ	MPM	90%	MPM	90%	μ	σ
Surge [m]	51.5	56.7	20.7	16.5	35.0	4.2	53.4	61.1	6.7	-2.8	32.5	6.4
Sway [m]	37.2	40.2	8.6	3.0	26.0	4.0	40.7	46.6	2.7	-5.6	25.3	5.5
Heave [m]	7.5	9.4	-8.3	-10.0	-0.2	2.1	7.7	9.6	8.4	-10.1	-0.2	2.2
Roll [deg]	3.7	5.1	-5.1	-6.8	0.2	1.0	3.7	4.7	-5.3	-7.6	0.2	1.1
Pitch [deg]	6.9	8.5	-7.4	-8.9	0.2	1.9	7.3	8.9	-7.8	-9.5	0.2	2.0
Yaw [deg]	166.7	170.3	134.1	132.5	157.0	3.6	169.7	175.5	133.5	132.2	156.9	3.9
	Co-linear Weather ALS Condition											
	Riflex						**Simo**					
	Max		**Min**		**Stat**		**Max**		**Min**		**Stat**	
	MPM	90%	MPM	90%	μ	σ	MPM	90%	MPM	90%	μ	σ
Surge [m]	32.7	37.6	4.9	1.9	17.5	3.9	36.4	44.1	-7.4	-15.9	16.1	6.2
Sway [m]	-6.2	-2.7	-30.1	-33.7	-15.9	3.3	2.6	10.3	-35.7	-42.2	-15.0	5.6
Heave [m]	7.2	8.9	-8	-9.6	-0.2	2.1	7.3	9.1	-8,1	-9.6	-0.2	2.1
Roll [deg]	0.7	1.0	-0.6	-0.7	0.1	0.2	0.8	1.2	-0.6	-0.8	0.1	0.2
Pitch [deg]	6.9	8.5	-7.3	-8.9	0.2	1.9	7.2	8.9	-7.8	-9.4	0.2	2.0
Yaw [deg]	139.8	140.3	135.2	134.2	137.7	0.75	140.0	141.2	134.7	133.6	137.6	0.9

7.4 Ultimate Limit State Tension Analyzes

As shown earlier in the section 7.2, large motions of the vessel's COG are excited when the moored floating FPSO are exposed to extreme weather conditions. As mentioned earlier in section 3.1.1, the turret motions are important because they excite dynamic tension loads in the mooring lines. The turret's heave-pitch-surge elliptic motions are observed in both ULS and ALS simulations. Figure 7.19 shows the turret's elliptic heave-surge motion pattern in an ULS simulation in spread weather conditions.

The straight lines in the figure are the mooring lines which extends from the anchor positions to the turret. Notice that the lines are formed as catenaries in the simulations and not straight like in the figure. The Long lines are the windward lines which experiences a large mean tension, but a smaller dynamic tension. The Longer and Longest lines are the leeward lines which experiences a larger dynamic tension due to the larger elliptic diameter which can be observed in the figure.

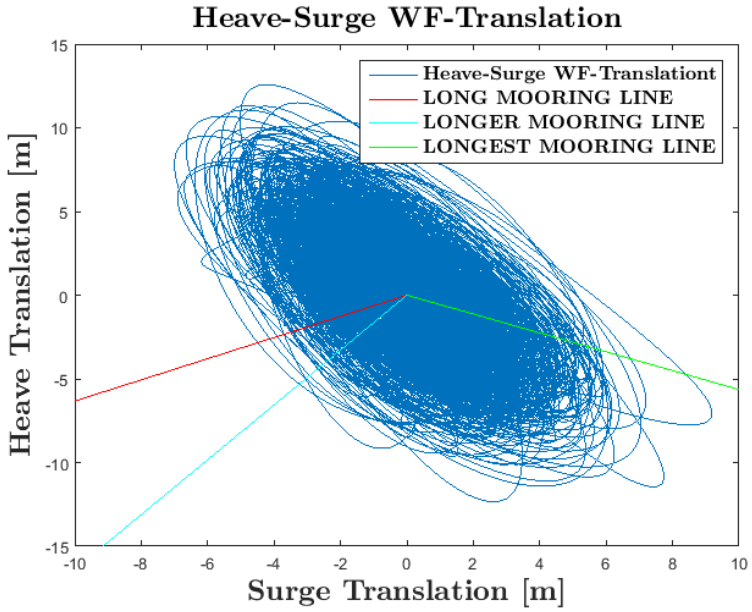

Figure 7.19: Turret's heave-surge WF-translation in ULS spread weather in Riflex.

The line tension results will in the sections below be presented. One windward and leeward line will be discussed and presented in form of time series, PSDs and statistics.

7.4.1 Windward Line Long 4

Time Series

Figure 7.20 shows the total, low frequency and wave frequency filtered time series of line Long 4. The WF filtered time serie gives a great illustration of the dynamic differences between Simo and Riflex, where the latter achieves a much greater dynamic tension response. The vessel's heave-pitch-surge motions excite dynamic top end motions, which creates dynamic line motions and thus dynamic tension responses. The LF filtered time serie shows that Simo achieves a larger LF tension response com-

pared to Riflex. The slowly varying tension loads in the cutted time serie have a period of approximately 180s. It is noticeable that among the total time series of line Long 4, the largest tension response in Riflex occurs during spread environment, which is probably a result of the weathervaning difficulties in spread weather.

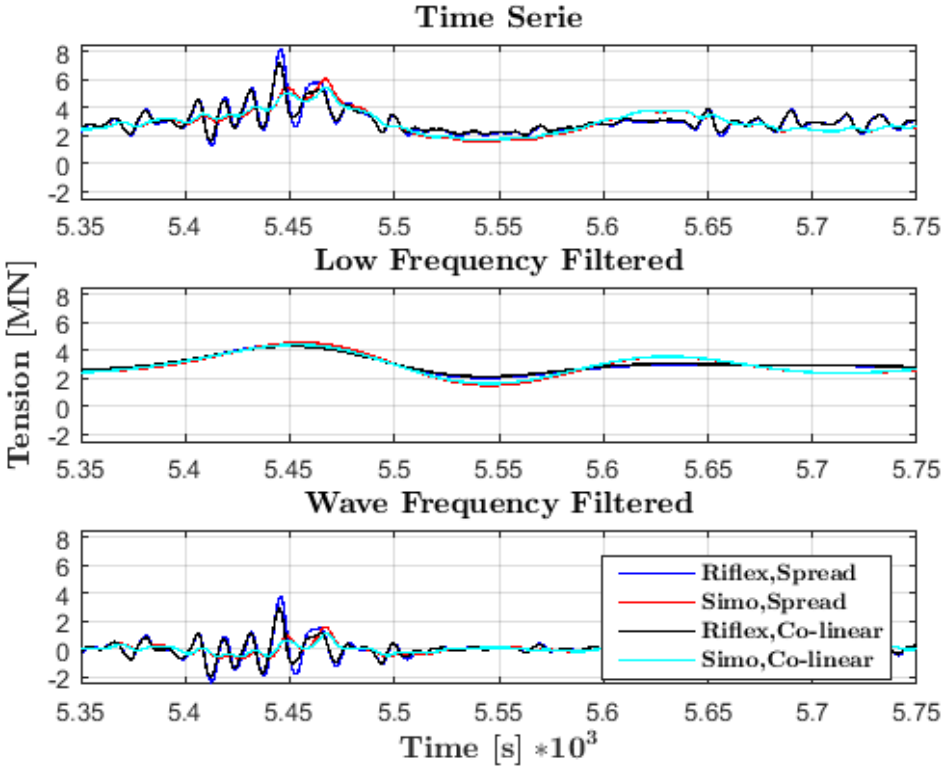

Figure 7.20: Total, LF and WF tension time series of line Long 4.

Tension statistics of line Long 4 is presented in Table 7.9. The statistics show that the percentage difference in the maximum dynamic WF line tension between Riflex and Simo is 57.3% and 52.3% in spread and co-linear weather, respectively. Riflex obtains over twice as much dynamic tension than Simo, and the difference is because of the mass and damping forces that are excited from the dynamic line motions, which are not considered in Simo. The maximum LF line tension is slightly larger in Simo, and the difference between Riflex and Simo is 3.1% and 5.6% in spread and co-linear weather respectively. Even though Simo slightly overestimates the maximum LF tension forces, the LF standard deviation in Simo is 34.9% and 31.8% larger than in Riflex in respectively co-linear and spread environment. The LF tension variation is thus larger in Simo however, the WF tension variation is larger in Riflex. It is noticeable that the mean tension forces are larger in Riflex during both weather conditions,

thus the mean tension forces are underestimated in Simo. The max LF forces are larger than the max WF forces.

Table 7.9: Max, min, μ and σ of the tension in windward line Long 4.

	Spread							
	Riflex [kN]				**Simo [kN]**			
Long 4	MAX	MIN	μ	σ	MAX	MIN	μ	σ
Total	8162.4	131.0	2867.9	583.0	6055.5	1586.3	2779.2	463.1
LF	4419.9	2035.9	2867.5	276.8	4560.8	1493.6	2778.5	405.65
WF	3762.3	-2955.0	-0.1	503.2	1605.2	-711.3	0.1	161.5
	Co-linear							
	Riflex [kN]				**Simo [kN]**			
Long 4	MAX	MIN	μ	σ	MAX	MIN	μ	σ
Total	7163.7	254.6	2901.7	525.0	5902.3	1609.9	2805.1	455.9
LF	4293.9	2131.2	2901.3	263.4	4547.8	1586.4	2804.4	404.5
WF	2888.0	-2847.6	0.0	444.6	1377.7	-606.7	0.2	147.9

PSD

The figure below shows the PSD spectrum of Long 4. The spectrum verifies that the LF tension forces dominates the total tension in Simo, and that Simo achieves greater LF tension response compared to Riflex. The LF energy peak is concentrated around f = 0.005284s^{-1} which corresponds to a slowly varying period of 189s. Energy is also concentrated around f = 0.054s^{-1} which is the frequency of the waves. The energy in this region verifies that the dynamic WF tension is larger in Riflex, and it also show that the dynamic WF tension is larger in spread environment.

The spectrum in Riflex shows that there exist energy within the frequency interval f = [0.065 0.09]s^{-1}, which corresponds to a period interval of T = [15.4 11.1]s. The FPSO's heave and pitch natural period is respectively 12 and 15 seconds, and heave and pitch resonance may be the reason for the tension energy within the energy interval in question.

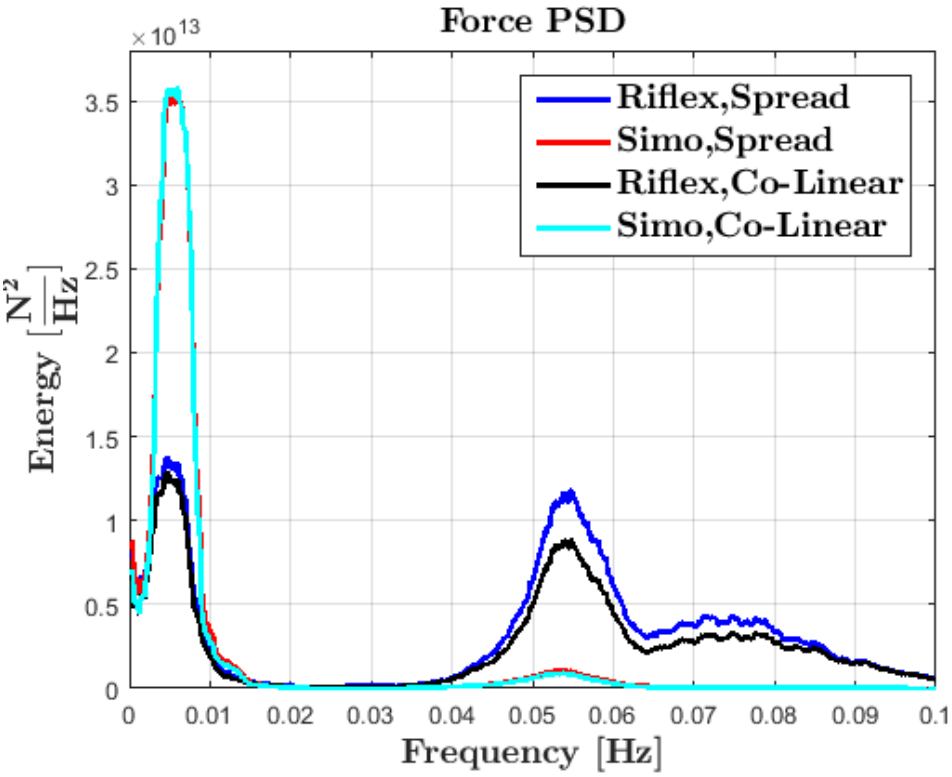

Figure 7.21: Caption

Figure 7.22: Tension energy spectrum of line Long 4.

7.4.2 Leeward Line Longest 4

Time Series

In this section, the tension in leeward Longest 4 from cluster 3 will be discussed. The tension time series of Longest 4 in Figure 7.23 shows that the largest line tension occur in spread weather. The wave frequent line tension in Simo is significantly lower than the WF line tension in Riflex when studying the WF filtered time serie. The WF tension in Simo is visually the same in co-linear and spread weather with a small amplitude, however the WF line tension in Riflex is larger in spread compared to co-linear weather. The dynamic WF tension is significantly larger in Riflex than Simo. The LF filtered time series show that the spread weather excite larger LF motions than co-linear weather.

An interesting phenomenon occurs in the total time serie. The tension in Longest 4 goes to zero and the term for this is slack. Slack in Longest 4 occurs three times con-

secutively during the cutted time serie, and causes large stresses in the line. These cyclic slack events is very important with regards to fatigue limit state analyzes, however this have not been studied in this thesis.

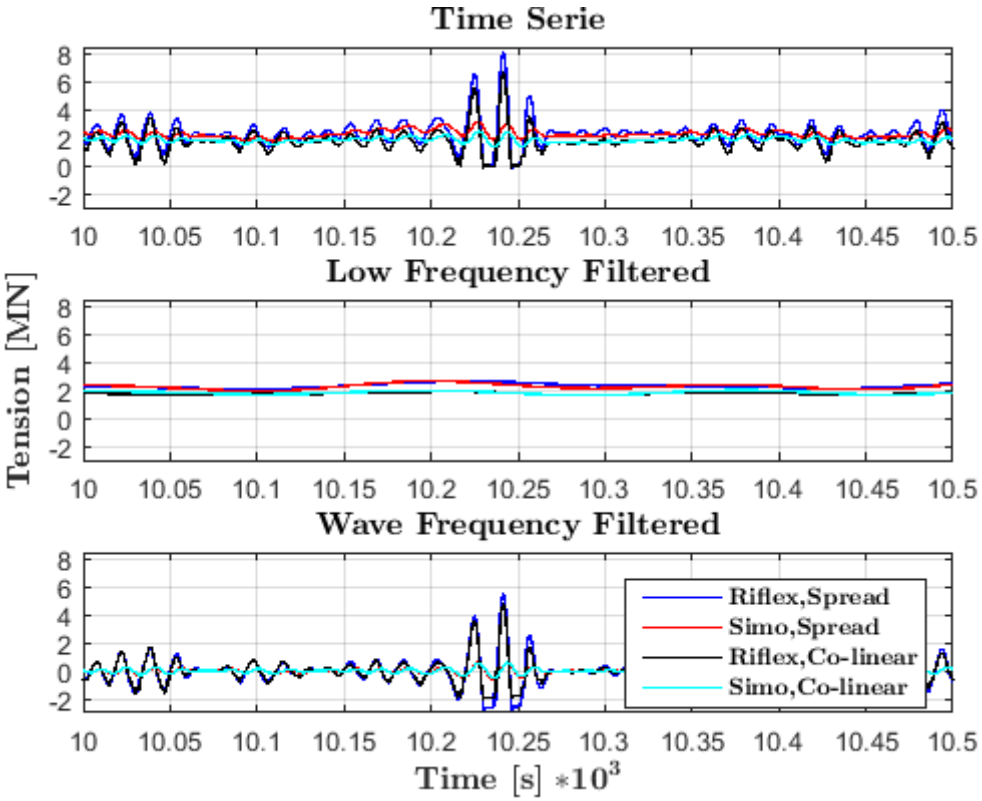

Figure 7.23: Total, LF and WF tension time series of line Longest 4.

The table below shows the time series' statistics. The first thing that attracts attention, is the significant differences between the WF line tension between Riflex and Simo of 89.0% and 88.0% in spread and co-linear weather respectively. Here the important dynamic contribution from the mooring line motions is observed. The maximum LF line tension is however larger in Simo compared to Riflex with a percentage difference of 5.8% and 9.2% in spread and co-linear. The vessel's offset motions are dampened by the mooring lines in Riflex which will result in smaller LF tension loads. The line damping is not considered in Simo thus larger LF motions and tensions will occur.

The statistics from the total time serie shows that the maximum line tension differences between Riflex and Simo is 61.3% and 63.1%, in spread and co-linear weather respectively. The difference is dominated by the WF dynamic forces which are much

larger in Riflex. Notice that in the total minimum value in Riflex is negative comapred to Simo which occurs in both weather conditions. This means that Longest 4 goes slack in Riflex, but not in Simo. It is also noticeable that the WF differences between Riflex and Simo, are larger in the time series for the leeward Longest 4 compared to the windward Long 4.

Table 7.10: The max, min, μ and σ of the tension in leeward line Longest 4.

	Spread							
	Riflex				**Simo**			
Long 4	MAX	MIN	μ	σ	MAX	MIN	μ	σ
Total [kN]	8117.3	-225.3	2301.7	691.1	3141.9	1562.0	2268.2	247.3
LF [kN]	2664.3	1955.6	2301.7	123.0	2827.8	1673.1	2268.8	193.6
WF [kN]	5499.6	-2816.6	-0.2	678.6	606.4	-622.1	0.1	133.5
	Co-linear							
	Riflex				**Simo**			
Long 4	MAX	MIN	μ	σ	MAX	MIN	μ	σ
Total [kN]	6686.0	-260.6	1769.2	609.1	2465.1	123.9	1839.2	175.5
LF [kN]	1991.4	1595.4	1769.2	66.2	2193.0	1549.6	1839.5	116.5
WF [kN]	4840.5	-2086.6	-0.1	605	582	-534.3	0.2	123.2

PSD

Figure 7.24 shows the PSD spectrum which shows where the tension energy is concentrated in the frequency domain. There are three energy peaks that attracts attention, and these occur at $0.005189 s^{-1}$, $0.05481 s^{-1}$ and $0.07094 s^{-1}$ and corresponds to a period of 193, 18.2 and 14.1 seconds. The energy peaks at 193 and 18.2 seconds is a result of line tension excited by the slowly varying wave motions and the wave frequent wave motions respectively. The energy peak at 14.1 second is close to the pitch natural period, and dynamic line tensions may occur because the vessel achieves pitch resonance.

The dynamic line tension dominates the total tension in Riflex, however in Simo the slowly varying line tensions are dominating. Notice that Riflex achieves both a larger WF and LF energy in spread weather compared to co-linear.

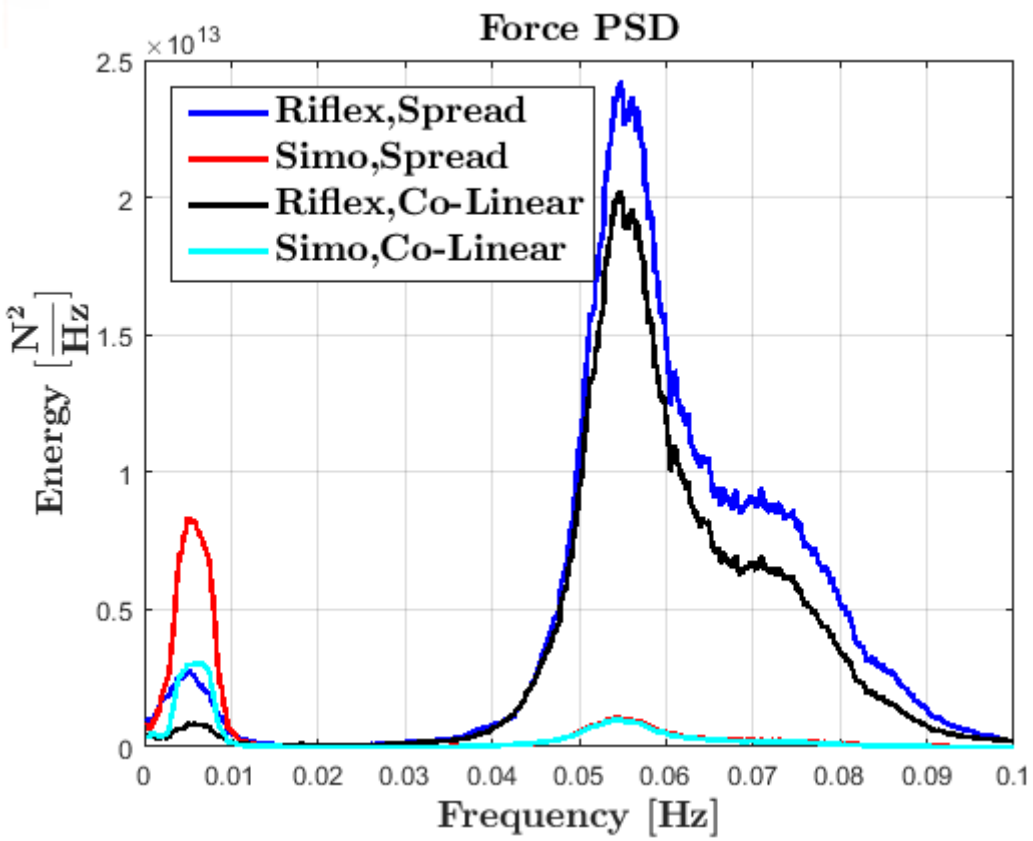

Figure 7.24: Tension energy spectrum of line Longest 4.

7.4.3 Line Characteristics of Windward Long 4

The figure below illustrates the difference in tension behavior of line Long 4 in both Riflex and Simo. The line characteristic in Riflex is more chaotic compared to the line characteristics in Simo. The line characteristic in Simo goes back and forth in a slightly non-linear curve, with some dynamics which is due to the dynamic top end motions of the vessel. Riflex however, achieves greater tension dynamics due to the dynamic top end motion of the vessel in combination with the dynamic motion of the mooring lines. It can also be observed that the vessel's surge motion is dampened in Riflex as a result from the damping provided by the mooring lines.

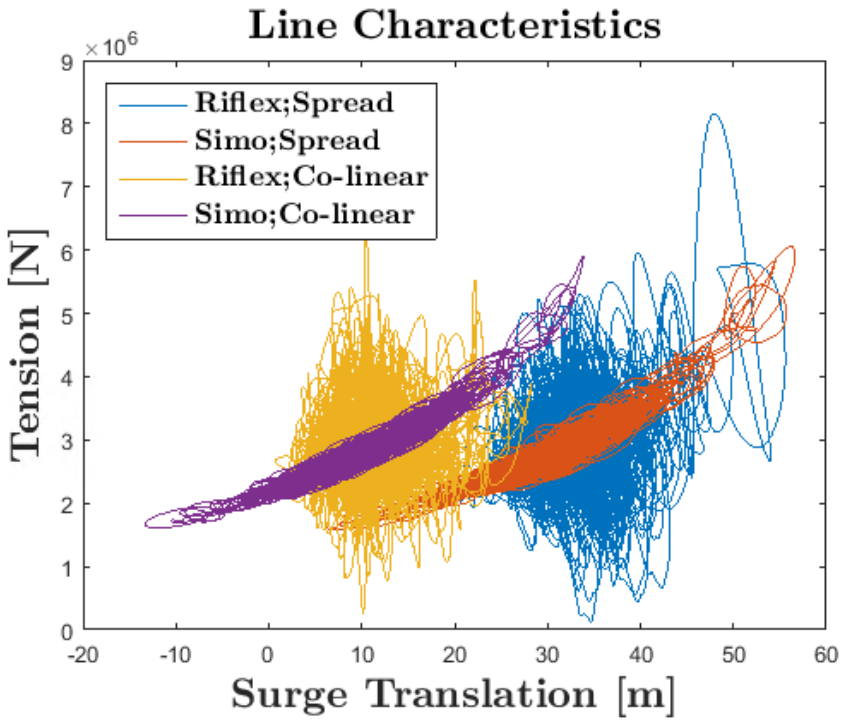

Figure 7.25: Surge line characteristic of the vessel's COG.

7.4.4 Most Probable Maximum, Minimum and 90% Fractile Tensions

The extreme line tension statistics are based on the Gumbel distribution and is presented and discussed in this section. The characteristic design line tension are similar to the vessel's offset given as the most probable maximum, and will be presented.

Spread Weather

Figure 7.26 is based on the each line's gumbel probability distribution, and gives an illustration of the most probable- and 90% fractile- max and min of each line during spread environment. The most probable max(MPM_{MAX}) line tension during spread weather is largest in the Longest lines, and the smallest most probable max is in the Longer lines in Riflex. In Simo however, the most probable max is largest in the Long lines and smallest in the Longer lines. The most probable min(MPM_{MIN}) in Riflex is positive in the Long lines, which means that the Long lines are most probably not going slack. The Longer and Longest lines however have a negative most probable min and are most probably going slack. The most probable minimum in Simo is however positive in all lines, and no lines go slack.

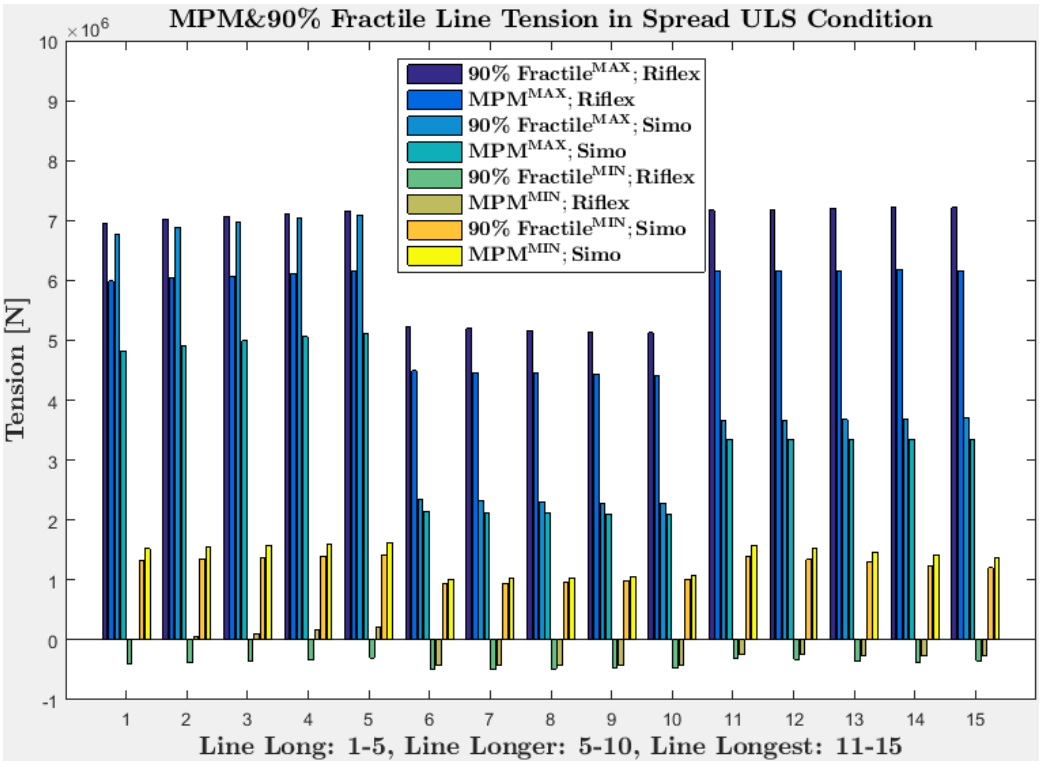

Figure 7.26: The MPM_{max}, 90%$_{max}$, MPM_{min}, 90%$_{min}$ line tension in Riflex and Simo during spread weather.

The table below show the statistics values of the most exposed cluster Long and Longest in Figure 7.26. Based on the 50 simulations, the mean line tension values between Riflex and Simo are quite similar where the mean tension values in Riflex is slightly larger than in Simo. The mean line tension, as observed from the previous line tension time series, has only a contribution from the slowly varying LF tension forces which is quite similar between Riflex and Simo. The standard deviation however, is larger in Riflex due to the large WF dynamic tension responses which creates a larger variation in the tension response. Based on the statistics, it is the line Longest 3 which achieves the second largest line tension and is thus chosen to be removed in the ALS spread simulations.

Table 7.11: The most probable and 90% fractile max, min, and μ and σ of the most exposed lines' tension in spread simulations.

	Spread Weather Condition					
	Riflex [kN]					
	MPM_{MAX}	$90\%_{MAX}$	MPM_{MIN}	$90\%_{MIN}$	μ	σ
Long 1	5990	6958	20	-398	2745	560
Long 2	6036	7020	63	-373	2792	563
Long 3	6077	7074	110	-357	2837	564
Long 4	6112	7118	160	-332	2881	565
Long 5	6145	7151	208	-298	2923	564
Longest 1	6155	7171	-236	-307	2446	653
Longest 2	6160	7184	-251	-323	2394	665
Longest 3	6168	7204	-268	-355	2345	676
Longest 4	6174	7213	-273	-365	2299	688
Longest 5	6162	7211	-269	-348	2249	696
	Simo [kN]					
	MPM_{MAX}	$90\%_{MAX}$	MPM_{MIN}	$90\%_{MIN}$	μ	σ
Long 1	4820	6771	1529	1335	2680	438
Long 2	4911	6886	1551	1353	2719	444
Long 3	4992	6982	1576	1373	2756	448
Long 4	5063	7049	1602	1394	2793	451
Long 5	5116	7082	1629	1418	2827	452
Longest 1	3352	3650	1577	1398	2390	240
Longest 2	3352	3664	1521	1344	2350	248
Longest 3	3352	3677	1467	1291	2310	256
Longest 4	3350	3692	1417	1245	2270	263
Longest 5	3345	3705	1368	1202	2230	269

The breaking strength of the top chain segment of each mooring line is $T^{BS} = 24073kN$, and the Norwegian ULS safety factor is given as 2.2 in Table 2.1. Line Longest 4 and Long 5 achieves the largest line tension of all the lines during spread weather in Riflex and Simo respectively. The MPM_{MAX} tension value is taken to be the characteristic tension, and is multiplied with the Norwegian safety factor to see if the design tension exceed the breaking strength. This design check is performed and the results are shown in the table below. The design tension is far below the breaking strength for both simulation softwares.

Table 7.12: Design check between the line's breaking strength (T^{BS}) and characteristic design tension (T_{Ch}^{DLS}) in spread weather

Design Check [kN]	
T_{Ch}^{DLS} Riflex	13582.8
T_{Ch}^{DLS} Simo	11255.2
T^{BS}	24073

Co-linear Weather

The figure below illustrates the most probable- and 90% fractile- max and min of each line in co-linear. The most probable max line tension during co-linear weather is largest in the Long cluster, and the smallest most probable max is in the Longer cluster in both Riflex and Simo. Similar to the most probable min in spread weather, the MPM_{MIN} of the Long cluster in Riflex is positive which means that the Long lines are most probably not going slack. On the other hand, the minimum 90% fractile tension is negative, so there exists a 10% possibility that the Long lines goes slack in this extreme weather. The Longer and Longest lines however have a negative most probable min and are most probably going slack. The most probable minimum in Simo is however positive in all lines, and no lines go slack. This is verified in Table 7.13 which shows the tension statistics of cluster Long and Longest in Figure 7.27. Based on the statistics in the table, it is line Long 5 which achieves the second greatest tension and is thus removed when performing the co-linear ALS simulations.

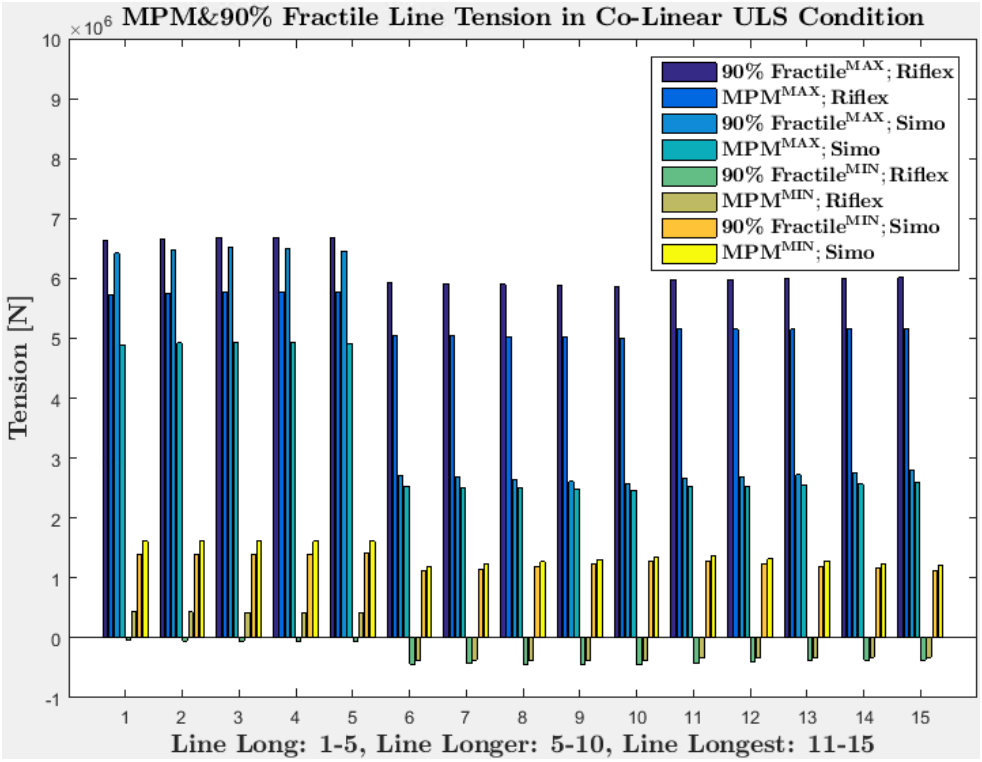

Figure 7.27: The MPM_{max} 90%$_{max}$, MPM_{min}, 90%$_{min}$ line tension in Riflex and Simo during ULS co-linear weather conditions.

Table 7.13: The most probable and 90% fractile max, min, and μ and σ of the most exposed lines' tension in the co-linear simulations.

	Co-linear Weather Condition					
	Riflex [kN]					
	MPM_{MAX}	$90\%_{MAX}$	MPM_{MIN}	$90\%_{MIN}$	μ	σ
Long 1	5731	6636	434	-44	2904	506
Long 2	5751	6663	429	-51	2910	509
Long 3	5762	6678	425	-58	2913	511
Long 4	5768	6684	420	-63	2914	5121
Long 5	5765	6678	416	-70	2912	512
Longest 1	5148	5977	-340	-425	1851	592
Longest 2	5148	5982	-337	-405	1821	598
Longest 3	5149	5991	-330	-386	1793	604
Longest 4	5148	6006	-321	-373	1769	610
Longest 5	5154	6013	-325	-376	1743	614
	Simo [kN]					
	MPM_{MAX}	$90\%_{MAX}$	MPM_{MIN}	$90\%_{MIN}$	μ	σ
Long 1	4892	6420	1615	1403	2809	447
Long 2	4920	6482	1614	1401	2814	450
Long 3	4933	6509	1614	1402	2817	451
Long 4	4930	6501	1615	1403	2818	451
Long 5	4913	6460	1618	1406	2816	448
Longest 1	2523	2658	1364	1286	1908	157
Longest 2	2538	2690	1322	1239	1885	166
Longest 3	2554	2724	1281	1196	1863	174
Longest 4	2569	2757	1242	1156	1842	182
Longest 5	2585	2790	1206	1120	1822	189

The tension response in co-linear weather is smaller than in spread weather, thus the design tension is below the breaking strength in both Riflex and Simo.

7.5 Accidental Limit State Tension Analyzes

Figure 7.28 shows the turret's elliptic heave-pitch-surge motion pattern in an ALS simulation in spread weather conditions. As shown in the previous time series and PSD spectrum from the ULS analyzes, this motion plays an important role with regards to the dynamic tension in the mooring lines. Similar to the turret's elliptic motion in ULS, the Long lines are the windward lines which experiences a large mean tension, but a smaller dynamic tension in ALS. The Longer and Longest lines are the leeward lines which experiences a larger dynamic tension due to the larger elliptic diameter.

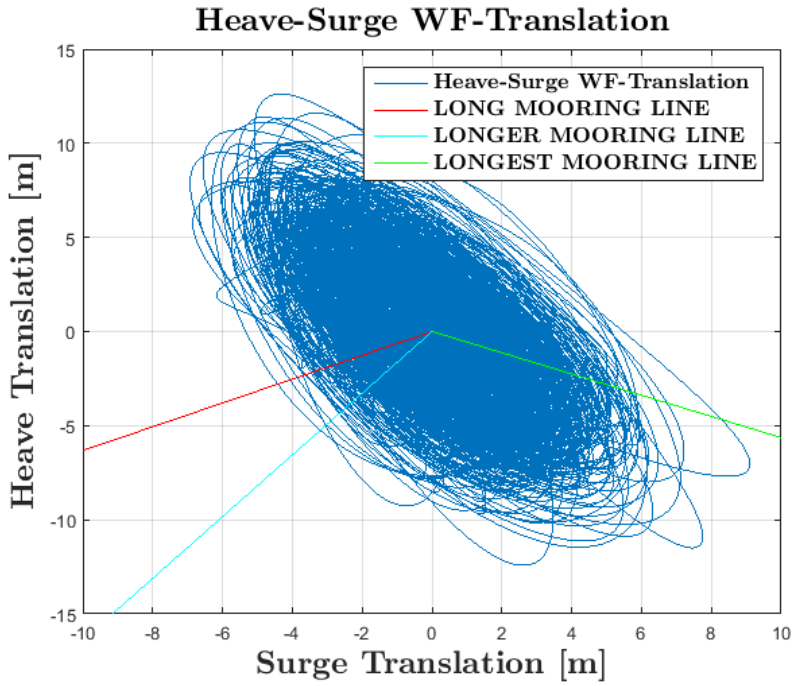

Figure 7.28: Turret's heave-surge WF-translation in ALS spread condition in Riflex.

The line tension results will in this section will be presented in form of extreme statistics from the gumbel distributions. Line tension time series, PSD spectrum and time series statistics in ALS can be found in D.

7.5.1 Most Probable Max and 90% Fractile Tensions

Spread Weather

Studying Figure 7.29, the Longest cluster achieves the largest most probable max in Riflex which is expected because Longest 3 is broken and removed from the ALS simulations. The Longest lines must therefore compensate by absorbing more loads. However, the most probable max tension in Simo is largest in the Long lines. The Longer cluster achieves least line tensions in both Riflex and Simo. Both the cluster Longer, Longest and line Long 1 are most probable to experience slack lines in Riflex, however the margin for line Long 2, 3, 4 and 5 to experience fully slack lines is not large. The lines in Simo are not probable to achieves slack lines, not even for the minimum 90% fractile value. The statistical extreme MPM and 90% fractile values are presented in Table 7.14.

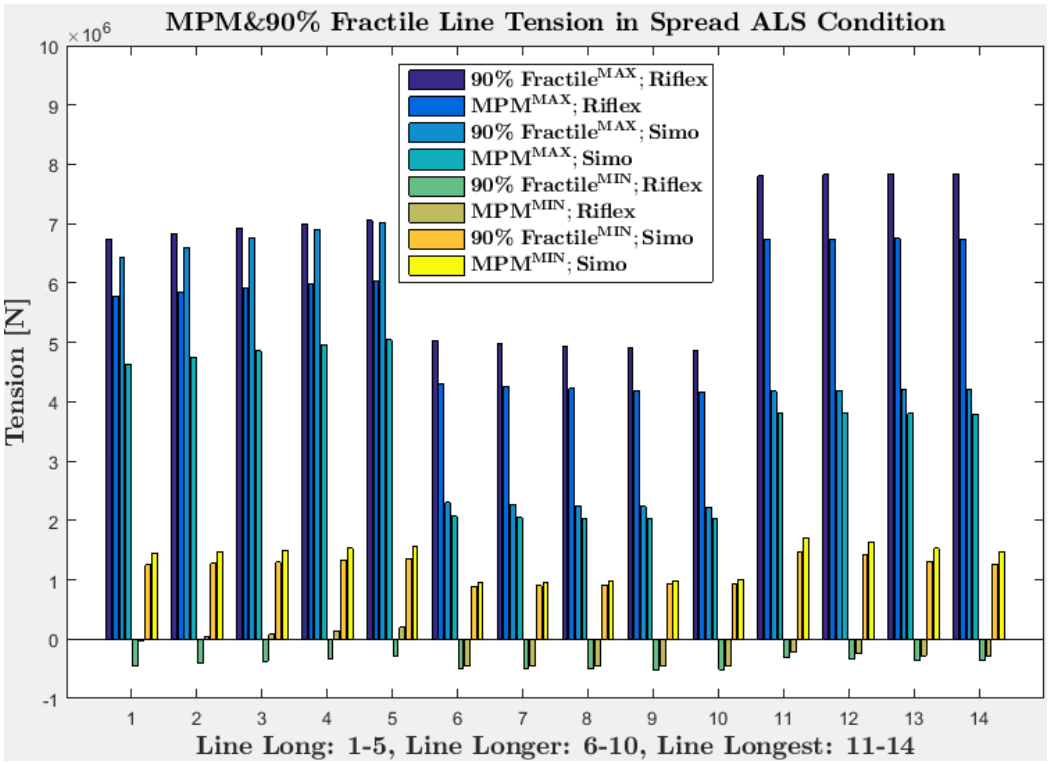

Figure 7.29: The MPM_{max}, 90%$_{max}$, MPM_{min}, 90%$_{min}$ line tension in Riflex and Simo in ALS spread weather conditions.

Table 7.14: MPM, 90% fractile, μ and σ of the most exposed lines' tension in ALS spread simulations.

	Spread Weather Condition					
	Riflex [kN]					
	MPM_{MAX}	$90\%_{MAX}$	MPM_{MIN}	$90\%_{MIN}$	μ	σ
Long 1	5781	6745	-21	-450	2620	541
Long 2	5852	6835	33	-406	2680	546
Long 3	5910	6917	82	-370	2738	551
Long 4	5918	6993	138	-323	2797	554
Long 5	6041	7059	194	-283	2854	557
Longest 1	6738	7806	-224	-312	2751	730
Longest 2	6744	7826	-250	-335	2689	745
Longest 4	6752	7846	-276	-364	2574	772
Longest 5	6735	7837	-280	-362	2513	781
	Simo [kN]					
	MPM_{MAX}	$90\%_{MAX}$	MPM_{MIN}	$90\%_{MIN}$	μ	σ
Long 1	4626	6430	1444	1248	2560	430
Long 2	4743	6600	1472	1271	2612	438
Long 3	4853	6756	1502	1295	2663	446
Long 4	4953	6896	1534	1322	2713	452
Long 5	5045	7014	1568	1351	2762	457
Longest 1	3808	4174	1704	1470	2685	285
Longest 2	3811	4184	1644	1415	2637	294
Longest 4	3805	4198	1529	1310	2540	311
Longest 5	3796	4200	1473	1260	2491	317

Line Longest 4 and Long 5 achieves the largest line tension of all the lines during spread weather in Riflex and Simo respectively. This design check is performed for these lines, and the results are shown in the table below. The design tension is far below the breaking strength for both simulation tools.

Table 7.15: Design check between the line's breaking strength and design tension in spread weather.

Design Check [kN]	
T_{Ch}^{DLS} Riflex	10102.5
T_{Ch}^{DLS} Simo	7567.5
T^{BS}	24073

Co-linear Weather

The illustration in Figure 7.30 shows that the Long cluster achieves the largest most probable max in both Riflex and Simo, which is expected because Long 5 is broken

and removed from the co-linear ALS simulations. The Long lines are therefore absorbing more loads getting a larger tension, while the Longer cluster achieves least line tensions in both Riflex and Simo. Both the cluster Longer and Longest are most probable to experience slack lines in Riflex, however the margin for cluster Long to most probably experience fully slack lines is not large. Similar to the spread weather simulations, the lines are not probable to achieve slack lines. The statistical extreme values can be found in Table 7.17.

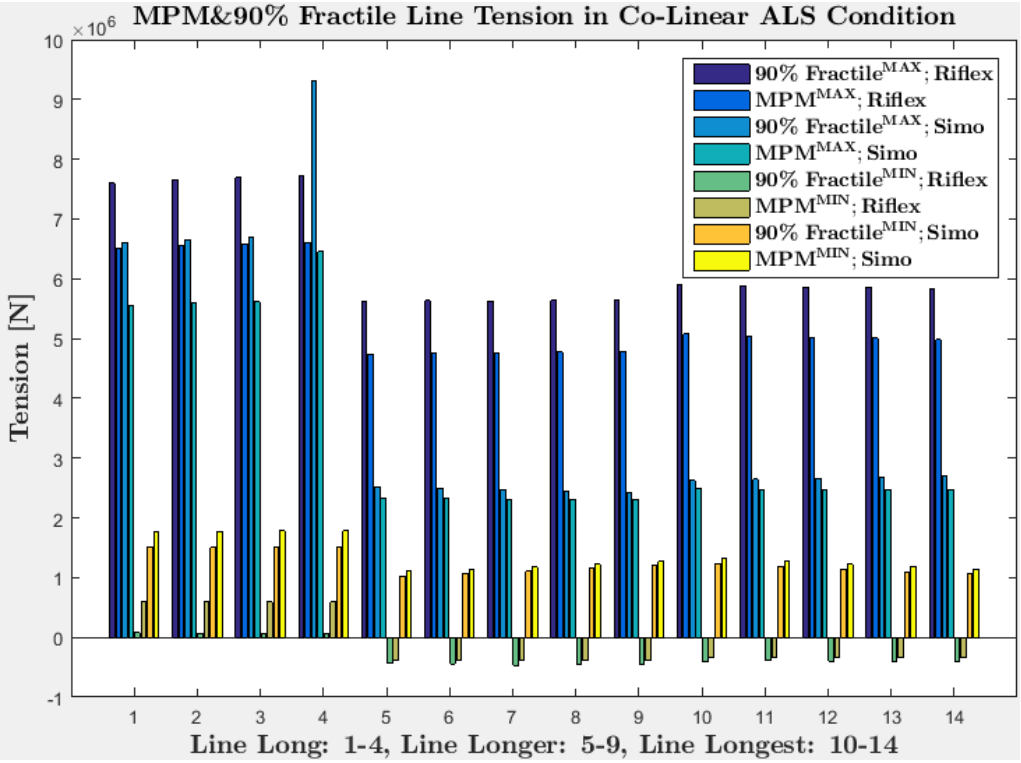

Figure 7.30: The MPM_{max} 90%$_{max}$, MPM_{min}, 90%$_{min}$ line tension in Riflex and Simo in ALS co-linear weather conditions.

Table 7.16: MPM, 90% fractile, μ and σ of the lines' tension in ALS co-linear simulations.

	Co-Linear Weather Condition					
	Riflex [kN]					
	MPM_{MAX}	$90\%_{MAX}$	MPM_{MIN}	$90\%_{MIN}$	μ	σ
Long 1	6513	7600	598	78	3310	584
Long 2	6557	7660	596	74	3323	589
Long 3	6585	7698	594	70	3332	592
Long 4	6599	7717	591	66	3337	594
Longest 1	5074	5906	-337	-403	1807	579
Longest 2	5047	5886	-330	-387	1767	581
Longest 3	5025	5865	-331	-394	1730	583
Longest 4	5011	5859	-336	-396	1698	585
Longest 5	4982	5839	-337	-395	1664	585
	Simo [kN]					
	MPM_{MAX}	$90\%_{MAX}$	MPM_{MIN}	$90\%_{MIN}$	μ	σ
Long 1	5558	6613	1776	1505	3198	535
Long 2	5594	6660	1779	1506	3210	539
Long 3	5614	6684	1782	1508	3218	540
Long 4	6454	9310	1785	1511	3236	570
Longest 1	2480	2627	1318	1238	1859	160
Longest 2	2479	2644	1268	1184	1826	167
Longest 3	2478	2661	1221	1137	1794	174
Longest 4	2479	2678	1179	1096	1764	180
Longest 5	2479	2696	1140	1056	1735	186

The tension response in co-linear weather is smaller than in spread weather, thus the design tension is below the breaking strength in both Riflex and Simo.

7.6 Turret Forces Analyzes in ULS

As the title describes, the turret forces will be presented and discussed in this section. The time series and PSD spectrum with the largest response of the boogie forces, moments, and radial wheel forces and their contributions will be presented in the co-linear environment, because this environment excite the largest turret load response. The time series and PSD spectrum of the boogies and radial wheels in spread weather is attached in the Appendix E, and is not presented in the report because the time series and PSD spectrum are similar to the co-linear weather.. Extreme turret statistics based on the gumbel distributions have been investigated and will be presented in both weather conditions.

7.6.1 Turret Forces and Moments

Time Series

Figure 7.31 below shows three time series: radial wheel forces, vertical boogie forces, boogie moments and their contributions. The contributions to the radial wheel forces come from the turret and added water inertia, turret mass and mooring shear force. The inertia and turret mass forces are oscillating in the wave frequency interval with a mean equal to zero, and from the time series it looks like they often are out of phase and cancelling occur. The total radial wheel forces are therefore dominated by the shear force from the mooring lines. Looking at the time series, the mooring shear forces is oscillating with the wave frequency but also with a slow varying period.

The turret and added water inertia, turret mass and the mooring axial force are the contributions to the vertical boogie forces. These force contributions is oscillating with the wave frequency, however the turret's mass oscillation is so small that it can not be observed in the time serie. The inertia and axial mooring force are sometimes out of phase and some cancelling will occur. This happens because the dynamic mooring force accelerates the FPSO, however the FPSO's inertia will resist the outer force by accelerating in the opposite direction. The turret mass is supported by the boogies, thus the non-visual variation in the turret mass contribution. The turret mass is the largest force contribution to the vertical boogie forces.

The boogie moment is a result of the moment contributions from the turret's inertia, radial wheel and mooring shear force. The radial wheel moment is so small compared to the other forces due to its small moment "arm". The moment from the inertia and shear force are often out of phase, but there are some occurrences where they are in phase and creating larger boogie moment responses. The moment from inertia is oscillating with the wave frequency with a mean equal zero. The shear moment also oscillates with the wave frequency, however it also oscillates with a low frequency and has a large mean value. The significant contributions to the boogie moment is mainly the mooring shear moment and secondly the inertia from the turret and added water mass.

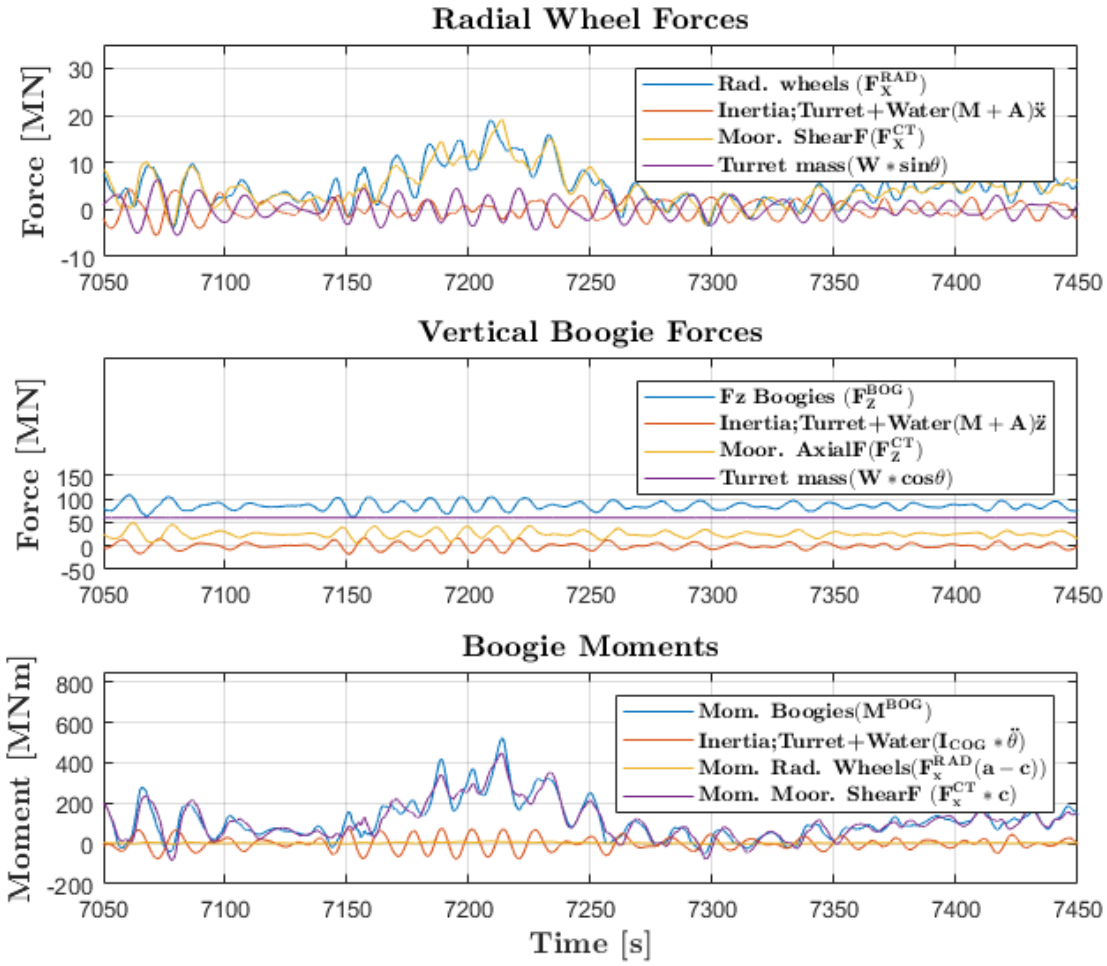

Figure 7.31: The force and moment time series of the radial wheels (F_X^{RAD}), boogies (F_Z^{BOG} & M^{BOG}) and their force and moment contributions in co-linear weather conditions.

In the table below, the statistics of the radial wheel and boogie time series are shown to quantify the forces and moments contributions. The largest contribution to the radial wheels is the mooring shear force, which actually is larger than the maximum radial wheel force. This means that force cancelling occurs due to the different phases of the force contributions, which was mentioned earlier. The percentage difference between the mean radial wheel and mooring shear force is 4.4%, thus the mean forces is dominated by the shear force.

The largest contribution to the vertical boogie forces is the turret weight, which is almost not varying by looking at the small standard deviation. The contribution from the axial mooring force is also important, however some of the force magnitude is

cancelled by the inertia due to different phases. The difference between the mean boogie and turret mass force is 29.4%, thus approximately 70% of the mean boogie force results from the turret weight.

The boogie moment is dominated by the mooring shear moment where the percentage difference between the maximums is 14.6%, which means that other forces contributes to the maximum boogie moment. The boogies also absorbs some moment from the turret inertia, however the contribution from the radial wheel forces is negligible compared to the other moments. The mean forces are dominated by the mooring moment.

Table 7.17: Max, min, μ and σ of the radial wheel forces, boogie forces and moments and their contributions in co-linear environment.

	Radial Wheel Forces [kN]			
	MAX	MIN	μ	σ
F_X^{RAD}	18933.7	-8063.0	3756.7	2487.4
$(M+A)\ddot{x}$	6781.3	-7323.9	0.1	1668.2
F_x^{CT}	19006.1	-8702.7	3589.9	2360.6
$W * sin\theta$	7263.5	-6658.7	166.7	1991.4
	Vertical Boogie Forces [kN]			
F_z^{BOG}	115212.7	57114.7	84684.5	7319.9
$(M+A)\ddot{z}$	23048.6	-20108.7	0.2	5717.4
F_z^{CT}	57695.7	3172.8	24876.6	6052.0
$W * cos\theta$	59841.0	59398.5	59807.6	46.0
	Boogie Moment [kNm]			
M^{BOG}	522876.9	-176567.3	86522.0	55652.1
$I_{COG} * \ddot{\theta}$	98851.3	-106365.6	-0.3	26800.5
$F_x^{RAD}(a-c)$	10886.9	-4636.2	2160.1	1430.2
$F_x^{CT} * c$	446643.5	-204514.2	84362.2	55474.6

PSD

The PSD illustrations of the radial wheel forces, vertical boogie forces, boogie moment and their contributions are showed in Figure 7.32. The radial wheel forces have a LF and two WF energy peaks at frequencies 0.005, 0.05462 and 0.07566s^{-1} respectively. These energy peaks is a result from the second order slowly varying and first order wave loads. There exist also shear force energy for frequencies close to zero, and this energy is excited by the extremely slow varying wind gusts. The energy peak

at 0.07566^{-1} corresponds to a period of 13.2 seconds which is 1 seconds away from the heave natural period, thus heave resonance could be the reason for this energy. There exist also a lot of energy in the frequency interval [0.06057 0.09208] which corresponds to a period interval of [16.5 10.9]seconds. The pitch natural period is 15 seconds which is within the energy interval and could be the reason for some of this energy. Notice that the radial wheel WF energy is lower than all the WF energy contributions at frequency 0.05462, which represents the generated waves with a period of 18.5 seconds. This verifies that the force contributions are out of phase and cancelling occurs. The turret mass is responsible for a lot of the energy within the frequency interval that was previously discussed, which may be a result of heave and pitch resonance. The LF energy consists only of the mooring shear force.

The vertical boogie energy is concentrated in the WF region and both the shape and the frequency range are almost identical to the pitch motion PSD in Figure 7.13. The vertical boogie response is thus a result from the first order generated waves, where pitch resonance occur and a possibility for a pitch-heave coupling. According to the PSD, there are only two contributions to the vertical boogie force. The PSD only considers loads that are significant when oscillating, thus the turret mass contribution can not be seen in this scale. The PSD shows that the boogie forces is a combination of both the axial mooring force and the turret's inertia.

The boogie moment energy consists of both LF and WF energy. The LF energy contribution comes from the slowly varying moment loads of the mooring shear moment, while the WF energy contribution comes from both the shear moment and the turret's moment of inertia. The turret's moment of inertia achieves two energy peaks, one representing the wave period and one at a frequency of 0.07s^{-1} which corresponds to a period of 14.3 seconds. The pitch and heave natural period are 0.7 and 2.3 seconds away from this energy peak, and thus some pitch resonance and heave-pitch coupling may contribute to this energy. The shear moment energy is similar to the shear force energy in the PSD of the radial wheel forces, where there slowly varying wave and wind loads excite shear moment energy, and the first order wave forces excite the WF loads. The PSD shows that the boogie moment consists of a moment contribution from the mooring and the inertia, and that the contributions must be out of phase since the boogie PSD in the WF interval is lower than the mooring contribution.

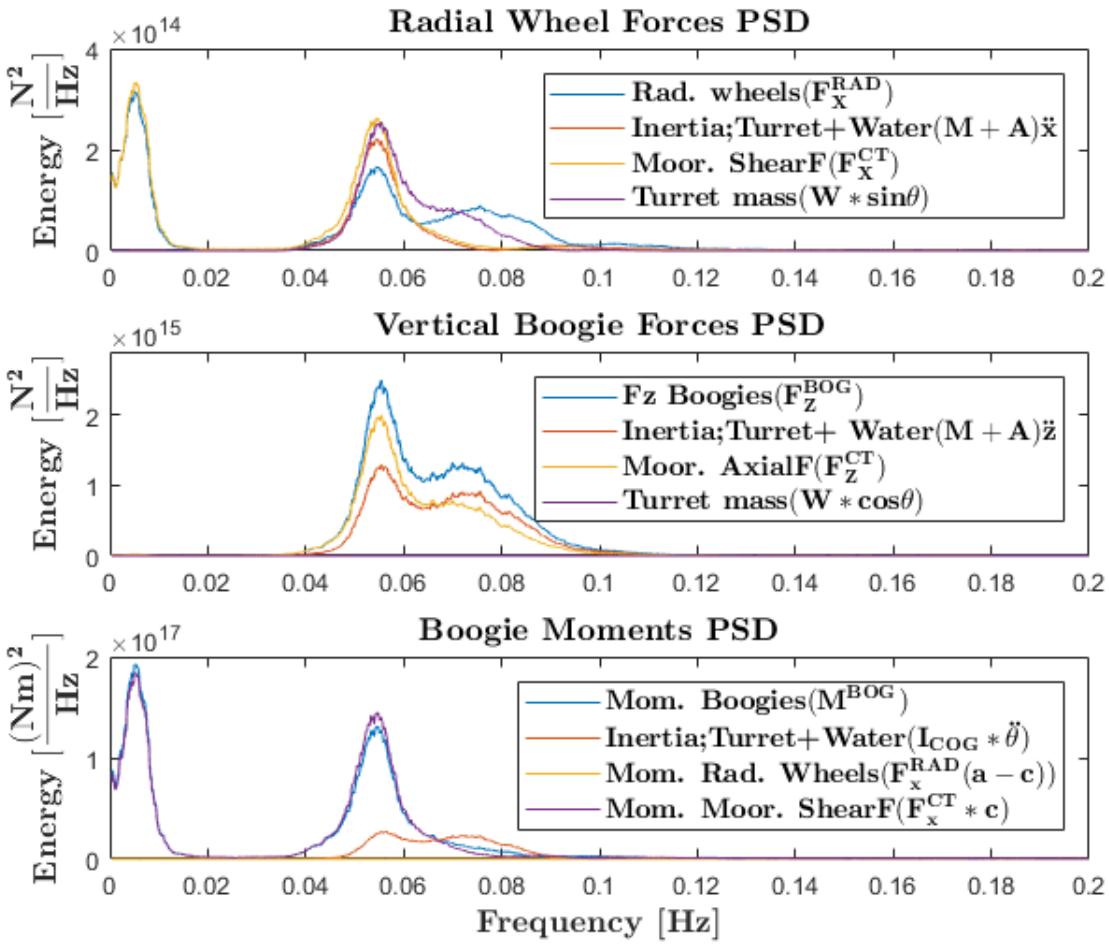

Figure 7.32: Shows the force and moment PSDs of the radial wheel (F_X^{RAD}), boogie (F_Z^{BOG}&M^{BOG}) and all of their force and moment contributions in ULS co-linear weather conditions.

7.6.2 MPM and 90% Fractile Forces & Moments

This section will present the MPM and 90% fractile forces and moments in the radial wheels and boogies. The extreme statistics will be presented in tables, and are based on the Gumbel probability distributions in Figure 7.33. The figure gives an illustration of the quantity of the most probable maximum and 90% fractile forces and moments within the turret. The characteristic design loads in the turret is given by the 90% fractile value and will be investigated.

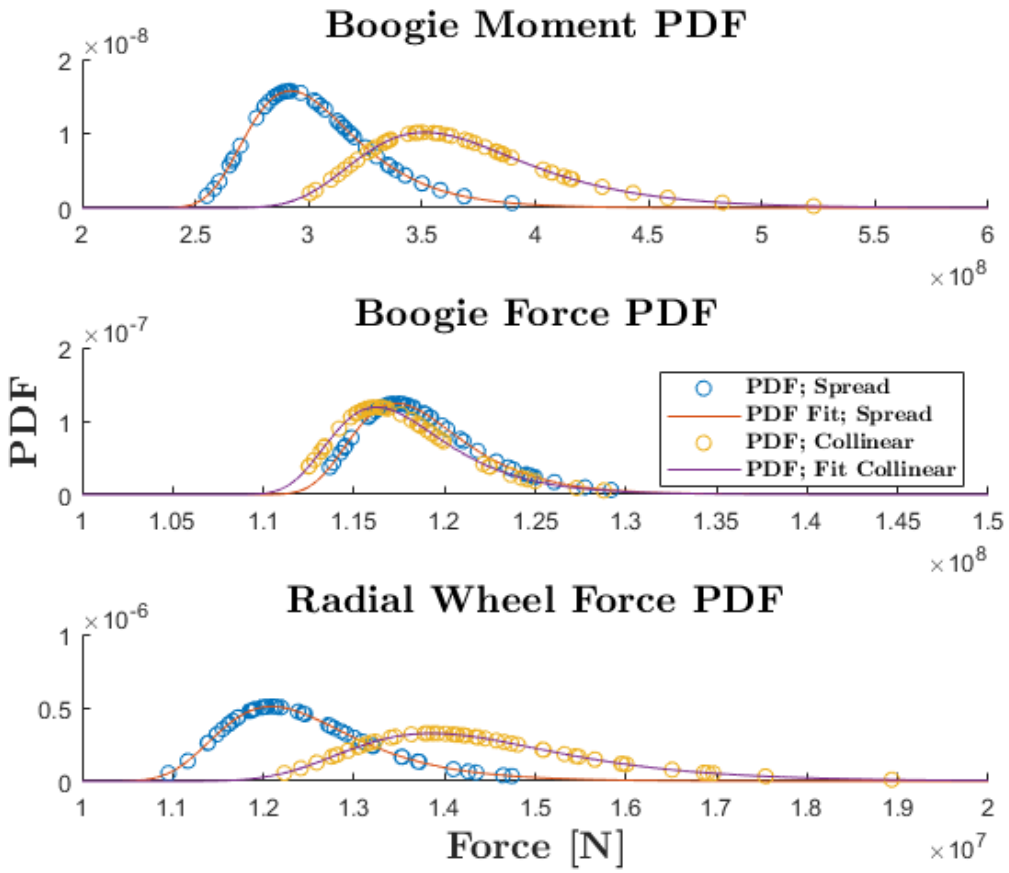

Figure 7.33: Gumbel distribution of the radial wheel forces and boogie forces and moments in ULS weather conditions.

The extreme boogie and radial wheel loads are presented in the table below. The radial wheel forces and boogie moments are larger in the co-linear weather compared to spread, while the vertical boogie forces are larger in spread weather. The significant difference between the 90% fractile boogie moment in co-linear and spread weather attracts the immediate attention, where the percentage difference is 20.4%. The mean boogie moment is however larger in spread weather. The standard deviation of the boogie moment is 37.9% larger in the co-linear weather compared to the spread weather, which means that the dynamic turret loads are varying more in the co-linear environment.

Table 7.18: The MPM, 90% fractile, μ and σ of the forces in the radial wheels(F_X^{RAD}) and boogies(F_X^{BOG} & M^{BOG}).

	Co-Linear Weather Condition			
	MPM_{MAX}	$90\%_{MAX}$	μ	σ
F_X^{RAD}[kN]	13859.0	16406.0	3765.3	2399.7
F_Z^{BOG}[kN]	116244.0	123214.0	84692.1	7327.0
M^{BOG}[kNm]	351142.0	432724.0	86732.8	52824.4
	Spread Weather Condition			
F_X^{RAD}[kN]	12092.0	13724.0	4864.2	1809.2
F_Z^{BOG}[kN]	117333.0	124010.0	84990.5	7561.1
M^{BOG}[kNm]	292016.0	344654.0	113134.5	32827.5

7.6.3 Forces in One Boogie & Radial Wheel

The figure below shows the time series of the total boogie force and its contributions in the most and least exposed boogies. Boogie 1 and 2 to have the same contribution from the vertical boogie force, however since these boogies are on the opposite side of the turret, the moment contribution will work in opposite direction which is observed in the figure. Both boogies achieves a moment contribution larger than the vertical boogie force, thus one of the boogies experience uplift. The figure shows that Boogie 1 experience a large down force while Boogie 2 experience uplift. The time series show that it is the dynamic boogie moment which is the crucial factor that decides whether uplift occurs or not.

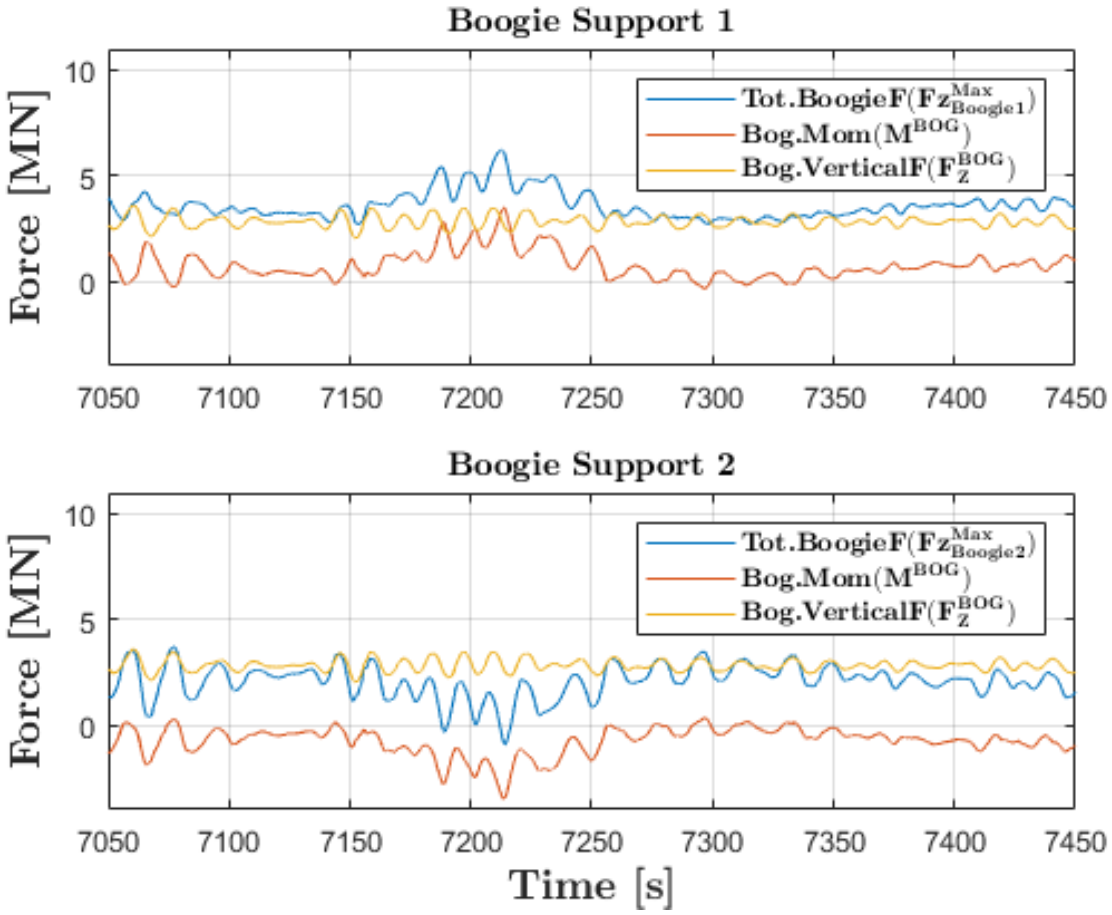

Figure 7.34: Force time series of boogie 1 & 2 and its force contributions during ULS co-linear weather condition.

Figure 7.35 shows the Gumbel probability density distributions of the forces in boogie 1 & 2 and in one radial wheel during co-linear and spread environment. The minimum PDF of boogie 2 show that the most probable minimum force is negative in co-linear weather, which means that the turret is most probable to achieve uplift in boogie 2. In spread weather however, the most probable minimum in boogie 2 is positive but the 90% fractile minimum may be negative. The statistics from the figure below and the 50 simulations are presented in Table 7.19 . The statistics show in fact that the 90% min fractile force in boogie 2 is negative during spread weather, which means that there is a 10% probability of experiencing turret uplift. To prevent uplift and satisfy the 90% fractile design load criteria in spread and co-linear weather, the turret weight must be larger than 6778 and 9440 tonnes respectively.

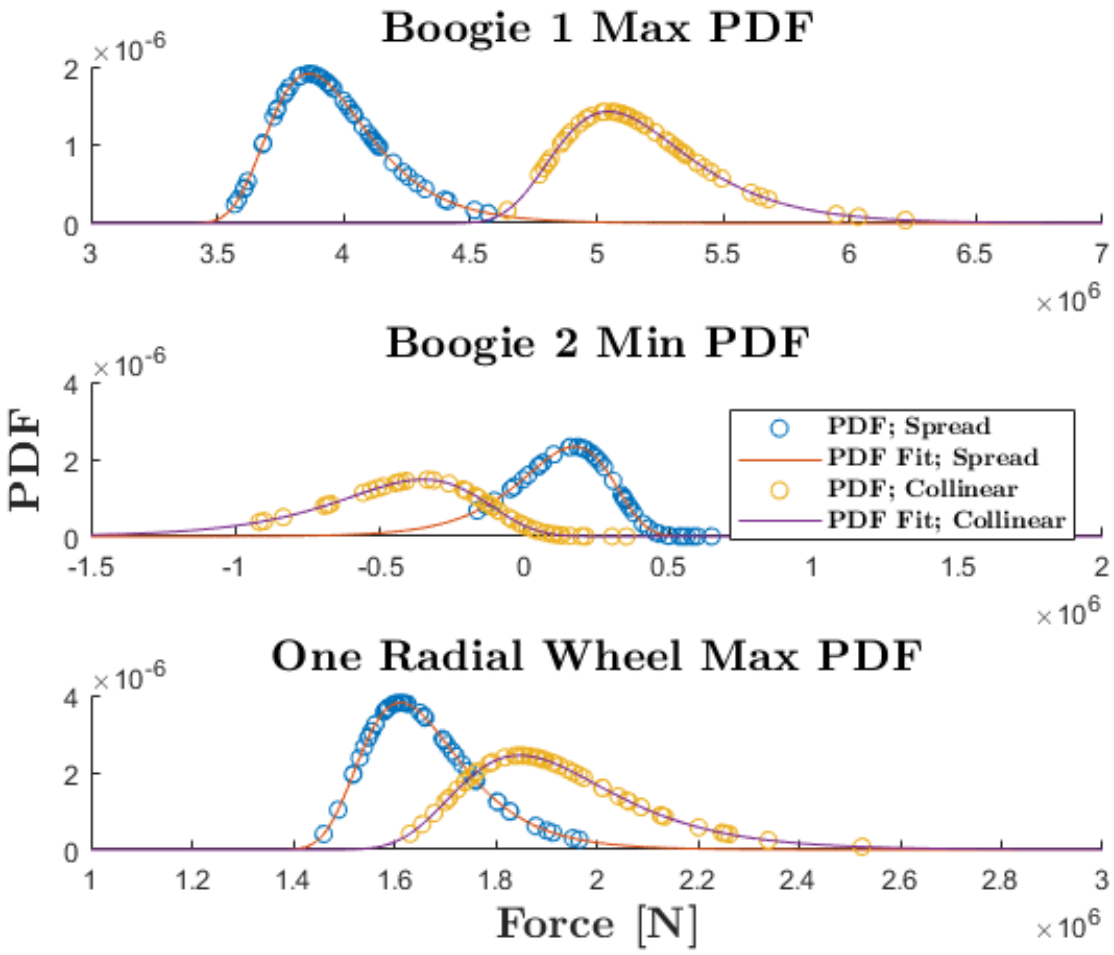

Figure 7.35: Gumbel pdf of the extreme forces in boogie 1 & 2 and in one radial wheel.

Table 7.19: The most probable and 90% fractile max, min, and μ and σ of the forces in boogie 1 & 2 and one radial wheel. The required turret weight to prevent uplift is also presented.

	ULS Spread									
	MPM_{MAX}	$90\%_{MAX}$	MPM_{MIN}	$90\%_{MIN}$	μ^{BOG1}	σ^{BOG1}	μ^{BOG2}	σ^{BOG2}	μ^{RAD}	σ^{RAD}
Boogie[kN]	3863.0	4297.0	174.0	-182.0	3587.2	252.5	2078.8	398.9	-	-
Radial Wheel[kN]	1612.0	1830.0	-	-	-	-	-	-	648.6	241.2
Req. Weight[ton]	-	-	-	6778	-	-	-	-	-	-
	ULS Co-linear									
Boogie[kN]	5046.0	5628.0	-350.0	-912.0	3401.3	280.2	2244.9	537.4	-	-
Radial Wheel[kN]	1848.0	2188.0	-	-	-	-	-	-	502.0	320.0
Req. Weight[ton]	-	-	7355	9440	-	-	-	-	-	-

7.7 Turret Forces Analyzes in ALS

As the title describes the analyzes of the turret forces in ALS will be studied. The results from the ALS analyzes will be presented in the form of extreme turret load statistics from the Gumbel probability distributions. The total forces in all and one single boogie and radial wheel will be presented and turret uplift in ALS will be investigated. The ALS turret time series and PSDs is not presented in the report, but is attached in the Appendix F

7.7.1 Most Probable Max and 90%Frac. Forces&Mom.

The gumbel probability distribution of the radial wheel and boogie forces and moments during both weather conditions in ALS are illustrated in the figure below. The Gumbel distributions in ALS is almost identical to the ones in ULS, which indicates that a line break will not affect the turret forces. They are found to be quite similar thus only the extreme statistics from the Gumbel distributions will be investigated.

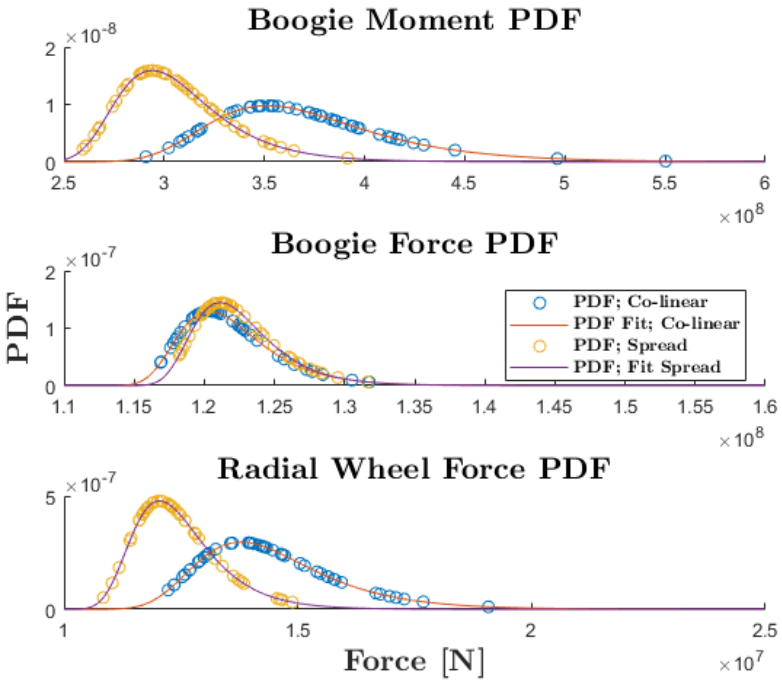

Figure 7.36: Gumbel pdf of the radial wheel and boogie forces and moments in ALS weather conditions.

The extreme turret loads Gumbel statistics from the ALS study are shown in the table below. The boogie moment gets slightly larger while the boogie and radial wheel

forces are slightly smaller in ALS compared to the ULS extreme statistics in Table 7.21, however the difference is small.

Table 7.20: The most probable and 90% fractile max, min, and the μ and σ of the forces in the radial wheels(F_X^{RAD}) and boogies(F_X^{BOG}&M^{BOG}) based on the 50 ALS co-linear simulations.

	Co-Linear Weather Condition			
	MPM_{MAX}	$90\%_{MAX}$	μ	σ
F_X^{RAD}[kN]	13516.0	16363.0	3750.0	2285.5
F_Z^{BOG}[kN]	112665.0	119154.0	82838.2	7048.4
M^{BOG}[kNm]	351627.0	436250.0	86639.2	51415.2
	Spread Weather Condition			
F_X^{RAD}[kN]	11729.0	13437.0	4849.3	1721.0
F_Z^{BOG}[kN]	113415.0	119333.0	83278.7	7258.5
M^{BOG}[kNm]	294270.0	346336.0	113029.9	32727.2

The previous table showed that there was a slightly increase in the boogie moment in ALS compared to ULS. It was shown in the ULS boogie uplift time serie that the boogie moment contribution is the crucial factor in deciding whether uplift occurs, thus it is interesting to see if the required turret weight to avoid uplift is larger in ALS than ULS. According to the table below, the required turret weight that prevents uplift and satisfies the 90% fractile design load in ALS during spread and co-linear weather is 6850 and 9653 tonnes respectively. The percentage difference between the required turret weight in ULS and ALS is 1.1% and 2.2% in spread and co-linear weather respectively. A system with a line break will thus lead to a slightly larger turret uplift than an intact system, however the difference is small.

Table 7.21: The most probable and 90% fractile max, min, and μ and σ of the forces in boogie 1 & 2 and one radial wheel. The required turret weight to prevent uplift is also presented.

	ALS Spread									
	MPM_{MAX}	$90\%_{MAX}$	MPM_{MIN}	$90\%_{MIN}$	μ	σ	μ^{BOG2}	σ^{BOG2}	μ^{RAD}	σ^{RAD}
Boogie[kN]	4722	5028.0	157.0	-198.0	3529.5	250.3	2022.4	386.8	-	-
Radial Wheel[kN]	1564.0	1792.0	-	-	-	-	-	-	646.6	229.5
Non-Uplift[ton]	-	-	-	6850	-	-	-	-	-	-
	ALS Co-linear									
Boogie[kN]	4927.0	5519.0	-407.0	-980.0	3338.9	267.5	2183.7	523.3	-	-
Radial Wheel[kN]	1802.0	2182.0	-	-	-	-	-	-	500.0	304.7
Non-Uplift[ton]	-	-	7555	9653	-	-	-	-	-	-

Chapter 8

Summary, Conclusion and Further Work

8.1 Summary

Spread mooring, single point mooring, and thruster assisted mooring systems are considered permanent, while dynamic positioning and mobile mooring systems are mobile station keeping systems. Mooring systems have typically a catenary or a taut configuration or a mix of both, where the mooring hardware components can consists of buoyancy elements, clump weights, connection links, anchor, and lines of chain, steel wire, synthetic fibre or a combination of these. The station keeping system studied in this thesis is a single point turret moored FPSO, with a line configuration of studless chain in the top and bottom section, whereas the midsection consists of a spiral strand steel wire. The lines are anchored with suction anchors.

In the design of a mooring system there are three design limit states that must be investigated: Ultimate limit state ensures that the mooring lines remain intact after a 100 year storm, Accidental limit state ensures that the system remain stable after one or two line failures in a 100 year storm, Fatigue limit state ensures that the mooring lines withstands cyclic loading. The Norwegian safety factors for the mooring lines of permanent oil storage and production units, are in a 100 year storm 2.2 and 1.5 in ULS and ALS, respectively. The fatigue safety factor for mooring lines which are not regularly inspected is given as a function of the fatigue damage ration between to adjacent lines and is minimum 5.0.

The FPSO's RAOs show that the FPSO achieves a surge, heave and pitch cancelling effect when the the wavelength is approximately same as the vessel length. The vessel's natural period in heave, roll and pitch are 12, 25.5 and 15 seconds respectively. The FPSO's most critical response is in roll with a maximum response of 9.9 deg/m, thus it is very important for the FPSO to be able to weathervane. The sway-yaw stability is thus a crucial factor to consider. The simple sway-yaw stability calculations show that the vessel is stable and is able to weathervane with a distance of 120 and 70 meters between the center of gravity and turret, and is unstable with a distance of

30 meters.

The software Sima have two numerical tools called Simo and Riflex which are used to analyze different marine systems and operations. Simo performs a quasi-static time domain analysis and captures the vessel's six degree of motions due to WF and LF loads. In Simo the mooring lines are modeled by the catenary equations and are functioning as springs that provides stiffness.
Riflex performs a non-linear time domain finite element analysis of slender systems, for instance a mooring system, and describes the lines' fully behavior by solving the whole equation of motions. A Simo-Riflex coupled analysis will solve all the contributions in the equation of motions, thus the vessel's and the mooring lines' fully behaviour will be captured.

The turret moored FPSO is modeled in Simo and Riflex, whereas the model in Riflex performs a Simo-Riflex coupled analysis by solving the fully behaviour of the vessel and the mooring lines. Simulations performing a system characteristic and surge decay test is conducted in order to investigate the surge natural period and the system stiffness between Riflex and Simo. The results show a 1.2% difference in surge natural period between Simo and Riflex, whereas the system characteristic show that the system in Riflex is at most 3.3% stiffer than in Simo. The larger stiffness in Riflex is a result of an increased elastic stiffness due to a larger bottom friction in Riflex, however the bottom friction in Simo is unknown thus this should be more closely investigated. The larger stiffness in Riflex will lead to a slightly smaller motion and tension response than if the stiffness was the same as in Simo.

Wave contour analyzes are performed in Riflex to find the system's worst significant wave height and peak period, and is found to be 15.5m and 18.5 seconds respectively. ULS and ALS simulations is performed in both Simo and Riflex, and co-linear and spread weather conditions is compared. 50 simulations is found to be sufficient to properly describe the line tension, and thus 50 simulations is performed in each analysis.

The systems responses that is investigated in this thesis are the vessel's six degree of freedom motions, the mooring lines' tension response and the turret loads. 50 simulations are performed in ULS and ALS conditions in spread and co-linear weather in both Riflex and Simo. The Gumbel distribution is used to distribute the maximums and minimums and to find the MPM and 90% fractile motions, line tension and turret loads.

8.2 Conclusions

As mentioned in the summary, the systems responses that is investigated in this thesis is the vessel's six degree of freedom motions, the mooring lines' tension response and the turret loads. The following conclusions are made:

- The motion analyzes in ULS and ALS shows that the FPSO's surge, sway, roll and yaw motions are larger in spread weather conditions, whereas the heave and pitch motions are more or less the same in spread and co-linear weather. The extreme motion statistics show that Simo overestimates the vessel's extreme surge, sway, and yaw motions, while the extreme heave, pitch and roll motions are approximately the same as in Riflex. The mean surge, sway and yaw motions are however larger in Riflex. The damping provided by the mooring lines are not considered in Simo thus the low frequent slowly varying surge and sway motions will be larger in Simo. Keep in mind that mooring system in Riflex is slightly stiffer than in Simo, and that the motions in Riflex would be slightly larger if the system stiffness was the same. In the ALS the vessel's extreme surge, sway and yaw motions gets larger, however the heave, roll and pitch motions are the same as in the ULS results. Simo can be used in the early stages of the FPSO's motion design, however a Simo-Riflex coupled motion design is necessary to describe the correct motions.
- The ULS and ALS line tension analyzes show that the tension loads are larger in spread weather compared to the co-linear condition. The time series of the windward and leeward lines clearly show that Simo does not consider the dynamic behavior of the line, and thus neither the dynamic line tension that occurs from this behaviour. By looking at the PSD spectrum in Riflex, the dynamic line tension are concentrated in the wave frequency range where the heave and pitch natural frequencies are located. This indicates that the dynamic tension responses are a result from the dynamic surge-heave-pitch coupled motions.
- The windward lines in Riflex achieves a combination of both a large LF mean tension and a WF dynamic tension, while the leeward lines is dominated by the WF dynamic tension loads. The mean LF tension loads in the leeward lines are much smaller than the large WF dynamic loads, thus these lines often becomes slack. In Simo however, both the windward and leeward lines are dominated by the LF slowly varying tension loads and does not go slack. Due to the cyclic events where the leeward lines becomes slack it is recommended to reassess

the pre-tension of the lines. The large line tension differences between Riflex and Simo is so large that it is not recommended to use Simo in ULS and ALS design. However, in operations where the dynamic line behaviour is negligible, Simo can be used in the early design stages.

- The ULS and ALS results in Riflex show that the Longest lines achieves the largest line tension in spread weather, closely followed by the Long lines, whereas the Longer lines achieves least line tension. However, in co-linear weather the Long lines achieves the largest line tension, closely followed by the Longest and then the Longer lines. All the mooring lines in both weather conditions satisfies both the ULS and ALS requirement for permanent mooring units on the Norwegian Continental Shelf.The turret mooring line system is thus well set-up and distributes the tension loads well.
- The largest load contribution to the turret's radial wheels and boogies are the forces from the mooring lines. Solutions to decrease the forces from the mooring lines should thus be investigated, like for instance by decreasing the "arm" or the distance between the mooring line fixing point and the turret's COG. The inertia forces are small in comparison. The radial wheel forces and the boogie moment consists of both LF and WF forces, while the boogie forces only consists of WF forces.
- The results show that the turret is more probable to experience uplift in co-linear compared to spread weather, and that uplift occurs in both the ULS and ALS simulations. The turret loads are designed such that the turret withstands uplift in the 90% fractile load in the extreme turret load statistics, however uplift occurs in both weather conditions in both ULS and ALS. To avoid uplift in the 90% fractile ALS turret load, the turret must gain weight and become 850 and 3653 tonnes heavier in spread and co-linear weather respectively.

8.3 Further work

Possible work in the future is to perform FLS-analyzes in the leeward lines which experiences cyclic occurrences of going slack. This is a fatigue problem that must be investigated. It would be interesting to study the occurrences of slack lines, and to investigate different solutions to this problem for instance by increasing the line pre-tension and length.

As mentioned turret uplift occurs in both ALS and ULS during co-linear and spread weather. Solutions to prevent uplift, like for instance increasing the turret weight or mooring line length should be investigated more closely. The turret is today designed to prevent uplift for a 90% fractile loading, but is it necessary to design the turret for such large loading? It would be interesting to do a literature review of all turret uplift coincidences, and to investigate if it is reasonable to design the turret loads with a most probable maximum instead of a 90% fractile turret load.

Analyzes and design of the mooring system together with the riser system should be conducted. The risers will also provide damping to the system which may lead to less vessel motions and system loads. The vessel's total offset should also be investigated with respect to the requirement of maximum riser offset.

Bibliography

DNV (2013). Offshore Standard DNV-OS-E301 - Position Mooring URL:https://rules.dnvgl.com/docs/pdf/DNV/codes/docs/2013-10/OS-E301.pdf.

DNV (2017a). *SIMO 4.10.1 Theory Manual*. DNV GL.

DNV (2017b). *SIMO 4.10.1 User Guide*. DNV GL.

Faltinsen, O. M. (1990). *Sea Loads On Ships and Offshore Structures*. Cambridge University Press, The Edinbugh Building, Cambridge.

H. Ormberg, K. L. (1998). *Coupled analysis of floater motion and mooring dynamics for a turret-moored ship*. Elsevier.

ISO (2013). ISO 19901-7. Stationkeeping systems for floating offshore structures and mobile offshore units.

Klingan, K. E. (2016). *Automated Optimization and Design of Mooring Systems for Deep Water*. NTNU.

Larsen, C. M. (2015a). *TMR 4182 Compendium in Marine Dynamics*. Norwegian University of Science and Technology, NTNU.

Larsen, K. (2014a). *Dynamic equilibrium of turret*. Power point slides.

Larsen, K. (2014b). *Stability of a turret moored tanker*. Power point slides.

Larsen, K. (2015b). Lecture Notes 8 and 9 TMR4225 Marine Operations Mooring and station keeping of floating structures.

Larsen, K. (2015c). *Static equilibrium of a mooring line*. NTNU.

Larsen, K. (2017). Lecture Notes 6b and 7 TMR4225 Marine Operations Station Keeping and Mooring Systems.

Leira, B. J. (2010). *Compendium TMR 4235 Stochastic Theory of Sealoads*. NTNU.

Tor Vinje, D. M. (2004). *Kompendium i Emne TMR 4180 Marin Dynamikk*. NTNU.

Vegard Aksnes (2016). Forankringshendelser på sokkelen URL: http://tekmar.no/wp-content/uploads/2016/09/13-SINTEF-MARINTEK-Vegard-%C3%98-Aksnes.pdf.

Øystein Ølund Bertelsen (2017). *Design of Mooring Systems and Quasi-static Analysis of a Turret Moored FPSO*. NTNU.

Appendices

Appendix A

Mooring Line Properties

```
'*********************************************************************
 VESSEL POSITION
'*********************************************************************
'chmoor
 15 mooring lines at 371m water depth
'x1ves x2ves x3ves x6ves
 0.0   0.0   0.0   0.0
'---------------------------------------------------------------------
 LINE DATA
'iline lichar inilin iwirun intact
 1     1      1      0      1
'tpx1 tpx2
 70.1 0.0
'alfa           tens           xwinch
 14.0           2097.0          0.0
'---------------------------------------------------------------------
 LINE DATA
'iline lichar inilin iwirun intact
 2     1      1      0      1
'tpx1 tpx2
 70.1 0.0
'alfa           tens           xwinch
 17.0           2097.0          0.0
'---------------------------------------------------------------------
 LINE DATA
'iline lichar inilin iwirun intact
 3     1      1      0      1
'tpx1 tpx2
 70.1 0.0
'alfa           tens           xwinch
 20.0           2097.0          0.0
'---------------------------------------------------------------------
 LINE DATA
'iline lichar inilin iwirun intact
 4     1      1      0      1
'tpx1 tpx2
 70.1 0.0
'alfa           tens           xwinch
 23.0           2097.0          0.0
```

```
 LINE DATA
'iline lichar inilin iwirun intact
 5     1      1      0      1
'tpx1 tpx2
 70.1 0.0
'alfa           tens           xwinch
 26.0           2097.0          0.0
'--------------------------------------------------------------------
 LINE DATA
'iline lichar inilin iwirun intact
 6     2      1      0      1
'tpx1 tpx2
 70.1 0.0
'alfa           tens           xwinch
 134.0          2097.0          0.0
'--------------------------------------------------------------------
 LINE DATA
'iline lichar inilin iwirun intact
 7     2      1      0      1
'tpx1 tpx2
 70.1 0.0
'alfa           tens           xwinch
 137.0          2097.0          0.0
'--------------------------------------------------------------------
 LINE DATA
'iline lichar inilin iwirun intact
 8     2      1      0      1
'tpx1 tpx2
 70.1 0.0
'alfa           tens           xwinch
 140.0          2097.0          0.0
'--------------------------------------------------------------------
 LINE DATA
'iline lichar inilin iwirun intact
 9     2      1      0      1
'tpx1 tpx2
 70.1 0.0
'alfa           tens           xwinch
```

```
 LINE DATA
'iline lichar inilin iwirun intact
 10     2      1      0      1
'tpx1 tpx2
 70.1 0.0
'alfa           tens           xwinch
 146.0           2097.0          0.0
'-------------------------------------------------------------------------
 LINE DATA
'iline lichar inilin iwirun intact
 11     3      1      0      1
'tpx1 tpx2
 70.1 0.0
'alfa           tens           xwinch
 254.0           2097.0          0.0
'-------------------------------------------------------------------------
 LINE DATA
'iline lichar inilin iwirun intact
 12     3      1      0      1
'tpx1 tpx2
 70.1 0.0
'alfa           tens           xwinch
 257.0           2097.0          0.0
'-------------------------------------------------------------------------
 LINE DATA
'iline lichar inilin iwirun intact
 13     3      1      0      1
'tpx1 tpx2
 70.1 0.0
'alfa           tens           xwinch
 260.0           2097.0          0.0
'-------------------------------------------------------------------------
 LINE DATA
'iline lichar inilin iwirun intact
 14     3      1      0      1
'tpx1 tpx2
 70.1 0.0
'alfa           tens           xwinch
```

```
 LINE DATA
'iline lichar inilin iwirun intact
 15     3      1      0      1
'tpx1 tpx2
 70.1 0.0
'alfa           tens           xwinch
 266.0           2097.0          0.0
'-------------------------------------------------------------------------
 LINE CHARACTERISTICS DATA
'lichar
 1
'linpty npocha npv
 2      40     1
'nseg ibotco icurli
 3    1      0
'anbot tpx3 x3ganc tmax    fric
 0.0   16.1 371.6  22000.0 1.0
'iseg ieltyp nel ibuoy sleng  nea brkstr
 1    0      100 0     520.0  1   21876.0
 2    0      50  0     355.0  1   22000.0
 3    0      10  0     50.0   1   24073.0
'iseg dia   emod   emfact uwiw    watfac cdn cdl
 1    0.170 4.72E7 2.0    4.983   0.87   2.4 1.15
 2    0.151 2.02E7 1.0    0.917   0.81   1.37 0.0
 3    0.170 4.77E7 2.0    4.983   0.87   2.4 1.15
'-------------------------------------------------------------------------
 LINE CHARACTERISTICS DATA
'lichar
 2
'linpty npocha npv
 2      40     1
'nseg ibotco icurli
 3    1      0
'anbot tpx3 x3ganc tmax    fric
 0.0   16.1 371.6  22000.0 1.0
'iseg ieltyp nel ibuoy sleng  nea brkstr
 1    0      100 0     420.0  1   19592.0
 2    0      50  0     355.0  1   22000.0
 3    0      10  0     50.0   1   24073.0
```

```
 LINE CHARACTERISTICS DATA
'lichar
 3
'linpty npocha npv
 2      40     1
'nseg ibotco icurli
 3    1      0
'anbot tpx3 x3ganc tmax    fric
 0.0   16.1 371.6  22000.0 1.0
'iseg ieltyp nel ibuoy sleng  nea brkstr
 1    0      100 0     720.0  1   24073.0
 2    0      50  0     355.0  1   22000.0
 3    0      10  0     50.0   1   24073.0
'iseg dia   emod   emfact uwiw    watfac cdn cdl
 1    0.170 4.77E7 2.0    4.983   0.87   2.4 1.15
 2    0.151 2.02E7 1.0    0.917   0.81   1.37 0.0
 3    0.170 4.77E7 2.0    4.983   0.87   2.4 1.15
END
```

Figure A.1: Mooring line data

Appendix B

Wind and Current Coefficients

Table B.1: Quadratic wind coefficients

No	Direction	C1	C2	C3	C4	C5	C6
1	0.0	2944.0	20.0	0.0	-797.0	0.0	11610
2	10.0	3305.0	768.0	0.0	-18330	0.0	-37810
3	20.0	3923.0	1860.0	0.0	-48130	0.0	-66340
4	30.0	3990.0	3188.0	0.0	-85270	0.0	-68030
5	40.0	3981.0	4762.0	0.0	-1.336e+05	0.0	-54530
6	50.0	3345.0	6043.0	0.0	-1.739e+05	0.0	-32900
7	60.0	2626.0	7312.0	0.0	-2.168e+05	0.0	-15130
8	70.0	1651.0	8405.0	0.0	-2.544e+05	0.0	26120
9	80.0	625.0	8912.0	0.0	-2.751e+05	0.0	68130
10	90.0	-412.0	9315.0	0.0	-2.921e+05	0.0	1.025e+05
11	100.0	-1190.0	8697.0	0.0	-2.77e+05	0.0	1.246e+05
12	110.0	-1891.0	8476.0	0.0	-2.732e+05	0.0	1.579e+05
13	120.0	-2534.0	8053.0	0.0	-2.615e+05	0.0	1.933e+05
14	130.0	-3042.0	7618.0	0.0	-2.491e+05	0.0	2.21e+05
15	140.0	-3262.0	6447.0	0.0	-2.117e+05	0.0	2.283e+05
16	150.0	-3222.0	4931.0	0.0	-1.634e+05	0.0	2.011e+05
17	160.0	-2899.0	3149.0	0.0	-1.074e+05	0.0	1.511e+05
18	170.0	-2626.0	1607.0	0.0	-59290	0.0	89070
19	180.0	-2435.0	202.0	0.0	-8766.0	0.0	7497.0
20	190.0	-2514.0	-1242.0	0.0	42870	0.0	-77900
21	200.0	-2718.0	-2791.0	0.0	91320	0.0	-1.418e+05
22	210.0	-2807.0	-4437.0	0.0	1.404e+05	0.0	-1.785e+05
23	220.0	-2859.0	-5972.0	0.0	1.887e+05	0.0	-2.037e+05
24	230.0	-2650.0	-7188.0	0.0	2.266e+05	0.0	-1.944e+05
25	240.0	-2377.0	-8184.0	0.0	2.574e+05	0.0	-2.009e+05
26	250.0	-1712.0	-8652.0	0.0	2.716e+05	0.0	-1.673e+05
27	260.0	-898.0	-8483.0	0.0	2.635e+05	0.0	-1.288e+05
28	270.0	-240.0	-9107.0	0.0	2.795e+05	0.0	-1.086e+05
29	280.0	712.0	-8593.0	0.0	2.579e+05	0.0	-64660
30	290.0	1790.0	-7982.0	0.0	2.356e+05	0.0	-16970
31	300.0	2729.0	-7266.0	0.0	2.097e+05	0.0	28640
32	310.0	3712.0	-6713.0	0.0	1.914e+05	0.0	45380
33	320.0	4051.0	-5256.0	0.0	1.439e+05	0.0	59040
34	330.0	4380.0	-3760.0	0.0	1.002e+05	0.0	64890
35	340.0	4080.0	-2075.0	0.0	51480	0.0	70490
36	350.0	3621.0	-859.0	0.0	20240	0.0	51500
37	360.0	2944.0	20.0	0.0	-797.0	0.0	11610

Table B.2: Quadratic current coefficients

No	Direction	C21	C22	C23	C24	C25	C26
1	0.0	1.592e+05	2210.0	0.0	-1.452e+05	0.0	0.0
2	10.0	1.718e+05	1.284e+05	0.0	2.396e+06	0.0	-1.27e+07
3	20.0	1.806e+05	4.051e+05	0.0	8.731e+06	0.0	-2.097e+07
4	30.0	1.76e+05	6.951e+05	0.0	1.704e+07	0.0	-2.991e+07
5	40.0	1.364e+05	9.873e+05	0.0	2.507e+07	0.0	-3.49e+07
6	50.0	79610	1.253e+06	0.0	3.037e+07	0.0	-3.59e+07
7	60.0	7910.0	1.485e+06	0.0	3.238e+07	0.0	-3.488e+07
8	70.0	-46090	1.605e+06	0.0	3.062e+07	0.0	-2.513e+07
9	80.0	-76820	1.738e+06	0.0	2.641e+07	0.0	-1.079e+07
10	90.0	-74950	1.846e+06	0.0	2.333e+07	0.0	3.585e+06
11	100.0	67510	1.871e+06	0.0	2.476e+07	0.0	2.862e+07
12	110.0	56330	1.713e+06	0.0	3.247e+07	0.0	4.267e+07
13	120.0	20020	1.594e+06	0.0	3.638e+07	0.0	5.008e+07
14	130.0	-54000	1.377e+06	0.0	3.618e+07	0.0	4.772e+07
15	140.0	-1.206e+05	1.054e+06	0.0	3.157e+07	0.0	4.549e+07
16	150.0	-1.732e+05	7.15e+05	0.0	2.349e+07	0.0	3.933e+07
17	160.0	-1.927e+05	4.228e+05	0.0	1.414e+07	0.0	2.849e+07
18	170.0	-1.797e+05	1.904e+05	0.0	5.518e+06	0.0	1.493e+07
19	180.0	-1.583e+05	15500	0.0	1.815e+05	0.0	0.0

Appendix C

Accidental Limit State Motion Response

C.0.1 Surge Translation

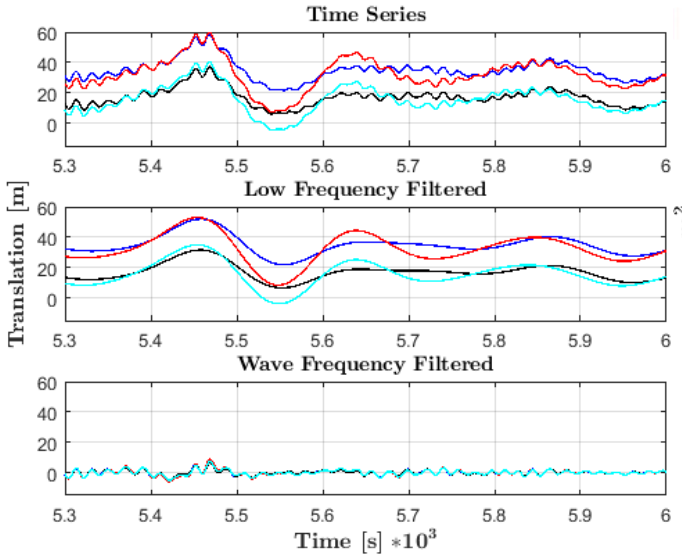

(a) Total, LF and WF surge time series.

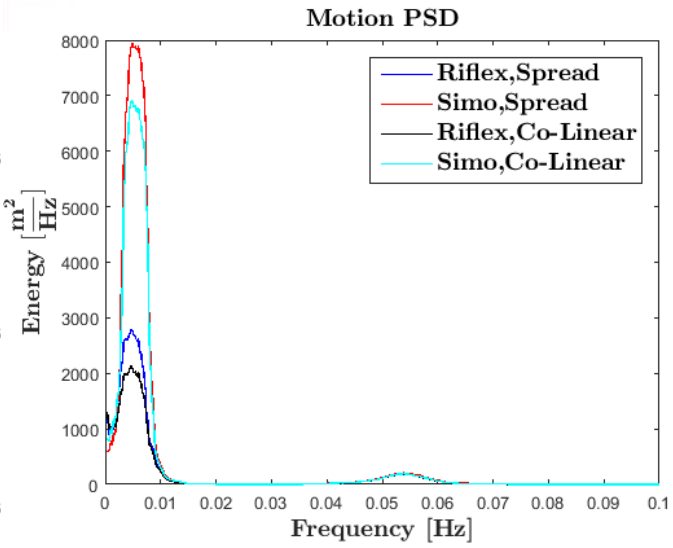

(b) Surge energy spectrum.

Figure C.1: Total, LF and WF surge time series of the vessel's COG, and the corresponding energy spectrum in both Riflex and Simo in ALS co-linear and spread weather.

Table C.1: The max, min, μ and σ of the vessel's COG surge translation in ALS spread and co-linear condition in Figure C.1a.

	Spread							
	Riflex				**Simo**			
Surge	MAX	MIN	μ	σ	MAX	MIN	μ	σ
Total [m]	58.4	21.5	34.7	4.4	59.6	7.3	32.3	6.6
LF [m]	52.0	21.9	34.7	3.8	53.0	8.4	32.2	6.0
WF [m]	7.1	-6.6	0.0	1.7	8.7	-6.7	0.0	1.8

	Spread							
	Riflex				**Simo**			
Surge	MAX	MIN	μ	σ	MAX	MIN	μ	σ
Total [m]	37.3	4.5	17.3	4.0	40.4	-7.0	15.8	6.2
LF [m]	31.6	6.6	17.3	3.5	34.9	-4.0	15.8	5.7
WF [m]	6.5	-6.4	0.0	1.7	7.3	-6.6	0.0	1.7

C.0.2 Sway Translation

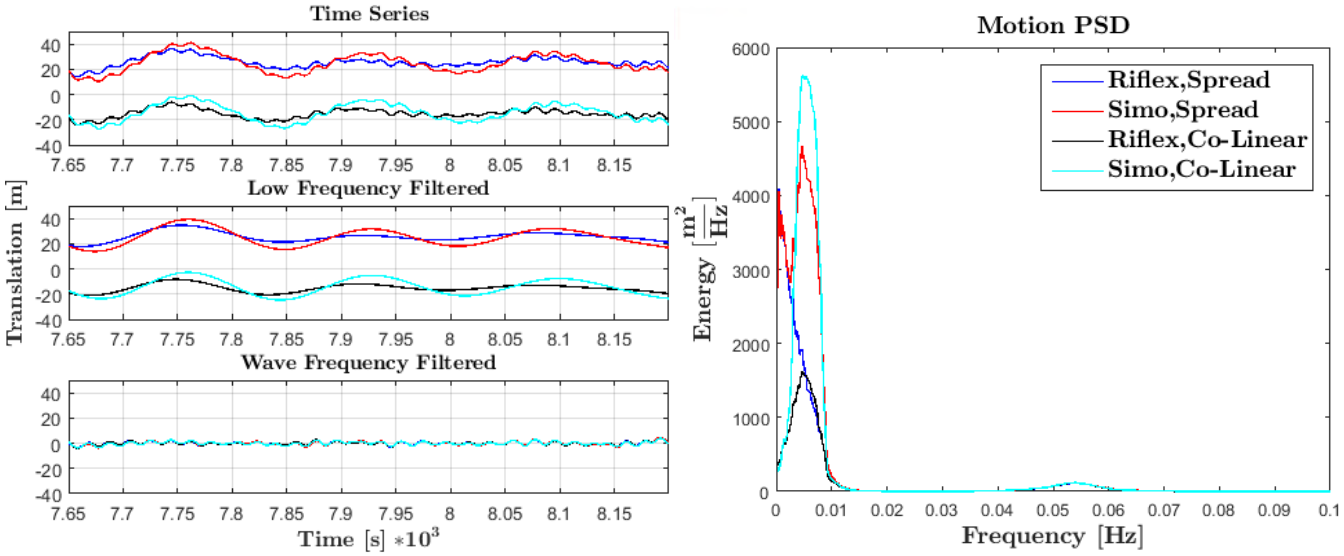

(a) Total, LF and WF surge time series.

(b) Sway energy spectrum.

Figure C.2: Total, LF and WF sway time series of the vessel's COG, and the corresponding energy spectrum in both Riflex and Simo in ALS co-linear and spread weather.

Table C.2: The max, min, μ and σ of the vessel's COG sway translation in ALS spread and co-linear condition in Figure C.2a.

	Spread							
	Riflex				**Simo**			
Sway	MAX	MIN	μ	σ	MAX	MIN	μ	σ
Total [m]	41.1	11.4	25.8	4.4	41.1	5.4	25.1	5.7
LF [m]	37.6	14.0	25.8	4.1	39.3	7.6	25.1	5.3
WF [m]	5.0	-5.2	0.0	1.4	5.1	-5.5	0.0	1.5

	Co-linear							
	Riflex				**Simo**			
Sway	MAX	MIN	μ	σ	MAX	MIN	μ	σ
Total [m]	-5.6	-27.4	-15.8	3.4	4.2	-32.5	-14.9	5.5
LF [m]	-8.3	-26.1	-15.8	2.9	1.5	-30.2	-15.0	5.0
WF [m]	4.9	-5.4	0.0	1.3	5.0	-5.7	0.0	1.4

C.0.3 Heave Motion

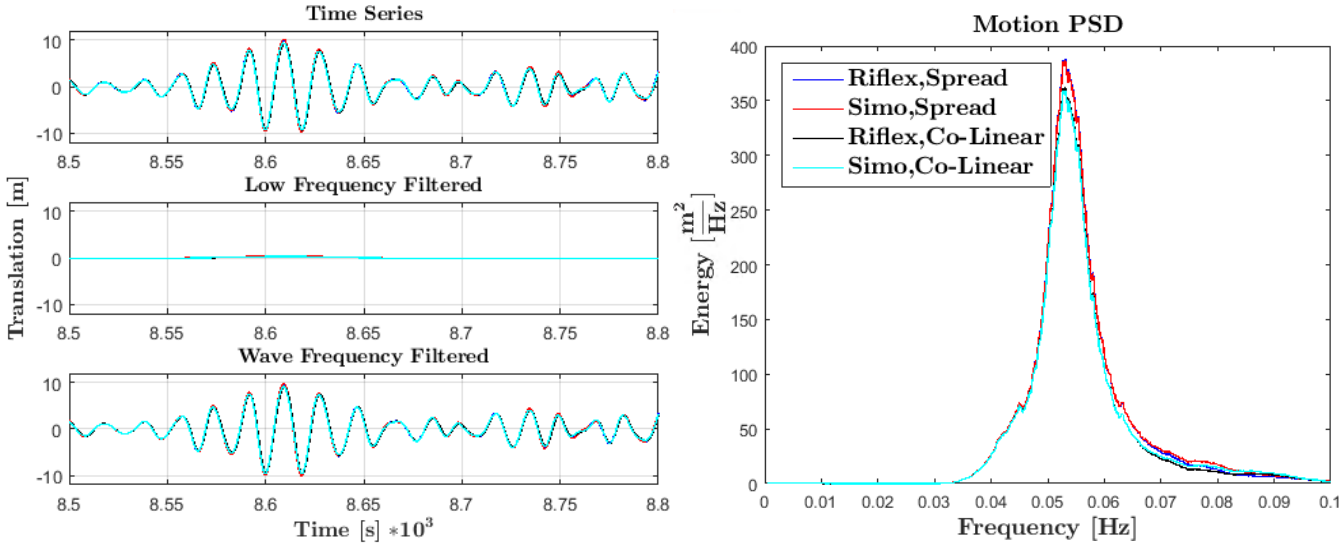

(a) Total, LF and WF surge time series.

(b) Heave energy spectrum.

Figure C.3: Total, LF and WF heave time series of the vessel's COG, and the corresponding energy spectrum in both Riflex and Simo in ALS co-linear and spread weather.

Table C.3: The max, min, μ and σ of the vessel's COG heave motion in ALS spread and co-linear condition in Figure C.3a.

	Spread							
	Riflex				**Simo**			
Heave	MAX	MIN	μ	σ	MAX	MIN	μ	σ
Total [m]	9.9	-9.7	-0.1	2.1	10.2	-9.7	-0.1	2.1
LF [m]	1.5	-0.4	-0.1	0.1	1.6	-0.4	-0.1	0.1
WF [m]	9.6	-10.0	0.0	2.1	9.9	-10.0	0.0	2.1
	Co-linear							
	Riflex				**Simo**			
Heave	MAX	MIN	μ	σ	MAX	MIN	μ	σ
Total [m]	9.2	-9.4	-0.2	2.0	9.4	-9.3	-0.2	2.1
LF [m]	1.6	-0.4	-0.1	0.1	1.5	-0.4	-0.1	0.1
WF [m]	9.0	-9.6	0.0	2.0	9.1	-9.6	0.0	2.1

C.0.4 Roll Motion

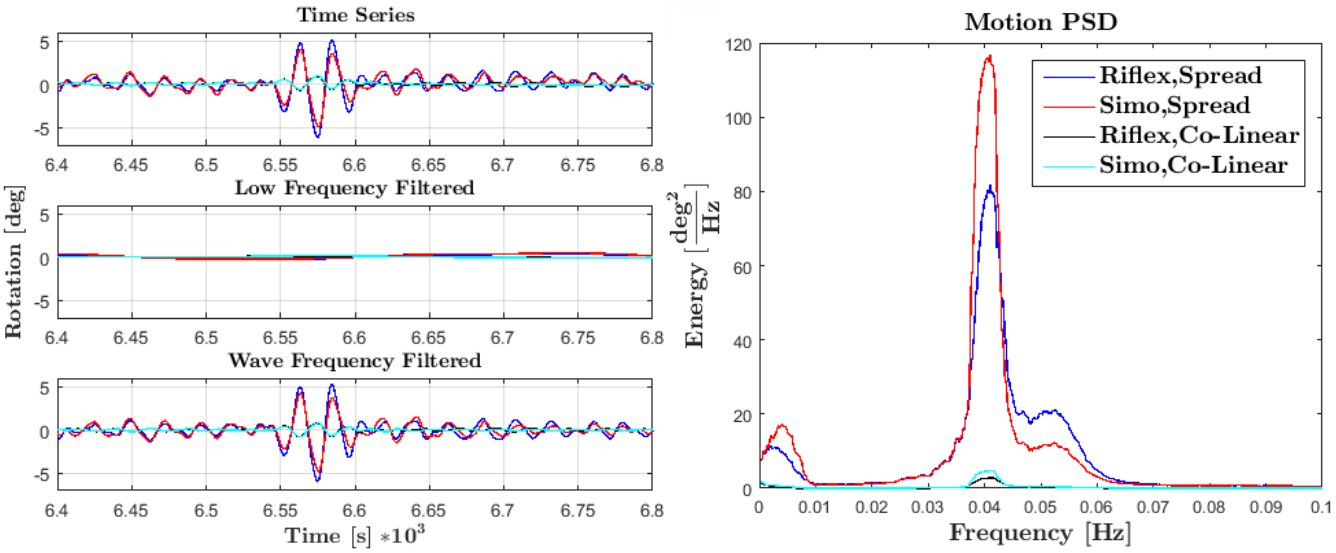

(a) Total, LF and WF surge time series.

(b) Roll energy spectrum.

Figure C.4: Total, LF and WF roll time series of the vessel's COG, and the corresponding energy spectrum in both Riflex and Simo in ALS co-linear and spread weather.

Table C.4: The max, min, μ and σ of the vessel's COG roll motion in ALS spread and co-linear condition in Figure C.4a.

	Spread							
	Riflex				**Simo**			
Roll	MAX	MIN	μ	σ	MAX	MIN	μ	σ
Total [deg]	5.2	-6.1	0.2	1.0	4.1	-4.9	0.2	1.0
LF [deg]	0.9	-0.7	0.2	0.3	1.1	-1.4	0.2	0.3
WF [deg]	5.3	-5.9	0.0	0.9	4.3	-4.8	0.0	0.9
	Co-linear							
	Riflex				**Simo**			
Roll	MAX	MIN	μ	σ	MAX	MIN	μ	σ
Total [deg]	0.9	-0.7	0.1	0.2	1.0	-0.6	0.1	0.2
LF [deg]	0.2	-0.1	0.1	0.1	0.3	-0.2	0.1	0.1
WF [deg]	0.8	-0.8	0.0	0.1	0.8	-0.8	0.0	0.2

C.0.5 Pitch Motion

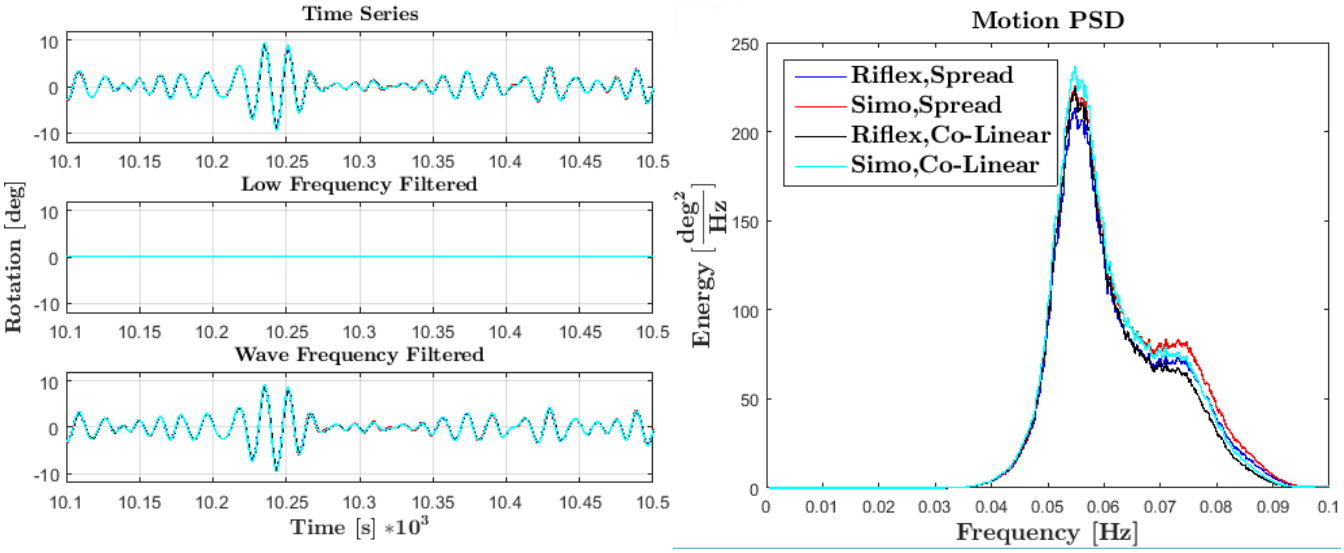

(a) Total, LF and WF surge time series.

(b) Pitch energy spectrum.

Figure C.5: Total, LF and WF pitch time series of the vessel's COG, and the corresponding energy spectrum in both Riflex and Simo in ALS co-linear and spread weather.

Table C.5: The max, min, μ and σ of the vessel's COG pitch motion in ALS spread and co-linear condition in Figure C.5a.

	Spread							
	Riflex				**Simo**			
Pitch	MAX	MIN	μ	σ	MAX	MIN	μ	σ
Total [deg]	9.0	-8.9	0.2	1.9	9.4	-9.4	0.1	2.0
LF [deg]	0.6	0.1	0.2	0.0	0.7	0.0	0.2	0.0
WF [deg]	8.8	-9.1	0.0	1.9	9.2	-9.6	0.0	2.0

	Co-linear							
	Riflex				**Simo**			
Pitch	MAX	MIN	μ	σ	MAX	MIN	μ	σ
Total [deg]	+ 9.0	-8.9	0.1	1.9	9.4	-9.4	0.1	2.0
LF [deg]	0.7	0.0	0.1	0.0	0.6	0.1	0.1	0.0
WF [deg]	8.8	-9.1	0.0	1.9	9.3	-9.6	0.0	2.0

C.0.6 Yaw Motion

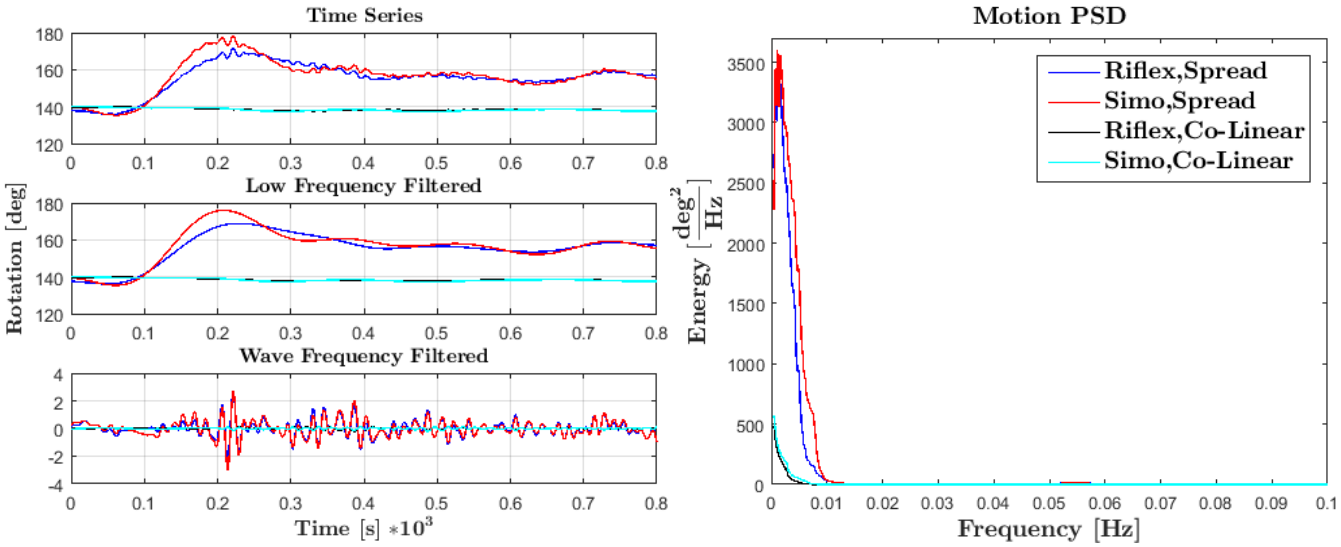

(a) Total, LF and WF surge time series. *(b) Yaw energy spectrum.*

Figure C.6: Total, LF and WF yaw time series of the vessel's COG, and the corresponding energy spectrum in both Riflex and Simo in ALS co-linear and spread weather.

Table C.6: The max, min, μ and σ of the vessel's COG yaw motion in ALS spread and co-linear condition in Figure C.6a.

	Spread							
	Riflex				**Simo**			
Pitch	MAX	MIN	μ	σ	MAX	MIN	μ	σ
Total [m]	171.3	135.8	156.9	3.6	178.0	135.1	156.8	4.1
LF [m]	168.9	136.1	156.9	3.6	175.9	135.4	156.8	4.0
WF [m]	2.6	-2.2	0.0	0.49	2.7	-3.1	0.0	0.5
	Co-linear							
	Riflex				**Simo**			
Pitch	MAX	MIN	μ	σ	MAX	MIN	μ	σ
Total [m]	140.1	135.3	137.7	0.8	140.8	134.6	137.6	1.0
LF [m]	140.1	135.7	137.7	0.8	140.8	135.0	137.6	1.0
WF [m]	0.4	-0.4	0.0	0.1	0.4	-0.5	0.0	0.1

Appendix D

Accidental Limit State Tension Response

D.0.1 Windward Line Long 4

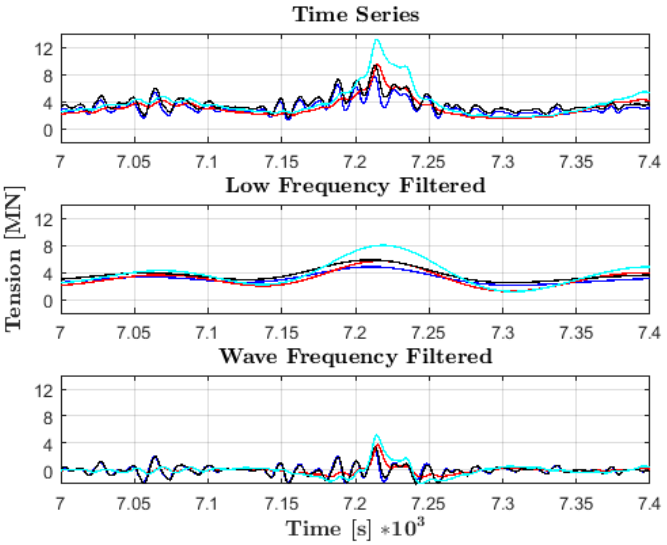

(a) Total, LF and WF tension time series of Long 4.

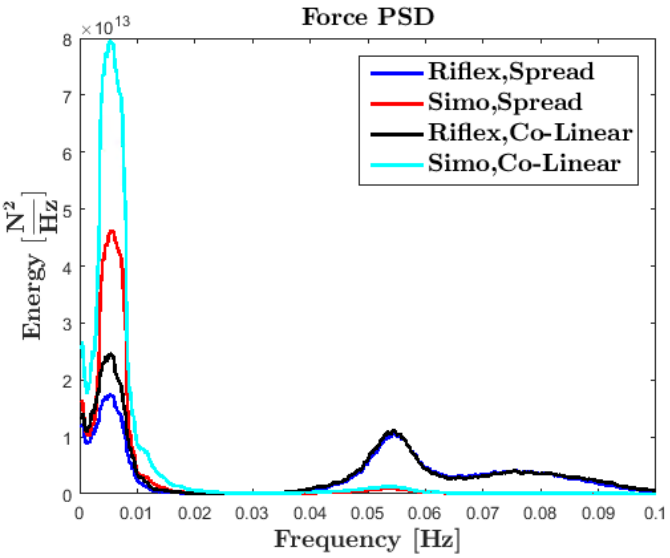

(b) Tension energy spectrum of Long 4.

Figure D.1: Total, LF and WF tension time series of windward line Long 4, and the corresponding energy spectrum in both Riflex and Simo in ALS co-linear and spread weather. In this case Simo actually achieves a larger line tension compared to Riflex in both weather conditions. This is because the effective line length is in Simo fully streched out and pulls on the anchor which is the reason for the large tension response in Simo.

Table D.1: The max, min, μ and σ of the tension time series of windward line Long 5 in ALS spread and co-linear weather conditions in Figure D.1a.

	Spread							
	Riflex				**Simo**			
Long 4	MAX	MIN	μ	σ	MAX	MIN	μ	σ
Total [kN]	7715.2	235.8	2796.1	588.2	9468.2	1444.2	2717.7	532.8
LF [kN]	4808.9	2090.9	2796.3	316.5	5677.5	1201.7	2717.7	469.6
WF [kN]	2912.1	-3060.8	-0.2	482.4	3797.9	-990.3	-0.3	179.8
	Co-linear							
	Riflex				**Simo**			
Long 4	MAX	MIN	μ	σ	MAX	MIN	μ	σ
Total [kN]	9286.1	561.9	3333.3	635.0	13140.0	1643.0	3247.0	710.2
LF [kN]	5832.1	2478.1	3333.1	371.2	7982.9	1157.4	3246.8	622.7
WF [kN]	3464.5	-3038.8	-0.2	496.4	5203.1	-1888.5	-0.3	252.1

D.0.2 Leeward Line Longest 4

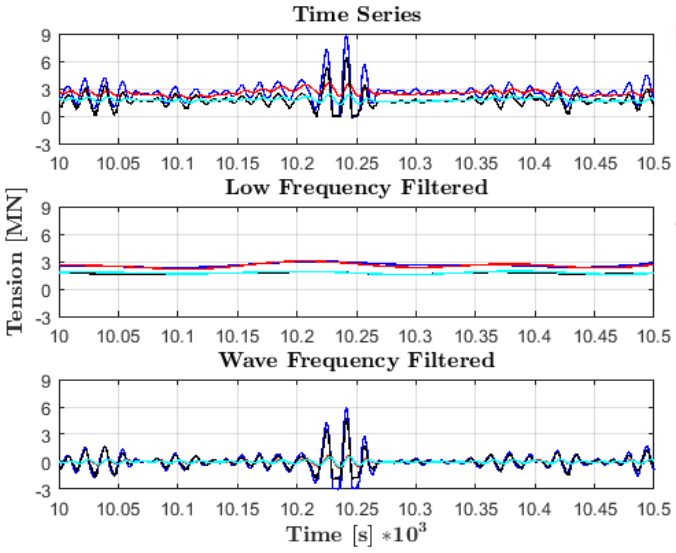

(a) Total, LF and WF tension time series of Longest 4.

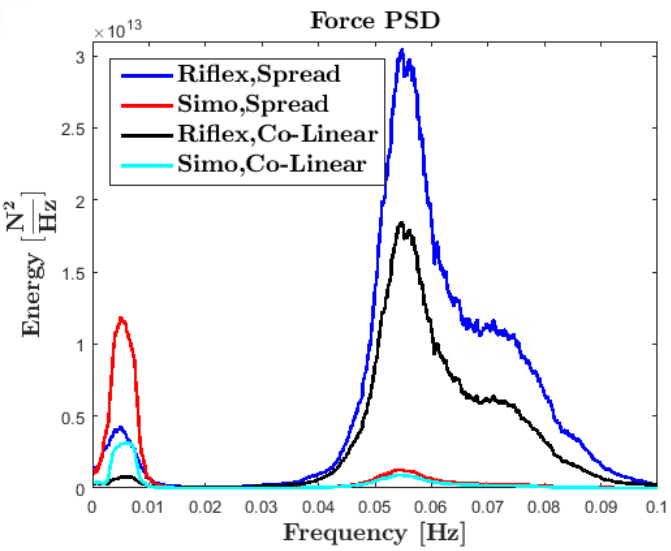

(b) Tension energy spectrum of Longest 4.

Figure D.2: Total, LF and WF tension time series of leeward line Longest 4, and corresponding energy spectrum in Riflex and Simo during ALS co-linear and spread weather.

Table D.2: The max, min, μ and σ of the tension time series of leeward line Longest 4 in ALS spread and co-linear weather condition in Figure D.2a.

	Spread							
	Riflex				**Simo**			
Long 4	MAX	MIN	μ	σ	MAX	MIN	μ	σ
Total [kN]	8784.7	-265.9	2577.7	774.6	3643.8	1738.8	2536.7	288.5
LF [kN]	3025.1	2118.1	2577.8	152.1	3188.9	1794.4	2537.4	234.7
WF [kN]	5841.1	-3161.4	-0.3	757.8	689.2	-696.5	0.1	146.3
	Co-linear							
	Riflex				**Simo**			
Long 4	MAX	MIN	μ	σ	MAX	MIN	μ	σ
Total [kN]	6485.6	-242.2	1698.2	584.9	2394.1	1189.5	1761.8	172.6
LF [kN]	1928.2	1527.1	1698.2	63.9	2109.1	1462.8	1762.0	118.5
WF [kN]	4702.5	-2038.5	-0.1	50.9	567.6	-512.2	0.2	118.3

Appendix E

Ultimate Limit State Turret Forces

E.1 Spread Weather

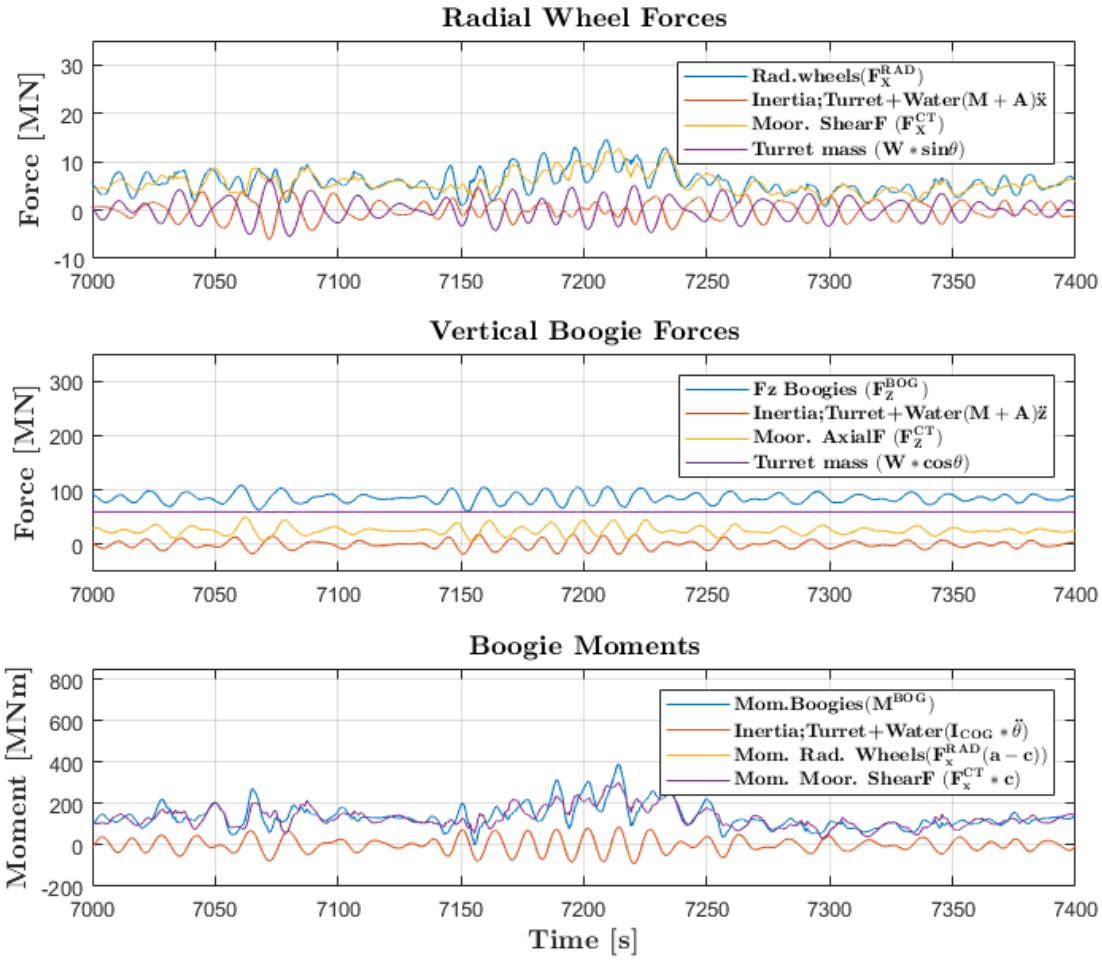

Figure E.1: Force and moment time serie of (F_X^{RAD}), (F_Z^{BOG}&M^{BOG}) and all of their force and moment contributions in ULS spread weather.

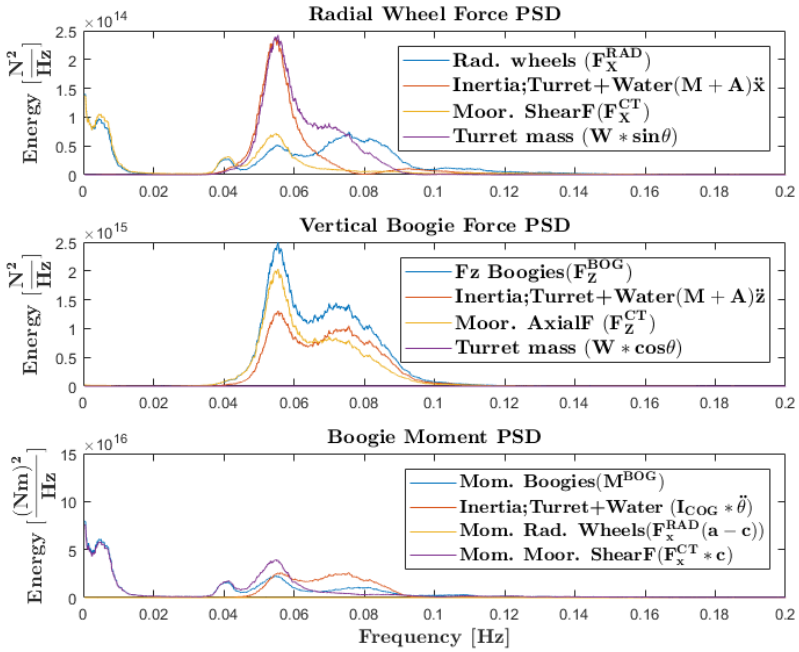

Figure E.2: Force and moment PSDs of (F_X^{RAD}), (F_Z^{BOG}&M^{BOG}) and their force and moment contributions in ULS spread weather.

Table E.1: Max, min, μ and σ of (F_X^{RAD}), (F_Z^{BOG}&M^{BOG}) and their contributions in spread environment in Figure E.1.

	Radial Wheel Forces [kN]			
	MAX	MIN	μ	σ
F_X^{RAD}	14645.6	-4078.9	4836.0	1850.8
$(M+A)\ddot{x}$	6494.1	-7850.4	0.2	1743.8
F_x^{CT}	12747.5	-3046.2	4666.8	1489.1
$W*sin\theta$	7261.8	-6645.4	169.	1996.8
	Vertical Boogie Forces [kN]			
F_z^{BOG}	116992.0	56950.1	84990.5	7549.3
$(M+A)\ddot{z}$	25108.9	-21165.8	0.5	5955.2
F_z^{CT}	59896.9	2754.4	25182.6	6254.9
$W*cos\theta$	59841.0	59398.7	59807.4	46.2
	Boogie Moment [kNm]			
M^{BOG}	389744.2	-48593.5	112449.0	34342.0
$I_{COG}*\ddot{\theta}$	109861.0	-117729.9	-1.5	27818.5
$F_x^{RAD}(a-c)$	8421.2	-2345.4	2780.7	1064.2
$F_x^{CT}*c$	299565.8	-71586.5	109669.8	34994.8

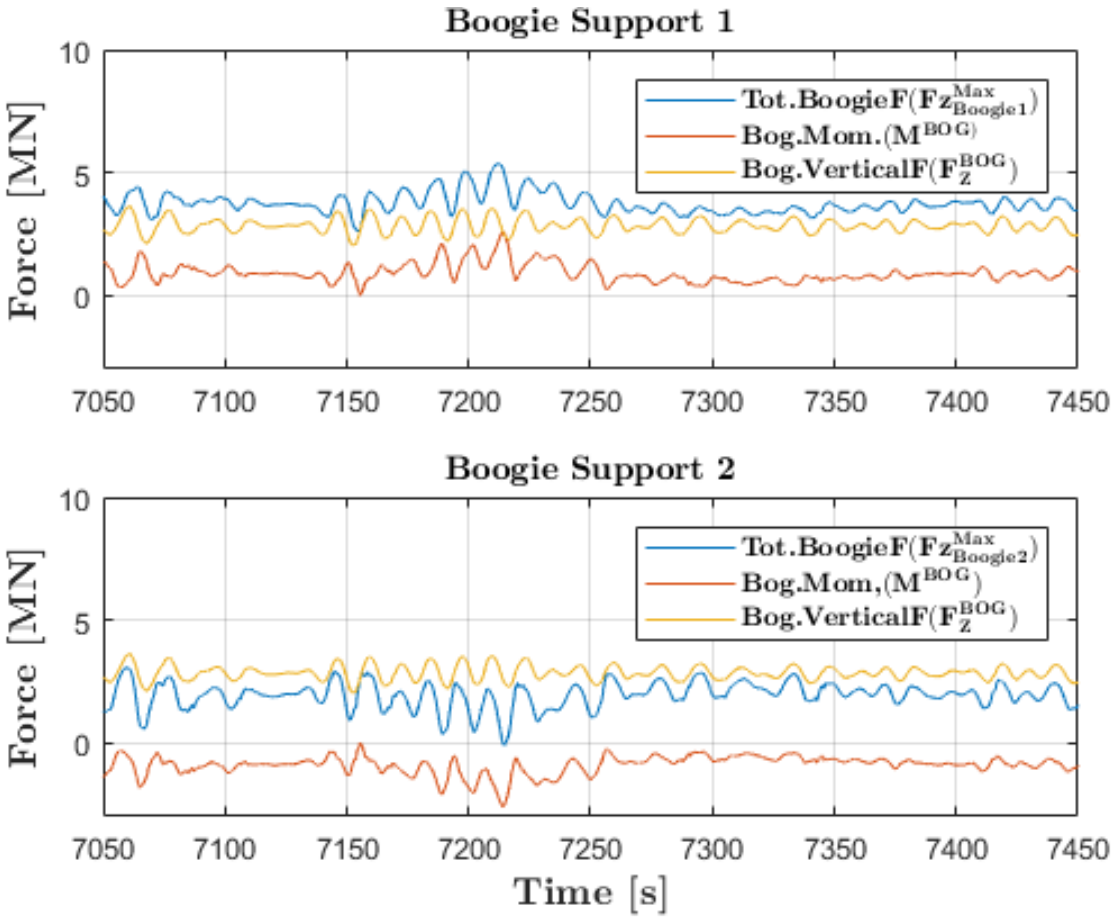

Figure E.3: Force time series of boogie 1 and 2, which are placed opposite of each other, and their force contributions in ULS spread weather.

Appendix F

Accidental Limit State Turret Forces

F.1 Spread Weather

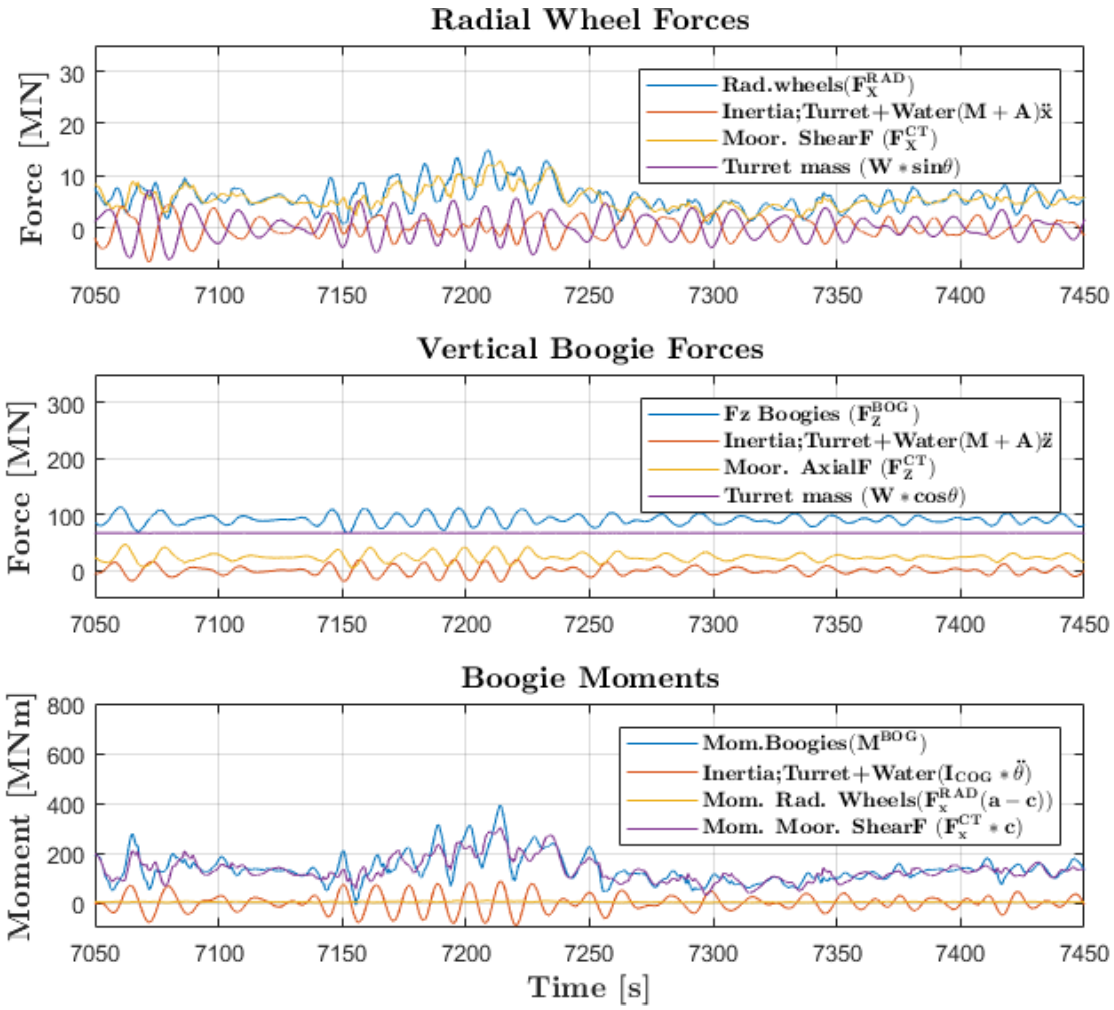

Figure F.1: Force and moment time serie of (F_X^{RAD}), (F_Z^{BOG} &M^{BOG}) and their force and moment contributions in ALS spread weather.

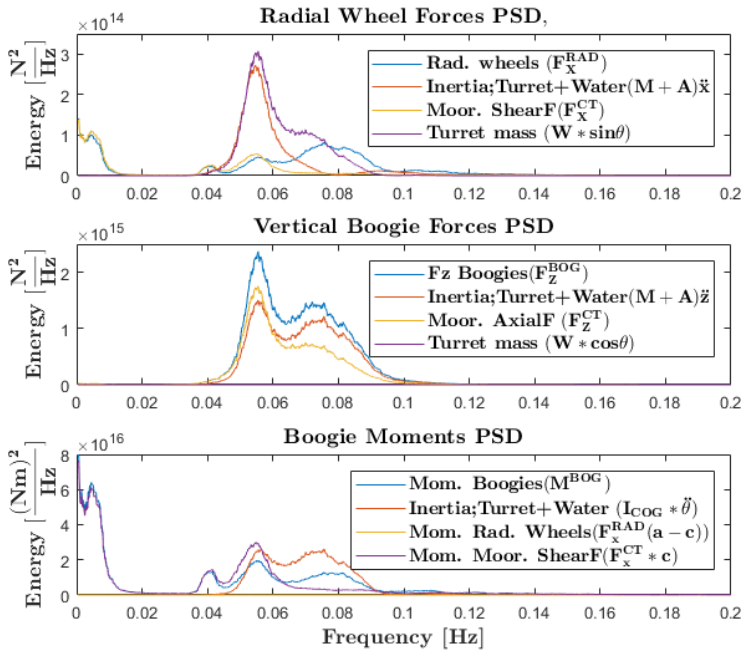

Figure F.2: Force and moment PSDs of (F_X^{RAD}), (F_Z^{BOG}&M^{BOG}) and their force and moment contributions in ALS spread weather.

Table F.1: Max, min, μ and σ of (F_X^{RAD}), (F_Z^{BOG}&M^{BOG}) and their contributions in spread environment in Figure F.1.

	Radial Wheel Forces [kN]			
	MAX	MIN	μ	σ
F_X^{RAD}	14882.5	-4059.6	4840.5	1881.3
$(M+A)\ddot{x}$	6900.1	-8396.4	0.3	1867.7
F_x^{CT}	12797.9	-2418.7	4662.7	1398.1
$W*sin\theta$	8182.1	-7516.2	177.6	2250.7
	Vertical Boogie Forces [kN]			
F_z^{BOG}	120644.8	62305.9	90633.5	7525.8
$(M+A)\ddot{z}$	26969.7	-22983.1	0.4	6414.2
F_z^{CT}	55430.5	2580.3	23472.5	5825.1
$W*cos\theta$	67198.5	66698.5	67160.5	52.3
	Boogie Moment [kNm]			
M^{BOG}	391550.6	-52936.9	112354.7	34251.2
$I_{COG}*\ddot{\theta}$	109979.2	-118557.3	-1.1	27956.6
$F_x^{RAD}(a-c)$	8557.5	-2334.3	2783.3	1081.8
$F_x^{CT}*c$	300750.2	-56839.5	109572.6	32855.7

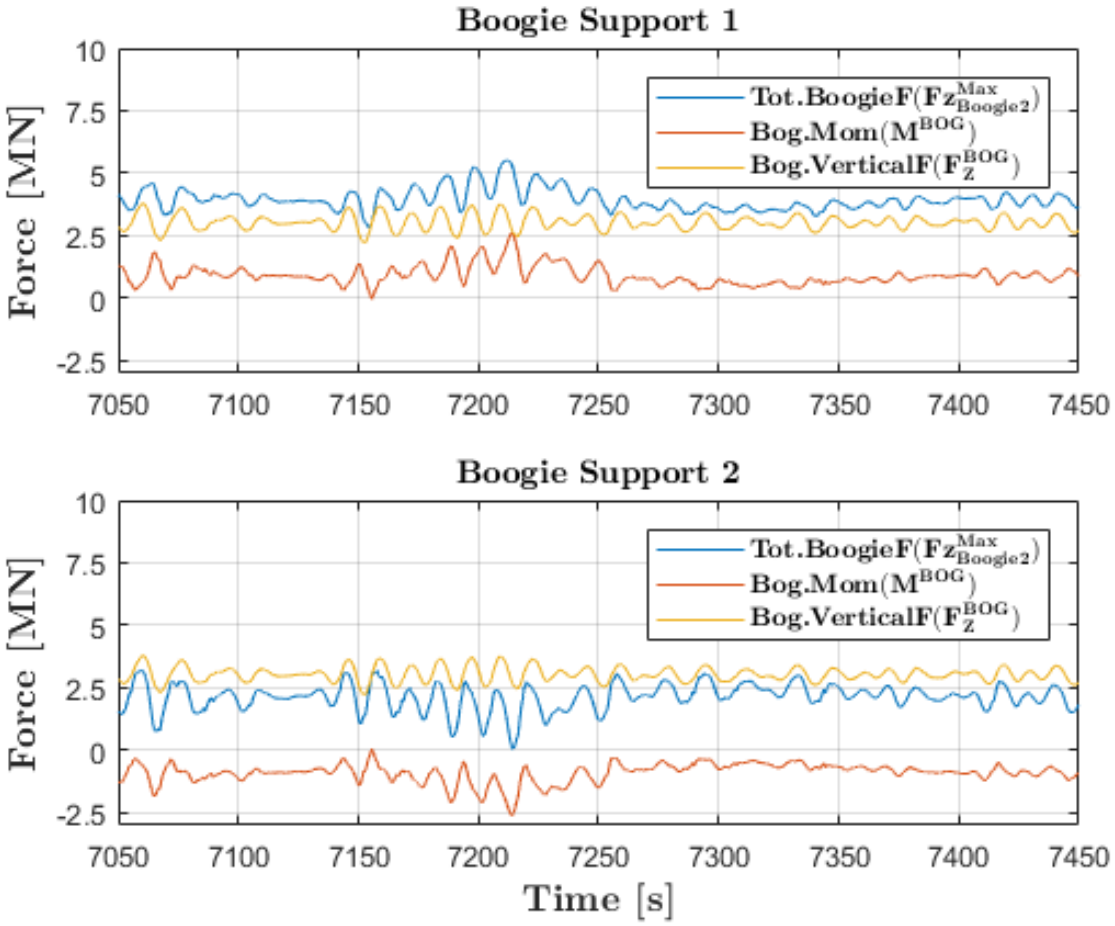

Figure F.3: Force time series of boogie 1 and 2, which are placed opposite of each other, and their force contributions during ALS spread weather.

F.2 Co-Linear Weather

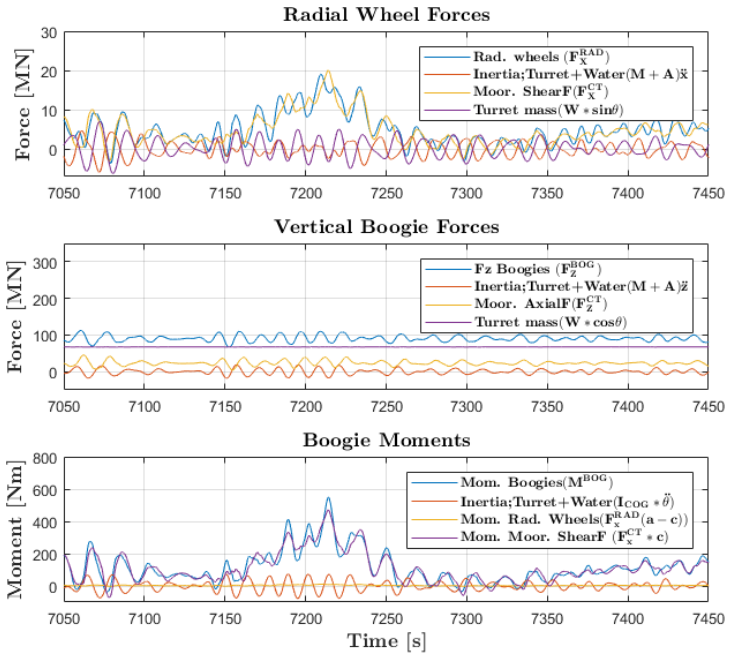

Figure F.4: Force and moment time serie of (F_X^{RAD}), (F_Z^{BOG}&M^{BOG}) and their force and moment contributions in ALS co-linear weather conditions.

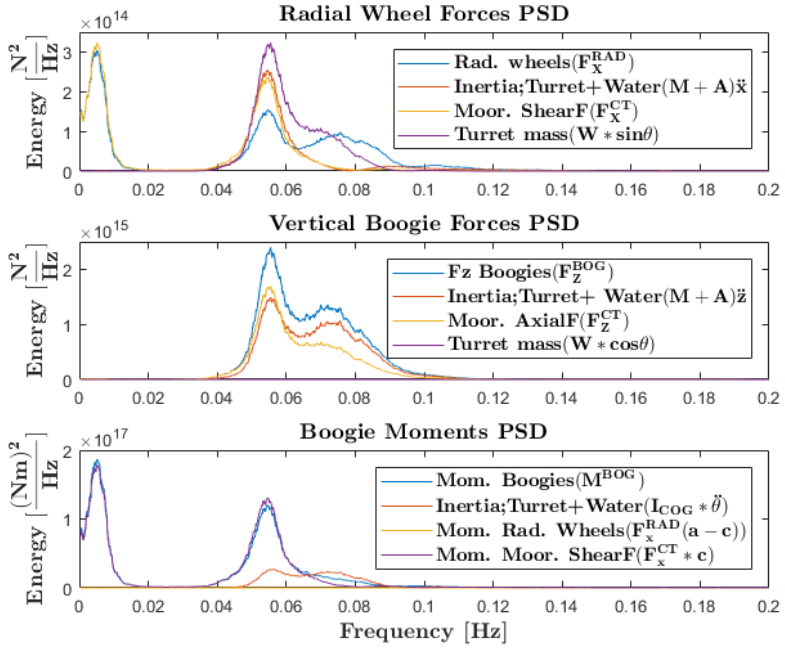

Figure F.5: Force and moment PSDs of (F_X^{RAD}), (F_Z^{BOG}&M^{BOG}) and their force and moment contributions in ALS co-linear weather conditions.

Table F.2: Max, min, μ and σ of (F_X^{RAD}), (F_Z^{BOG}&M^{BOG}) and their contributions in co-linear environment in Figure F.4.

	Radial Wheel Forces [kN]			
	MAX	MIN	μ	σ
F_X^{RAD}	19075.9	-7904.5	3760.2	2475.1
$(M+A)\ddot{x}$	7267.7	-7900.4	0.1	1787.6
F_x^{CT}	20084.4	-8387.0	3585.9	2266.1
$W * sin\theta$	8205.2	-7502.9	174.1	2244.1
	Vertical Boogie Forces [kN]			
F_z^{BOG}	119348.5	63217.7	90189.1	7308.4
$(M+A)\ddot{z}$	24992.4	-21563.8	0.5	6156.9
F_z^{CT}	53978.0	3315.4	23027.8	5604.9
$W * cos\theta$	67198.5	66695.7	67160.8	52.0
	Boogie Moment [kNm]			
M^{BOG}	550153.8	-168119.8	86430.9	54395.3
$I_{COG} * \ddot{\theta}$	100641.2	-106365.6	-0.9	26913.1
$F_x^{RAD}(a-c)$	10968.7	-4545.1	2162.1	1423.2
$F_x^{CT} * c$	471982.3	-197093.4	84269.7	53253.1

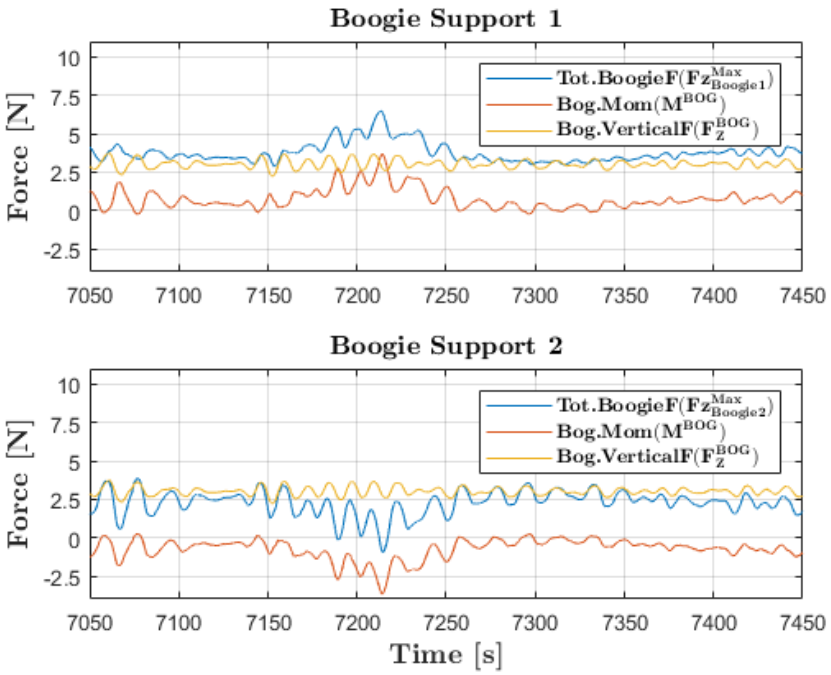

Figure F.6: Force time series of boogie 1 and 2, which are placed opposite of each other, and their force contributions during ALS co-linear weather.